Doctoral Thesis in Medical Technology

Minimally Invasive Catheter-Based Technologies

MIKAEL SANDELL

Stockholm, Sweden 2023

Karolinska Institutet

Minimally Invasive Catheter-Based Technologies

MIKAEL SANDELL

Academic Dissertation which, with due permission of the KTH Royal Institue of Technology and the Karolinska Institute, is submitted for public defence for the Degree of Doctor of Medical Technology on Friday the 8th of September 2023, at 9:30 a.m. in B2, Brinellvägen 23, Stockholm.

Doctoral Thesis in Medical Technology
KTH Royal Institute of Technology
Stockholm, Sweden 2023
The Karolinska Institute,
Stockholm, Sweden 2023

TRITA-CBH-FOU-2023:32
ISBN 978-91-8040-641-3

Printed by: Universitetsservice US-AB, Sweden 2023

Abstract

A simple incision procedure in a blood vessel makes the entire vascular system accessible. Through contrast injection and X-ray visualization, the vascular tree can be mapped and navigated through manual manipulation of thin tubes and wires. This utilization of the vasculature as internal pathways is commonly referred to as the endovascular technique. This technique can be used to deliver implants and drugs, retrieve problematic lesions or objects from the vasculature, or take tissue samples. Compared to open surgery, the advantage of this technique lies in the reduced invasiveness, ideally only leaving a small incision scar at the point of entry. Some interventions, however, are still associated with certain risks, requiring medication or complicating further interventions. The development of sequencing technologies presents an opportunity to improve and miniaturize devices, reducing invasiveness. This thesis aims to mitigate these risks and capitalize on the potential of next-generation sequencing through microfabrication technologies, producing devices that are less invasive than current methods or that enable a new procedure.

Initially, the aspect of endovascular heart biopsy is covered. The first work presents the fabrication and *in vivo* evaluation of a nitinol-based catheter device designed for extracting myocardial tissue. The device is fabricated through picosecond laser machining of nitinol tubes and wires, producing a device that is substantially smaller than what is currently used. The samples are evaluated and compared to samples extracted with conventional devices through RNA-Sequencing, verifying the proof of concept. The second work further emphasizes the device's functionality by evaluating it in a disease model of endomyocardial infarction. Tissue that is affected by the infarct and surrounding healthy tissue is extracted and compared in terms of its genetic expression. This comparison reveals a genetic discrepancy between the sick and healthy tissue, verifying the potential of using the device with RNA-sequencing for diagnostic purposes. The third work evaluates the safety aspects of the novel device in a head-to-head comparison with a conventional device. The study reveals a clear benefit of using the smaller device in terms of the complication rate during the procedure.

The fourth work presents the fabrication and *in vivo* evaluation of another nitinol-based catheter device designed for endothelial cell sampling. The device is fabricated through two-photon polymerization technologies, producing sub-mm brush structures mounted on a nitinol wire. Currently, there are no devices in clinical use that are capable of exclusively extracting endothelial cells. The novel device presents a solution for selective interaction with the innermost layer of the blood vessel. It represents an important step toward sampling endothelial cells for diagnostic and research purposes.

The fifth and sixth works collectively present two different aspects of a third nitinol-based catheter device designed to sample tissue from soft organs anywhere in the body. The device is fabricated using laser micromachining, grinding, and two-photon polymerization. The work is separated in terms of the *in vivo* evaluation and the technical solution. The technical aspects of the device are examined in terms of force generation in miniaturized catheter systems and the problems that arise in terms of mechanical scaling. These problems are solved by attaching pistons along the wire surface coupled with applied pressure to increase the force generated. The sampling with this device is realized, similar to the fourth work, with sub-mm brushes mounted on the wire. *In vivo* evaluation of this device reveals successful sampling of minute tissue quantities from the liver and kidney, in the size range of 10-100 cells per sample.

The seventh work presents the *in vivo* and *in vitro* performance of a nanostructure coating on nitinol-based stents. Patients with a stent implant are prescribed an extensive medication regimen to counteract the metal implant's effects on the blood and surrounding tissue. This issue is being continuously targeted by new stent platforms, either with a drug-eluting polymer layer or by being resorbable by the body or through various other means. These implants all have a transient behavior, resulting in different issues over time. Paper VII presents an alternative approach to this problem by instead applying a nanostructure coating that is designed to interact with the blood to a much lesser degree, as demonstrated by CT-angiography and the measurement of multiple biomarkers.

Mikael Sandell, misande@kth.se
Division of Micro and Nanosystems
School of Electrical Engineering and Computer Science
KTH Royal Institute of Technology, SE 100 44 Stockholm, Sweden

Sammanfattning

Med ett snitt i ett blodkärl tillgängliggörs hela kärlsystemet. Genom kontrastinjektion och röntgenvisualisering kan man kartlägga och navigera kärlträdet med hjälp av manuell manipulation av tunna rör och trådar. Användandet av kärlträdet som interna vägar kallas i dagligt tal för den endovaskulära tekniken. Med denna teknik kan man leverera implantat och mediciner, extrahera problematiska lesioner eller objekt, eller ta vävnadsprover. Jämfört med öppen kirurgi så är fördelen med denna teknik den minskade invasiviteten, där ett litet sår vid ingången till kärlträdet är det enda som återstår, i idealfallet. Vissa procedurer är dock fortfarande förknippade med vissa risker som kräver medicinering eller som försvårar vidare behandlingar. Utvecklingen av sekvenseringstekniker möjliggör förbättring och miniatyrisering av verktyg och på så sätt en minskning av dess invasivitet. Denna avhandling ämnar att minska riskerna som förknippas med endovaskulära procedurer och att kapitalisera på potentialen som sekvensering representerar. Genom tekniker för mikrofabrikation tillverkas verktyg som är mindre invasiva än nuvarande metoder eller som möjliggör en ny procedur.

Inledningsvis kommer endovaskulär hjärtbiopsi att beskrivas. Det första arbetet presenterar tillverkningen och *in vivo*-utvärderingen av ett nitinol-baserat kateterverktyg designat för att extrahera vävnad från myokardiet. Verktyget är tillverkat med laserbearbetning av nitinolrör och trådar, med hjälp av en pikosekundlaser. Verktyget är avsevärt mindre än de som används kliniskt idag. Proverna som tas utvärderas och jämförs med prover som tas med konventionella verktyg genom RNA-Sekvensering, där konceptets genomförbarhet bevisas. Det andra arbetet fördjupar utvärderingen av verktygets funktionalitet genom att utvärdera det i en sjukdomsmodell, specifikt en modell av hjärtinfarkt. Vävnad som påverkas av infarkten och omkringliggande, frisk vävnad extraheras med verktyget och dess genuttryck jämförs. Denna jämförelse avslöjar en genetisk diskrepans mellan sjuk och frisk vävnad, vilket verifierar potentialen med att använda RNA-sekvensering för diagnostik. Det tredje arbetet utvärderar säkerhetsaspekterna hos det nya verktyget genom en direkt jämförelse med det konventionella verktyget. Studien visar på en klar fördel i att använda det nya verktyget med avseende på incidensen av komplikationer under proceduren.

Det fjärde arbetet presenterar tillverkningen och *in vivo*-utvärderingen av ytterligare ett nitinol-baserat kateterverktyg designat för att provtagning av endotelceller. Verktyget tillverkas med hjälp av tvåfotonpolymerisering, där sub-mm borststrukturer tillverkas och monteras på nitinoltråd. För närvarande finns inga verktyg i kliniskt bruk som klarar att selektivt extrahera endotelceller. Det nya verktyget presenterar en lösning för att selektivt interagera med det innersta lagret av blodkärlet och motsvarar ett viktigt steg mot provtagning av endotelceller för diagnostiska syften och för forskning.

Det femte och sjätte arbetet presenterar två aspekter av ett tredje nitinol-baserat kateterverktyg designat för att ta prover från mjuka organ i kroppen. Verktyget tillverkas med laserbearbetning, slipning och tvåfotonpolymerisering. Arbetena är separerade i *in vivo*-utvärderingen och den tekniska lösningen. De tekniska aspekterna av verktyget utvärderas vad gäller kraftgenerering hos miniatyriserade kateter-system och de problem som uppstår med mekanisk skalning. Dessa problem löses genom att tillsätta pistonger längs tråden och applicera ett tryck för att öka kraftgenereringen. Provtagningsmekanismen liknar den som presenteras i det fjärde arbetet, där liknande sub-mm borststrukturer tillsatts på en tråd. *In vivo*-utvärdering av verktyget visar på framgångsrik provtagning från lever och njure, i storleksordningen 10-100 celler per prov.

Det sjunde arbetet presenterar *in vivo*- och *in vitro*-utvärderingen av en nanostruktur-beläggning på nitinol-baserade stentar. Patienter med ett stent-implantat ordineras en extensiv medicinering för att kontra effekterna som implantatet har på blodet och omkringliggande vävnad. Nya stentplattformar utvecklas löpande för att kontra dessa effekter, exempelvis genom beläggningen av ett polymerlager som innehåller medicin, genom resorberbara implantat och många andra sätt. Dessa implantat har ett transient beteende som resulterar i olika problem på längre sikt. Det sjunde arbetet presenterar en alternativ lösning till dessa problem genom att applicera en nanostruktur-beläggning som är designat att interagera med blodet till en mindre grad. Detta demonstreras med CT-angiografi och mätningen av flertalet blodmarkörer.

Mikael Sandell, misande@kth.se
Division of Micro and Nanosystems
School of Electrical Engineering and Computer Science
KTH Royal Institute of Technology, SE 100 44 Stockholm, Sweden

Contents

List of publications

This thesis is based on the following papers published in *peer-reviewed international journals* and manuscripts:

I. "Myocardial micro-biopsy procedure for molecular characterization with increased precision and reduced trauma", R. Grankvist*, A. Chireh*, **M. Sandell,** A. K. Mukarram, N. Jaff, I. Berggren, H. Persson, C. Linde, F. Arnberg, J. Lundberg, M. Ugander, G. La Manno, S. Jonsson, C. O. Daub & S. Holmin, *Scientific Reports,* 10, 8029, 2020.

II. "Micro-biopsy for detection of gene expression changes in ischemic swine myocardium: A pilot study", A. Chireh*, R. Grankvist*, **M. Sandell**, A. K. Mukarram, F. Arnberg, J. Lundberg, C. O. Daub, and S. Holmin. *PLOS ONE,* 16(4): e0250582. 2021.

III. "Safety evaluation of high-risk myocardial micro-biopsy in a swine model," A. Chireh, **M. Sandell**, R. Grankvist, V. Lövljung, J. Al-Saadi, F. Arnberg, J. Lundberg, M. Settergren, and S. Holmin, *Heart and Vessels,* 37, 697–704, 2022.

IV. "Endovascular Device for Endothelial Cell Sampling," **M. Sandell,** A. Chireh, A. Spyrou, R. Grankvist, J. Al-Saadi, S. Jonsson, W. van der Wijngaart, G. Stemme, S. Holmin, and N. Roxhed, *Advanced NanoBiomed Research*, 2: 2200023, 2022.

V. "Sampling through a transvascular working channel," **M. Sandell**, A. Chireh, A. Spyrou, J. Al-Saadi, S. Jonsson, W. van der Wijngaart, G. Stemme, N. Roxhed, and S. Holmin, manuscript

VI. "Hydraulic micropistons enable high force operations through miniaturized catheters," **M. Sandell**, S. Jonsson, W. van der Wijngaart, G. Stemme, S. Holmin and N. Roxhed, submitted manuscript, June 2023

VII. "A novel noble metal stent coating reduces in vitro platelet activation and acute in vivo thrombosis formation: a blinded study," **M. Sandell**, A. Ericsson, J. Al-Saadi, B. Södervall, E. Södergren, S. Grass, J. Sanchez, and S. Holmin, submitted manuscript, March 2023

The contribution of the author to each publication, major (X ≥ 80%) (• • •), substantial (80% ≥ X ≥ 33%) (• •), minor (X ≤ 33%) (•):

	Design	Fabrication	Experiments	Analysis	Writing
I.	• •	• • •	• • •	• •	•
II.	•	• • •	• •	•	•
III.	• •	• • •	• • •	• •	•
IV.	• • •	• • •	• • •	• • •	• • •
V.	• • •	• • •	• • •	• • •	• • •
VI.	• • •	• • •	• • •	• • •	• • •
VII.	• •	•	• • •	• •	• • •

This work has also been presented at the following *peer-reviewed international conferences* (not included as paper prints)

VIII. "An ultraminiaturized MEMS microbiopsy tool for trans blood vessel wall biopsies," **M. Sandell**, R. Grankvist, S. Jonsson, W. van der Wijngaart, G. Stemme, S. Holmin, and N. Roxhed, in *Proceedings of 33rd International Conference on Micro Electro Mechanical Systems (MEMS 2020),* IEEE, Vancouver, BC, Canada, pp. 10-12

IX. "3D printed micrograters for sampling of the blood vessel wall," **M.Sandell**, S. Jonsson, W. van der Wijngaart, G. Stemme, S. Holmin, and N. Roxhed, in *Proceedings of 34th International Conference on Micro Electro Mechanical Systems (MEMS 2021),* IEEE, Gainesville, FL, USA, pp. 548-550

Other *peer-reviewed papers* with contributions by the author not included in the thesis:

X. "Transcriptomic analysis of the harvested endothelial cells in a swine model of mechanical thrombectomy," N. Jaff, R. Grankvist, L. Muhl, A. Chireh, **M. Sandell**, S. Jonsson, F. Arnberg, U. Eriksson, and S. Holmin, *Neuroradiology*, 60, 759–768, 2018

List of abbreviations

2PP – Two-photon polymerization
BMS – Bare metal stent
BRS – Bio-resorbable stent
CT – Computed tomography
DAPT – Dual antiplatelet therapy
DAPI – 4',6-Diamidino-2-Phenylindole
DES – Drug-eluting stent
EC – Endothelial cell
EMB – Endomyocardial biopsy
HAZ – Heat-affected zone
ID – Inner diameter
ISR – In-stent restenosis
LAD – Left anterior descending artery
MEMS – Micro Electro Mechanical Systems
MI – Myocardial infarction
OD – Outer diameter
PCA – Principal component analysis
PTFE – Polytetrafluoroethylene
RNA – Ribonucleic acid
RNA-Seq – RNA Sequencing
SEM – Scanning electron microscope
SMC – Smooth muscle cell
SOI – Silicon on insulator
ST – Stent thrombosis
WBC – White blood cell

Introduction

This section introduces a brief overview of the field of endovascular devices, which is the overarching theme for this thesis work, both in terms of the clinical and engineering aspects. The scope of the thesis and the objectives for each journal publication are detailed in the later sections, as well as the overall thesis structure.

Endovascular devices

Endovascular devices are medical devices inserted into the body through a blood vessel, typically for diagnosing or treating a medical condition. These devices are visible under fluoroscopy and can be manually navigated through the vasculature. Examples of endovascular devices include angioplasty balloons designed to widen narrowed or blocked blood vessels, stents, metal mesh implants that maintain vessel patency after placement, and forceps, designed to extract a tissue sample from within the heart or other lesions. Endovascular interventions are commonly referred to as minimally invasive since they only require a small bodily incision. The devices used, however, can still exert unnecessarily invasive actions on the body, such as scarring at the site of tissue sampling and clot formation. The aspect of invasiveness is the unifying theme in the individual publications in this thesis, each attempting to reduce it. Another key development that is utilized in this thesis is the advent of molecular analyses, such as RNA-Seq, enabling the study of gene expressions and other aspects of minute quantities of cellular material, even as low as one cell. This is leveraged here by utilizing micro and nanofabrication technologies to create novel, miniaturized catheters to extract samples dedicated to these analysis modalities.

Catheter-based operations can be expressed in simple terms as operating tubes or wires within a larger set of tubes, which are ultimately navigated in an organic set of tubes, the vessel structure. The interaction between these tubes relies on having a good match between mechanical stiffness and low surface friction to enable good pushability while maintaining a low enough stiffness to avoid being invasive toward the vasculature. When attempting to miniaturize these systems to reduce invasiveness, one needs to keep the laws of mechanical scaling in mind, as the bending stiffness of a tube or wire scale with the radius to the power of 4. Drastically reducing the dimensions of a catheter will require innovative ways of achieving effects that would otherwise easily be done manually. In addition to that, there are devices, usually attached to the distal end of the catheter, that cannot simply be made smaller due to the same laws of mechanical scaling. The devices will not function if pushed beyond a certain size.

The clinical and engineering aspects presented here are explored in this thesis work, attempting to overcome the issues of enabling small-scale tissue sampling with RNA-Seq and reducing overall invasiveness through the use of state-of-the-art technologies for microfabrication.

Scope

The research covers the areas of heart, liver, kidney, and endothelial cell biopsies, either attempting to replace and improve upon existing devices or establishing entirely new methods of achieving tissue sampling. Additional focus is garnered toward reducing the invasiveness of devices used for endovascular implantation. This project builds on existing technologies for heart biopsy, super-selective tissue access, and stents. This work extends these technologies with novel functionality through the application of micro and nanofabrication technologies. Various technologies, such as laser micromachining, two-photon polymerization, and MEMS technology, are utilized

to create small devices and surface features to create the desired effect. The scope of this work has been to provide a preclinical evaluation of these techniques, with a focus on the functionality and safety of the devices. We have performed our work with translation in mind, but clinical translation has been beyond the scope of this project.

Thesis objectives

The common objective for all the projects in this thesis is to attempt to reduce catheter-related invasiveness in endovascular procedures. A significant part of the thesis objectives was to utilize the advances in molecular analyses of tissue samples through the realization that large-scale tissue samples might no longer be needed. Through the use of micro and nanofabrication technologies, this thesis presents a number of new types of devices for selective and miniaturized tissue sampling. Part of the thesis objective is also oriented towards the invasiveness of endovascular implants, presenting a way to reduce the foreign body response using an immobilized nanostructure coating of noble metals.

The specific objectives of this thesis were to:

1. Establish less invasive methods of obtaining tissue samples through the endovascular route. We demonstrate several nitinol-based catheter devices for a variety of applications. Through laser micromachining, a device is produced that features a new mechanism for obtaining endomyocardial tissue samples. The device is substantially smaller than the conventional device and provides several benefits in terms of flexibility and safety (*Paper I*). Through 3D-printing techniques, a device was produced for the sampling of endothelial cells (*Paper IV*) in small peripheral blood vessels. Additionally, a device is produced for soft tissue sampling from hard-to-reach areas (*Paper V*). The last device contains a new solution for deploying extremely thin wires (*Paper VI*).

2. Validate the new device in terms of the quality of the produced samples. We demonstrate the capability of producing high-quality sequencing data from the produced samples (*Papers I, II, &* IV). Furthermore, analysis of endomyocardial tissue samples enables the detection of pathological changes in an endovascular infarct model, further highlighting the quality of the samples produced (*Paper II*).

3. Verify the safety profile of the devices used for sampling. A head-to-head comparison of the device for taking endomyocardial biopsies with the conventional device proves that the incidence of major complications with the smaller device is significantly reduced (*Paper III*). The endothelial cell sampling device's safety aspects are briefly investigated regarding thrombo-embolic complications (*Paper IV*).

4. Reduce protein adhesion and thrombosis formation on endovascular implants. By applying a nanostructure on stent implants, we demonstrate the possibility of reducing the thrombo-inflammatory reaction and thrombosis formation *in vivo* (*Paper VII*).

Thesis structure

Chapter 1 provides a deeper background to the field of endovascular techniques, providing a historical perspective as well as the landscape of applications and developments relevant to this thesis. Chapter 2 outlines the technological framework relevant to the thesis work, describing the materials utilized, the major fabrication technologies that are used as well as what specific challenges exist when miniaturizing catheter technology. The overarching structure of chapters 3-6 is to focus each chapter on an individual project conducted in this thesis. It will be presented in a coherent chronological frame, where the problem is first introduced, followed by what novelty we are providing, how we reached that stage, what the main methods and results are, and short conclusions. Furthermore, chapters 3-6 are categorized based on four levels of operational invasiveness. The first level is described in Chapter 3, which entails stent implantation, where there is no focus on tissue sampling but rather on the effect of foreign materials in the vascular system. The second level, described in Chapter 4, entails sampling the blood vessel's innermost layer: the endothelial cells. In the third level, described in Chapter 5, we go beyond the primary layer and sample muscle tissue, in casu endomyocardial tissue. Lastly, the fourth level, chapter 6, entails sampling of tissue beyond the vascular structure. Chapter 7 concludes the thesis work and the future potential of the devices and solutions presented.

Chapter 1 – The endovascular technique

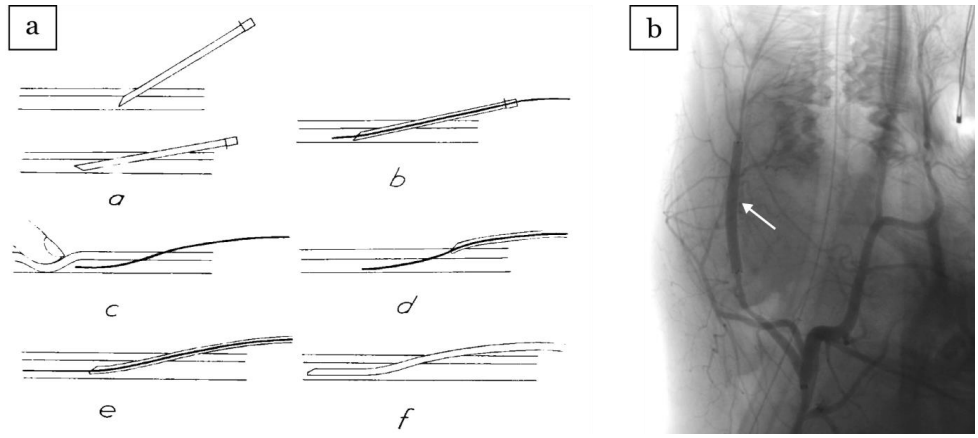

Figure 1. (a) The development of the Seldinger technique for safe access into the vasculature made endovascular surgery safe and accessible. (b) An example of an endovascular surgery that is common today, stent implantation, showing an angiogram of a stent implanted into the lingual artery (arrow) in a porcine model. Image (a) adapted from Informa UK Limited with permission from the publisher[1].

The endovascular technique involves entering the vascular system through a small incision and employing flexible catheters and guidewires to navigate the vasculature, Figure 1, under X-ray guidance[2]. Historically, this type of surgery was made widely available by the development of the Seldinger technique, providing a safe and reliable way of accessing the vasculature[1]. Several studies have since developed the field. A few among them are the advent of the percutaneous transluminal angioplasty for restoring blood flow in blocked vessels in 1964, the development of digital subtraction angiography, drastically increasing the usefulness and resolution of angiography images in 1980, and the first stent prototype to prevent vessel restenosis in 1987[3-5]. The state of the art of endovascular techniques has expanded a great deal since then. It can now be used to treat various vascular conditions such as stroke or aneurysms, perform implantations to restore or divert blood flow, or take biopsies[6-8]. Naturally, the main advantage of endovascular surgery is reduced invasiveness compared to traditional surgery, requiring only a small entry point, e.g., in the groin, forearm, or neck, depending on the procedure. These benefits entail reduced hospital stays and faster patient recovery compared to open surgeries[9]. Invasiveness relates to many more aspects of endovascular intervention other than size; it generally concerns how the procedure affects the patient. It could be related to the position of the required catheter access point and size, the scarring the utilized device performs, how the body reacts to a foreign object, and many more.

1.1 The biopsy procedure and its' use in diagnostics

A biopsy is a procedure where a tissue sample is extracted from a lesion or an area identified as problematic, and these samples can be extracted in several ways. For many conditions, biopsies form the gold standard for establishing a diagnosis[10-14]. Naturally, the reason for extracting tissue samples is to obtain prognostic information

on disease status. Diagnoses are typically established by tissue sampling followed by histologic or cytological evaluation of samples in combination with patient symptoms. There exists a multitude of ways to obtain tissue samples from the body, using devices such as core and aspiration needles and various kinds of forceps[15-17]. These can be used either percutaneously, guided by ultrasound or other imaging modalities, or with endo- or bronchoscopes through the airways or gastrointestinal tract. Percutaneous biopsies can reach a majority of lesions within the body and are advantageous when sampling from regions that are not in close proximity to sensitive regions and when there are no contraindications to the procedure, such as an increased risk of bleeding[18-20]. However, the endovascular technique carries less risk for areas that are otherwise hard to reach, such as the heart or pancreas. The indications for utilizing the endovascular route are endomyocardial biopsy, transjugular liver biopsy, and sampling of intravascular masses[8, 10, 18, 21]. Other applications, such as sampling of the endothelium, have been attempted, although this is not yet used in the clinical routine[22, 23].

The primary focus of this thesis is on devices for taking biopsies through the endovascular route, represented by papers I-V. Indications and details about the targeted procedures will be further described in the chapters relating to the separate studies. The reason for pursuing this research from the clinical perspective will be outlined here by going through the developments in the diagnostic procedure and what opportunities these represent.

1.1.1 Histopathology

Conventional diagnostics is performed with histopathology, the microscopic examination of fixated tissue. This process requires a macroscopic tissue sample with an intact cellular structure that is possible to slice into thin sections and stain with specific chemicals or antibodies to visualize the cellular morphology. This technique dates as far back as 1838 and has, since then, seen extensive development in fixation, sectioning, and image analysis techniques[24]. The basics of the method are, however, still very much the same; a tissue sample is sectioned and fixated, usually in formalin, and stained on glass slides with hematoxylin and eosin to highlight the interesting features of the tissue. This way, pathologic changes in the tissue morphology can be identified, and a diagnosis can potentially be established. At the moment, the size of extracted tissue samples is inherently limited by histopathology in that it is impossible to analyze tissue morphology if the samples are too small. The cellular structure is not maintained if they are, and microscopic evaluation will be inconclusive.

1.1.2 Cytopathology

Another important tool in clinical practice that complements histopathology is cytopathology, the examination of the morphology on a cellular level. Similarly, this technique was conceived in the 19th century and started seeing widespread use in the latter half of the 20th century[25]. The assessment of cellular features consists of fixating and staining a cell suspension or cell smear with a dye and examining the cells in a microscope. Abnormalities in the cell population can then be identified, aiding in establishing a diagnosis[26].

Cytopathology, in contrast to histopathology, is an improvement in the invasive aspect of sampling, usually performed on cell suspensions acquired from fine needle aspirations or brush samples. However, the acquired information depends heavily on the selected staining procedure. For established diagnostic procedures, this is not an

issue; however, if the mechanism of action and genes responsible for a disease are of interest, molecular analyses could provide more information.

1.1.3 Molecular analyses

The advent of next-generation sequencing can potentially mitigate the problems connected to histo- and cytopathology and alter the way diagnoses are established by enabling analysis of the genes expressed within the tissue[27]. Several methods are available to quantify levels of genetic expression, such as the quantitative polymerase chain reaction (qPCR) and microarray panels[28, 29]. Both methods target existing genetic markers, meaning unknown or altered genes cannot be detected[30]. The key enabler of the research conducted here, however, lies in the field of RNA sequencing (RNA-Seq), revealing the entire transcriptome of the samples, both known and unknown.

The importance of being able to study what genes are expressed in the tissue sample as it is being extracted cannot be understated. Gene expression analysis can potentially reveal hitherto unknown disease mechanisms, for instance, in cancer and cardiovascular disease, which can greatly expand our knowledge of how these diseases are initiated and progress[31]. Furthermore, these techniques are not limited by the tissue sample size; single-cell RNA-seq can provide the entire genetic sequence being transcribed within individual cells[32]. An additional benefit of molecular techniques is the potential for discovering pathologic genetic expressions earlier. Establishing a diagnosis using histopathology naturally requires that certain changes in the tissue morphology have already happened. Therefore, it follows that the changes to the genetic sequences responsible for producing proteins that change the tissue morphology occurred earlier. For example, it has been shown that the transcriptomic analysis of heart samples can detect tissue rejection earlier than when using histopathologic analysis[33]. With the rapidly decreasing costs of sequencing and other comparable techniques, the techniques for establishing diagnoses are bound to change in the foreseeable future. Especially in oncology, sequencing is already used to establish diagnoses and tailor treatments and drug regimens to the individual patient[31].

1.1.4 Implications for device design and use

The devices utilized for extracting tissue samples are currently constructed with histopathology in mind, producing larger-scale samples that can be reliably sectioned. In conjunction with the onset of RNA-Seq in diagnostic procedures, the overall trend identified here is the reduced need for large tissue samples. In essence, it would be enough with a few cells from the area of interest. Apart from the mentioned benefits of RNA-Seq, this presents a number of additional opportunities, such as increasing selectivity when sampling and reducing the procedure's invasiveness. Being able to miniaturize these devices could provide multiple patient benefits, such as enabling different and smaller access points and less damage at the sampling site. Lastly, if the devices are small enough, they could open up the possibility of sampling from areas that are not sampled through the endovascular route today, such as the brain.

The method with which to miniaturize these devices cannot be to simply reduce the size of existing designs. The mechanical functions of existing devices will quickly deteriorate if one attempts simple miniaturization. New and innovative ways of achieving the same effect, but on a much smaller scale, is necessary. The mechanical aspects of reducing device sizes will be further elaborated in Chapter 2. When attempting to extract samples in the size range of a few hundred cells, other questions arise, such as whether the acquired samples are representative. It could be enough to

be a few millimeters off when sampling, resulting in a cellular sample that consists of the wrong cell types. This limitation greatly depends on the pathology in question but can potentially be addressed with improvements in imaging techniques, such as the photon counting computed tomography (CT) scanner[34], promising a drastic increase in the acquired image resolution. Coupling this data with angiography during endovascular navigation would greatly improve the guidance to the target lesion.

1.2 Endovascular implantation

The other minor part of this thesis focuses on integrating a noble metal coating on stent implants. The historical development of the stent implant will be briefly elaborated here to explain the reasoning for the research conducted in paper VII. Chapter 3 will present a more thorough description of these developments, further highlighting the role that the novel coating could play in the clinical landscape.

Before the development of the stent, a common intervention for patients with vascular blockage was balloon angioplasty[35]. This procedure involves inflating the area of vessel blockage with a catheter-mounted balloon, and a common, potentially lethal complication is abrupt vessel closure[5]. The development of the stent solved this by keeping the vessel open after the intervention. The initial stent was a pure metal mesh, usually referred to as the bare metal stent (BMS). These suffered other issues such as the formation of thrombi on the implant surface, referred to as stent thrombosis (ST), neointimal hyperplasia or neoatherosclerosis, leading to a gradual decrease in lumen size, referred to as in-stent restenosis (ISR). The issue of ST has been addressed by prescribing dual antiplatelet therapy (DAPT) to patients undergoing stent implantation. However, this treatment puts the patient at an increased risk of bleeding, which is problematic if further surgical interventions are needed[36].

Furthermore, the stent platform has been developed beyond the BMS by coating it with drugs in certain polymeric substrates, called drug-eluting stents (DES). DES shows superior performance in ISR and is now the standard of care; however, the drug-carrying platform can lead to other problems, such as delayed healing, inflammatory reactions, and delayed endothelialization in the longer term[37, 38]. This problem is partially related to the fact that the drug capacity is depleted after a certain time and that the platform carrying the drug deteriorates over time. DES implants' drug and carrying platform combination is continuously evaluated to target the associated issues. Another technology initially perceived to change the area of endovascular stent implantation is the bioresorbable stent (BRS), intended to be adsorbed by the body over time[39]. These stents are either polymer or metal based, with advantages and drawbacks for each. Polymeric substrates are usually based on poly-lactic acid, which decomposes into safe by-products in the body. However, they require larger strut dimensions to maintain the necessary radial support, which is detrimental to vascular healing[40]. Metal-based BRS do not suffer reduced mechanical strength, but on the other hand, the by-products, when decomposed, are not yet fully understood and differ depending on the metal used[41].

1.2.1 Blood-surface interactions

Regardless of the implant type, they all suffer from the associated foreign body response. Implantation into the vasculature immediately initiates rapid protein adsorption on the surface that induces the activation of coagulation, platelets, and leucocytes, possibly causing adverse effects such as acute thromboembolic complications, bleeding, or pro-inflammatory reactions. This interaction has been extensively studied and involves a multitude of biological mechanisms[42-44]. Initially,

the proteins carried within the bloodstream are rapidly adsorbed to the foreign surface, which causes circulating platelets and leukocytes to adhere to the surface and activates factor XII. This leads to a cascade of subsequent reactions that ultimately lead to the generation of fibrin and a thrombus on the surface. This problem is an area of intense research and attempted solutions[45-48]. The ideal stent would behave as an extension of the vessel itself, essentially not inducing a foreign body response. To date, no one size fits all solution exists that responds to the entire spectrum of the coagulation cascade, necessitating further research.

1.2.2 Modulating protein adhesion

The initially adsorbed proteins heavily influence the coagulation cascade[43]. A method suggested and evaluated in paper VII for achieving improved blood compatibility on stent implants is to apply a coating that modulates the initial stages of protein adhesion. The coating presented in paper VII is a noble metal nanostructure that is believed to interfere with the adsorbed proteins and prevent conformational changes. The coating has proven antibacterial properties when used on other medical devices[49-52]. The study on the coating is further elaborated on in Chapter 3.

Chapter 2 – The technological framework

2.1 Nitinol as a material

The core material relevant to all the manuscripts in this thesis is the alloy nitinol. This alloy is mainly known for its superelastic or shape memory properties and has a precisely controlled ratio between Ni and Ti and a few trace elements, such as Co. The essence of these properties lies in a diffusionless phase transformation between an austenitic and martensitic phase, either dictated by mechanical stress or a temperature change[53]. The temperatures at which the austenite or martensite phase is stable are heavily reliant on changes in the Ni-content and alloying trace elements, where minute changes can change the transition temperature to anywhere between -20 and 100°C[54]. The temperature at which each phase is stable determines if the shape memory or superelastic effect is observed at room temperature.

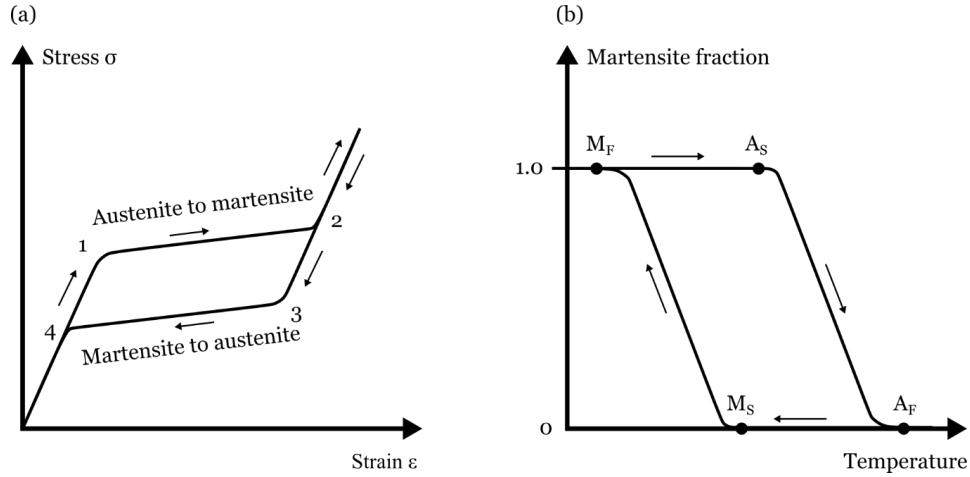

Figure 2. Stress-strain behavior for superelastic nitinol (a). Once the elastic limit of the austenite has been reached (1), the phase change to martensite is initiated. Once the phase change is complete (2), the elastic region for full martensite is reached. Unloading the material leads to an elastic recovery up to a certain point (3), where a phase change back to austenite is initiated. A full elastic recovery is subsequently achieved once the transformation is complete (4). The shape memory effect is instead governed by changes in temperature (b). $M_{S\text{-}F}$ and $A_{S\text{-}F}$ correspond to the start and finish of the respective phase change. An increase in temperature initiates the transition from martensite to austenite, which is fully reversible upon temperature decrease. Arrows are intended to highlight the transformation direction.

The superelastic behavior is observed if austenite is thermally stable from temperatures below room temperature and up. If mechanical stress is applied at room temperature, the austenite will gradually change phase to martensite, referred to as strain-induced martensite. Once the stress is released, the material will revert back to austenite since this is the thermally stable phase. This leads to hysteresis in the stress-strain curve, Figure 2, where this phase change leads to recoverable strains of up to 9%[55]. This can be compared to conventional, stainless steel alloys exhibiting recoverable elastic strains of less than 1%[56]. The shape memory effect is instead observed when the martensite phase is the parent phase at room temperature and

where austenite is stable at higher temperatures. Deforming the material permanently and heating it above the phase transition temperature will cause the lattice to revert back to the austenitic phase, recovering the deformation.

In the field of endovascular intervention, it is important to balance stiffness, good pushability, and flexibility, providing effortless navigation through tortuous vascular paths. The superelastic property of nitinol has proven valuable in endovascular devices in that it provides this balance. For example, navigating a nitinol wire would be possible in most complex vasculatures, whereas a stainless steel wire of the same size would be plastically deformed quickly upon moderate bending, complicating further navigation. In reality, however, devices are composed of a plethora of different material combinations to achieve a large variety of behaviors, such as varying the stiffness along different parts of a catheter[57]. Although nitinol is a wonderful material, in some cases, it is not feasible to fabricate or machine to the degree required in some of the projects of this thesis, necessitating the use of microfabrication technologies.

2.2 Microfabrication techniques

Several fabrication modalities appurtenant to microfabrication are utilized in this thesis; the set of fabrication techniques related to micro-electromechanical systems (MEMS), laser micromachining, 3D printing using two-photon polymerization (2PP), as well as grinding. One or more of these techniques are utilized in some way in each individual work to produce a device.

2.2.1 MEMS

The MEMS technology was initially utilized to explore the possibility of creating small silicon-based biopsy devices. The idea was to take advantage of the high strength of silicon as a material and the versatility of the MEMS technique to achieve very sharp features. However, the silicon-based devices did not achieve much success, as will be elucidated in Chapter 6.

The MEMS technology is derived from the technology used to create integrated circuits. It is a set of techniques that enable the structuring of silicon wafers to produce 3-dimensional, microscopic systems that either have an electrical or mechanical function, often both[58]. MEMS devices are widely utilized in everyday appliances; examples are the accelerometer or gyroscope in the smartphone, pressure sensors for blood, or gas sensors [59]. Typically, a MEMS procedure is initiated by spin coating a photoresist layer on top of the wafer, followed by ultraviolet lithography through a mask with a predefined pattern. Depending on the photoresist type, the exposed areas can either be made more soluble or hardened by UV exposure, facilitating selective removal of the exposed or unexposed regions of the polymer. Once the polymer removal is completed, an etching step is applied to transfer the polymer pattern to the wafer.

There are various ways of etching silicon wafers, but the most widely used method is deep reactive ion etching[60]. This manufacturing sequence can be combined with several steps, e.g., additional patterning of the backside of the wafer, bonding of additional wafers, coating metal layers, etc. Combining these steps allows one to create vastly complex systems with intricate functions. The process conducted in one of the works here is on silicon-on-insulator (SOI) wafers, Figure 3. SOI wafers feature three layers, two silicon layers, the device and handle layer, with a silicon oxide layer in between.

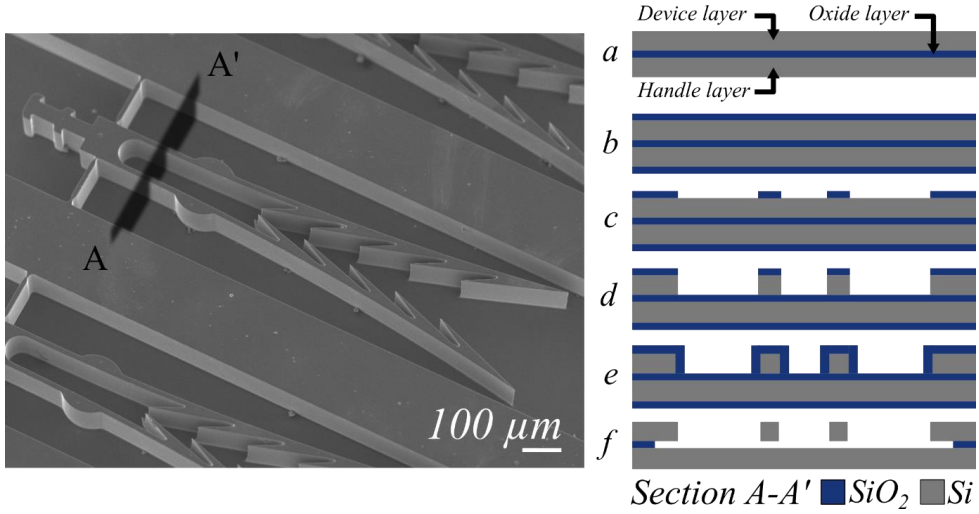

Figure 3. Overview of the MEMS procedure utilized in paper VIII. A scanning electron microscope (SEM) image (left) of a device freely suspended on a wafer and the corresponding fabrication process (right) of cross-section A-A'. A silicon wafer with a device, handle, and oxide layer (a) is oxidized (b), patterned (c), and etched (d). Subsequent oxidation (e) and HF release (f) lead to a device suspended above the handle layer.

After patterning and structuring the device layer, one can selectively etch the oxide layer to produce free-standing silicon structures. The free-standing structures were then subjected to oxidative sharpening, used to create extremely sharp silicon features to lower the penetration force of the intended device[61].

2.2.2 Laser micromachining

Laser micromachining has been used extensively throughout papers I-III, where large parts of the presented device are fabricated with this technique. This technique is used moderately in the other works but has been heavily utilized in the exploratory phase of device prototyping.

Laser micromachining of any material requires ultra-short laser pulses to reduce thermal effects on the laser-material interface that induce a heat-affected zone (HAZ), local melting, or micro cracks. The time scale of the laser pulse in contact with the material is of great importance in achieving adequate feature quality and size, where longer pulses generally transfer more heat, leading to more thermal effects. Early studies of femtosecond laser systems in the 1980s and 90s revealed the versatility of these short pulses through the demonstration of clean ablation of polymethylmethacrylate with a minor HAZ as well as the ability to ablate even transparent materials due to very high peak intensities[62, 63].

The fundamentals of laser processing vary greatly at different time scales, Figure 4. At the nanosecond range, thermal effects dominate, leading to a larger HAZ, a lower aspect ratio of the ablated area, and a larger degree of recast material[64]. At the femtosecond range, the energy exchange dynamics at the interface change, leading to a drastically reduced HAZ compared to using longer laser pulses.

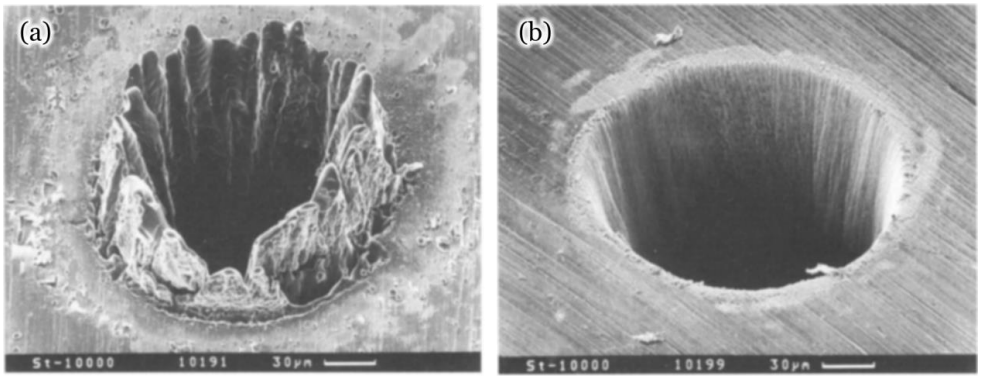

Figure 4. Scanning electron microscopy (SEM) images of a 100 µm steel foil ablated with a 3.3 ns laser pulse (a) and a 200 fs laser pulse (b) illustrate the difference in local heating and the resulting feature quality. Image adapted from Springer Nature with permission from the publisher[63].

In the picosecond range, the characteristics of material ablation is a mixture of the two, depending on the laser parameters and material properties. The reason for this change as a function of pulse duration is how fast the energy is deposited into the material. In theory, at the femtosecond range, the energy from the laser pulse is only transferred to the electrons in the material. The energy transfer to the electrons is too fast for the electrons to transfer heat to the surrounding lattice. Provided the energy is high enough, this increases the average energy of the electrons above the energy that binds the electron to its parent atom and the energy required for the electron to escape. This energy increase causes the electrons to escape from the solid, creating a strong electrostatic field that pulls ions out of the solid, referred to as electrostatic ablation. In the meantime, the lattice remains cold due to the fast energy deposition[63, 65]. This process produces no HAZ and more precise features than a longer pulse duration would. However, other ablation modes might induce heat transfer to the surrounding lattice if the energy is lower than this threshold.

In practice, these other modes of ablation do occur since high repetition rates of the laser pulses are used. Even at high scanning speeds, multiple pulses hit the same area, where the laser pulses interact to couple the heat transfer[65]. The applications in this work utilize both picosecond and femtosecond laser systems to create devices with sharp or otherwise precise features.

2.2.3 Two-photon polymerization

Another method of achieving extremely precise features is through the use of 2PP. 2PP is essentially a method of creating 3D micro/nanostructures using non-linear absorption of photons in various types of resin or hydrogels[66, 67]. This method has been extensively utilized in papers IV-VI in device manufacturing, both during the exploratory phase and in the final device as published.

The essence of the method is similar to regular photolithography 3D printing, with the key difference in how the material and laser light interact. In 2PP, high-intensity femtosecond laser pulses crosslink a photosensitive polymer resin. The process requires that two photons hit the photoinitiator simultaneously, which sets the

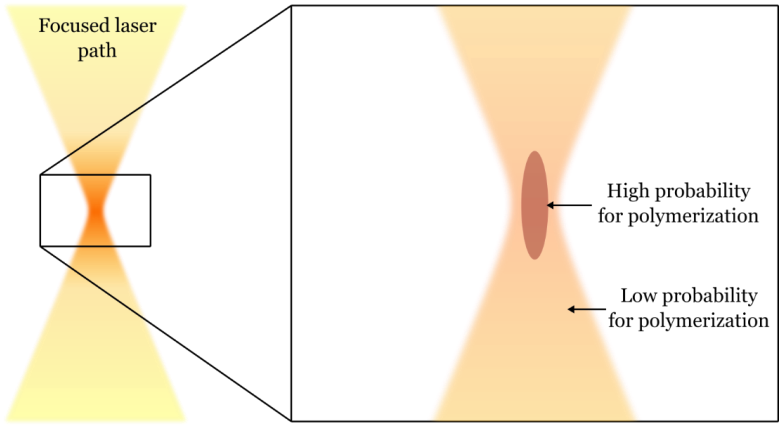

Figure 5. Schematic of the non-linear polymerization process. Along the majority of the focused laser path, no polymerization will occur. However, in the focal point's center, the photon density is high enough to initiate polymerization.

stage for the non-linearity of the polymerization process, Figure 5. The photon density in the focused laser pulses is generally too low to initiate polymerization, except at the focal point. It comes down to the probability of two incident photons hitting the same molecule simultaneously, and the probability outside of the focal point is essentially zero. Furthermore, the polymerization is further localized to the center of the focal point, leading to "printed" voxels even smaller than the width of the laser[68]. Depending on the optics of the laser system, this enables 3D printing of sub-micron voxels.

2.3 Downscaling of catheter systems

When considering the miniaturization of catheters, as described here, an intuitive thought is to make conventional devices smaller through an already established process. When attempting this, however, one will eventually conclude that it will not be possible to maintain the required mechanical properties of these devices due to the effects of mechanical scaling, specifically how it relates to bending and the area moment of inertia. This property is calculated according to eq. 1.

$$I_x = \int y^2 dA \qquad (1)$$

Where I_x denotes the area moment of inertia for bending along the x-axis, and y denotes the distance of an element dA from the x-axis. The area moment of inertia is a measure of a body's resistance to bending. This property typically scales with L^4, where L is the characteristic length of the system. It then follows that a 50% reduction in the dimensions of a body leads to a 16-fold reduction in bending stiffness. This scaling phenomenon directly relates to the properties of a potential device sitting at the distal tip, where one cannot miniaturize existing devices that often feature moving parts and subassemblies. They will break too easily, and achieving the same function on a smaller scale requires a new method.

Another property that is influenced by this scaling is the pushability of catheters. Advancing catheters through the vessel system and through other catheters inside the same is a complex process, and a lot of the properties of the catheter material come into play. One study has investigated how this interplay of physical properties affects

the pushability of different angiographic catheters[69]. Among the properties investigated are the bending stiffness, surface contact angle, surface free energy, and friction properties. In the study, it is recognized that bending stiffness is one of the major influences in being able to navigate through complex curvatures. The reason for this is the complex curvatures that are seen when navigating with endovascular devices. In a completely straight section of tubing, naturally, the stiffest catheter is easiest to push through. However, when curvatures are in place, an increased bending stiffness causes the catheter to press against the inner wall of the outer, larger tube, which increases the friction acting against the forward motion. This phenomenon is known as the capstan effect, which causes an exponential increase in friction depending on the degrees of curvature that a system of tubing is subjected to.

2.3.1 Capstan effect

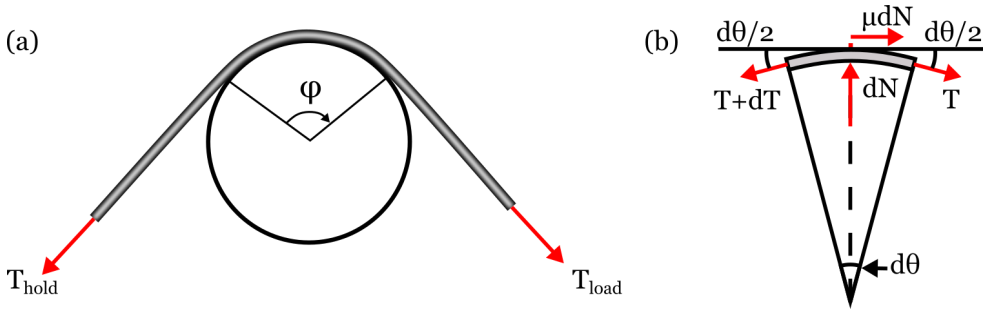

Figure 6. The capstan effect influences the loading force on a wire being pulled around a circular object in relation to the holding force (a). The Capstan equation describes an exponential relation between the two forces and is derived from an integration of the local force equilibrium (b).

The capstan equation describes the relation of pulling and holding force on a wire wrapped around a circular object, Figure 6. This effect, although not specifically describing them, can be directly extrapolated to catheter systems. The exact relation between these forces is shown in eq. 2.

$$T_{load} = T_{hold} e^{\mu\varphi} \qquad (2)$$

Where T_{load} and T_{hold} represent the holding and pulling force, μ represents the coefficient of friction, and φ represents the angle of rotation[70]. As one reaches high rotation angles, as in catheter-based systems, even small changes in the friction coefficient can drastically change the required pulling force. In the case of pulling, it is, as described previously, beneficial with a low bending stiffness to decrease the surface contact that the internal wire creates with the tubing. However, when reversing the motion, i.e., attempting to push a wire into a complex system of bends, it is instead important to be able to transfer the force into the rest of the system, commonly referred to as catheter pushability[69]. The capstan effect effectively inhibits the force transfer when attempting to push a wire into a tortuous path of tubing. It is especially troublesome when attempting to push a wire through extremely small catheters. In some cases of extreme tortuosity, applying manual force at the proximal end of very small catheter systems is not sufficient to achieve the necessary transfer of motion.

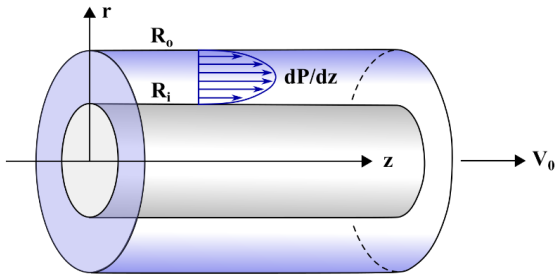

Figure 7. Flow through an annular section creates a shear force acting on the internal cylinder.

Furthermore, this issue is exacerbated when attempting to overcome an obstacle at the distal end of the catheter, e.g., when extracting a biopsy through such a catheter.

An effective way of overcoming the issue of tortuosity, i.e., the Capstan effect, is to apply liquid pressure into the catheter system, which is a method occasionally used when treating aneurysms with coils[71]. The flow generated in such an annular section, Figure 7, generates a shear force that drives the internal wire forward. This force depends on the catheter dimensions and the applied pressure according to eq. 3.

$$F_s = \frac{\pi P L}{2}\left(2R_i^2 + \frac{R_i^2 - R_0^2}{ln\frac{R_0}{R_i}}\right) \qquad (3)$$

In larger systems of tubing, such as power cables, there are solutions in place to overcome complex tortuous paths when installing cables into tubes. The solution encompasses placing structures along the wire in combination with applying pressure. The applied pressure pushes on the structures that are placed along the wire, effectively producing a differential pressure before and after these structures, pushing the entire cable forward[72].

Each biopsy-related project is to some extent affected by issues with miniaturization, especially in papers IV-VI, where solutions had to be developed to solve the Capstan effect and how to produce devices less sensitive to fracture.

Chapter 3 – Stent implantation

This chapter goes into greater detail on the endovascular implantation of stents. The chapter outlines the development of the stent historically and what challenges are associated with the implantation. The main results from paper VII, as well as additional data from trials that were not documented in the manuscript, will be presented and discussed in terms of how they are envisioned to change the clinical landscape.

3.1 The stent platform

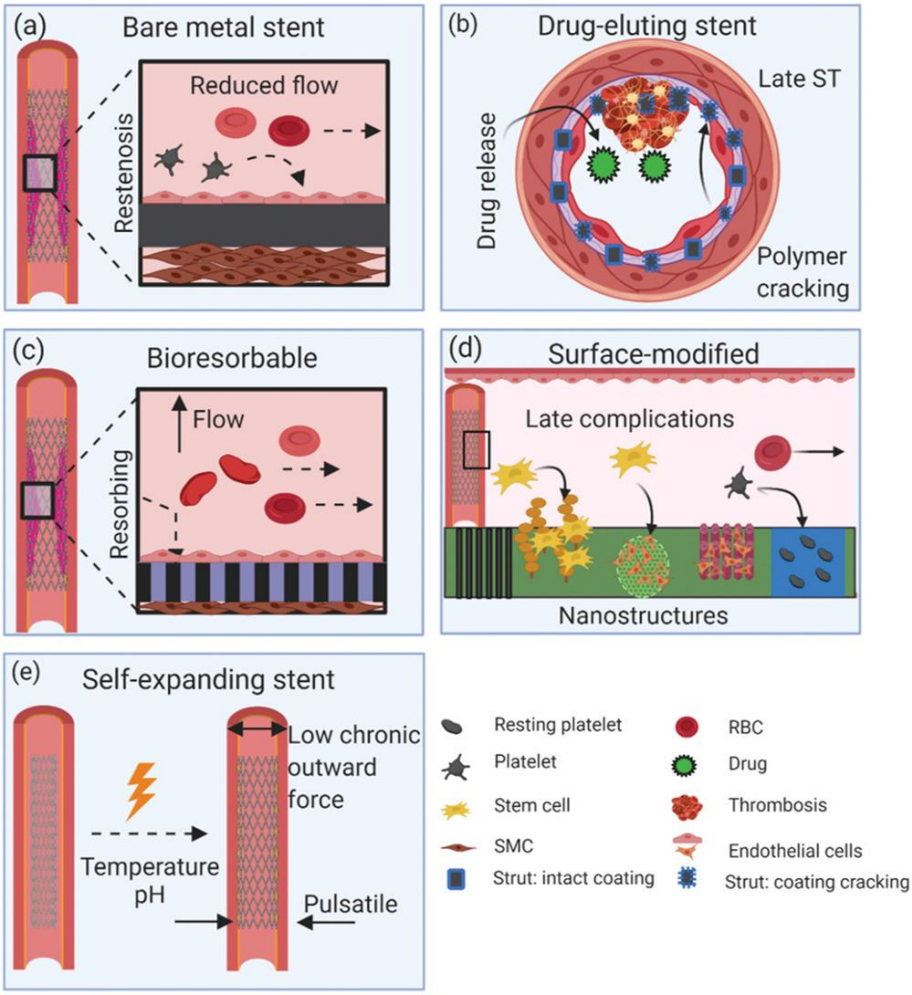

Figure 8. Overview of the current landscape of stent types available. Image reproduced from John Wiley and Sons[73] with permission from the publisher.

The development of the stent platform stems from the interventions of Charles Dotter, pioneering the procedure referred to as percutaneous transluminal angioplasty, where one recanalizes a blocked vessel with a catheter[3], which led to the subsequent development of balloon angioplasty, where one forcefully expands a vessel closure with

a catheter-mounted balloon. The balloon angioplasty procedure, however, suffered from a number of issues, such as vessel closure and elastic recoil[38]. Most of these issues were solved by the advent of the first stent prototype, the BMS[74]. The BMS is a tubular metallic mesh used to treat a variety of vascular conditions, mostly atherosclerotic lesions, that affect the flow through the vessel. By implanting it across a lesion, one relies on the expansive properties of the stent to regain vessel patency.

3.2 Challenges with stent implantation

Currently, there are a multitude of stent varieties available, Figure 8, that is being constantly updated, each attempting to target specific bodily responses, either through elution of drugs, by being absorbed by the body over time, or with a surface coating that prevents or promotes certain interactions with the body[73, 75, 76]. This subchapter will outline how the various stent types have been developed over time and the advantages and disadvantages of each stent type.

A common factor for all stent implants is the foreign body response, causing a variety of reactions on the surface of the implant. The moment the surface comes into contact with the blood stream, proteins in the blood are rapidly adsorbed onto the surface[43]. In the early stages, the adhesion of proteins is dominated by the Vroman effect, where higher molecular weight proteins, such as fibrinogen, are initially adsorbed and sequentially replaced by proteins with lower molecular weight[42]. Over longer time periods, the dynamics of protein adhesion are poorly understood in terms of its composition, which naturally varies a great deal across different surfaces. Regardless of the surface, however, the adhered proteins significantly influence the following cascade of reactions. The adsorbed proteins undergo a conformational change that induces the adhesion and activation of platelets and leucocytes, eventually resulting in a thrombus formation on the surface as well as local inflammation. To address this reaction, patients are administered a dual antiplatelet medication to reduce platelet activity and the risk of thrombosis[77]. This medication represents issues for patients that need additional interventions after the implantation in that they prevent clotting and can complicate surgical procedures.

Aside from this medication, a lot of focus is garnered toward improving the stent platform itself. The following subchapters briefly introduce some of the major stent platforms and the appurtenant issues. Paper VII demonstrates a coating on stents that significantly reduces the initially adsorbed proteins, which then influences thrombus formation. The main results and the difference compared to existing technologies will also be discussed.

3.2.1 Bare-metal stents

The BMS was, naturally, the earliest stent type and was first implanted in a peripheral artery in 1985[76]. The BMS was vastly superior to balloon angioplasty in terms of restoring vessel patency and overall clinical outcomes[38]. BMS exist in a variety of metallic alloys, including stainless steel, cobalt-chromium alloys, and nitinol, and are typically manufactured through laser cutting intricate patterns in a metallic tube, followed by surface processing, such as electropolishing, to create a smooth surface[78]. Although superior to previous methods, the BMS, by virtue of being a foreign material in the blood stream, suffers from later-stage issues during implantation, such as neointimal hyperplasia, ST, and ISR. A variety of mesh design alterations have been attempted in an attempt to mitigate these issues[78]. The design and geometry of the stent does influence the clotting response. For instance, the strut size is important, where smaller struts lead to fewer complications[73]. Attempting to

describe all possible variations is beyond the scope of this thesis, however. Apart from design alterations in terms of the stent geometry, other efforts were made to provide a polymer coating with embedded medication to address the neointimal hyperplasia, the DES.

3.2.2 Drug-eluting stents

The development of the DES can generally be divided into the first and second generation[38, 79]. The first generation utilized durable polymers with embedded drugs released slowly into the vessel surrounding the stent. The polymers were wide in variety but generally had poor biocompatibility.[37] The drugs were designed to prevent cellular proliferation and, as an effect of this, neointimal hyperplasia and restenosis. The first generation, however, suffered other later-stage issues, such as delayed vascular healing, which is attributed to the poor biocompatibility of the polymer used and the released drug's inhibitory effects [37]. The second generation of DES changed the drug-carrying polymer to more biocompatible ones, further reducing complication rates[37, 38, 46]. The use of the second generation of DES, although showing drastic improvements in clinical outcomes, still suffers from late-stage ST. These issues are believed to be partly caused by differences in mechanical properties between the metal and polymer coating, causing delamination or cracking of the polymer. These concerns have, in parallel, led to the development of the BRS where hope is put in eliminating late stage complications since the BRS is slowly absorbed over time.

3.2.3 Bioresorbable stents

The concept of acquiring a bioresorbable implant can be achieved either through the use of specific metal alloys or polymer substrates. The metal-based platforms have the advantage of providing a mechanically stiffer material, making a thinner strut dimension possible. However, they instead suffer the drawback of toxic metallic by-products during degradation[73]. The polymer-based platforms provide a material that generally degrades into safe by-products but instead suffers from weaker mechanical strength, necessitating larger struts that interfere with the vessel wall and patency to a larger degree[39]. Furthermore, the absorption times of the BRS in question vary greatly, between 6-42 months[40]. The absorption time is one of the transient aspects that is important to consider, especially since the stent should ideally provide vessel support to allow proper tissue healing before the resorption starts[73].

3.2.4 Surface-modified stents

Another approach to achieve a more biocompatible stent implant is to modify the surface through various means to target certain cellular interactions or modulate the protein adhesion. The examples are many, such as functionalized surfaces by laser ablation, CD34 antibody coating to enhance binding of circulating endothelial cells, silicon carbide coatings, and others[38, 73, 76]. Modifications to the surface can be generally divided into bio-active, attempting to target a cellular response, or passive, intending to passivate the surface and reduce the foreign-body response[80]. Several aspects are considered for passive surface modification, such as wettability, surface charge, and electronic properties. These properties are intended to achieve a selective interaction with certain proteins dissolved in the blood or to achieve a passive adhesion, leading to little or no conformational changes in the adsorbed proteins. For instance, superhydrophobic coatings are intended to prevent contact with the liquid that contains the dissolved proteins. In contrast, super hydrophilic surfaces aim to absorb water selectively, achieving a stealth effect and reducing protein adhesion[80]. Various types of modifications exist, each with its own advantage and disadvantage[47,

[48, 80, 81]. There is, however, no real consensus on a universal surface modification; the requirements naturally depend on the specific application.

3.3 Noble metal nanostructure coating

This subchapter presents a surface coating consisting of a mixture of noble metals arranged in a stochastic nanostructure. This surface coating has been clinically tested in other applications, mainly for urinary catheters, indicating a reduction in infection rates[50-52, 82]. It has been tested for blood-contacting devices previously, although the focus of those studies has been oriented toward the inflammatory response rather than thrombotic complications[83]. It has been shown in an *ex vivo* study, however, that the coating does exhibit increased blood compatibility[49]. The mechanism of action behind the coating is multifaceted, being both antimicrobial and hemocompatible. The antimicrobial aspect of the coating is attributed to induced microcurrents on the surface, Figure 9, whereas the blood compatibility is believed to be an effect of how the surface interacts with protein deposition and certain elements of the contact activation pathway.

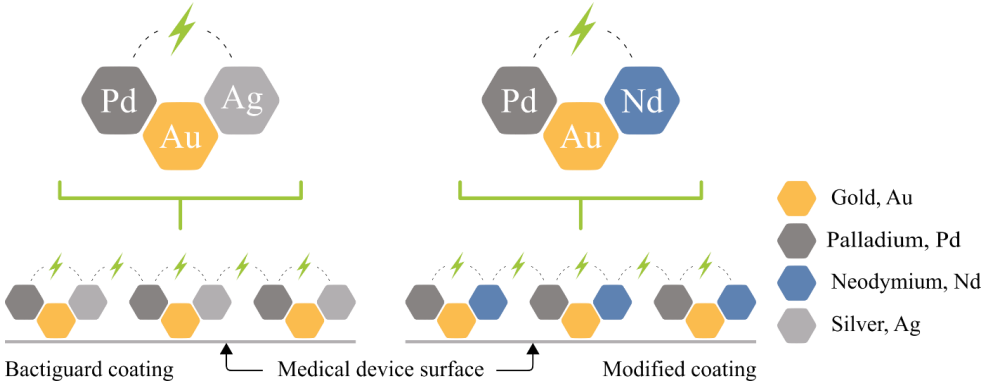

Figure 9. Conceptual sketch of the coating and the induction of microcurrents on the surface of the coating.

The latter mechanism is currently unknown but is speculated to be because adhered proteins are not activated, prohibiting further binding by platelets and subsequent reactions. The aim of paper VII was to evaluate the coating *in vivo* as applied to a stent substrate. The whole body of work consisted of an evaluation of the commercially applied coating, referred to as the Bactiguard coating, and a modified version of the same coating, where the silver component is replaced with neodymium. Neodymium, along with other rare earth metals, has been shown to interact with the coagulation cascade by interacting with binding sites on certain proteins in the blood, such as factor Xa and thrombin[84].

3.3.1 Evaluation of the coating

The coating was evaluated as a parallel *in vivo* and *in vitro* analysis, Figure 10, in a porcine model. Uncoated and coated stents were implanted pairwise in two groups of 12 animals, each group investigating one of the coatings. The stent implantations (n = 24) were blinded to ensure a similar analysis methodology between the groups. The *in vivo* analysis consisted of a 3D CT angiography scan of the implant at the time of the implantation as well as after 1 and 2 hours.

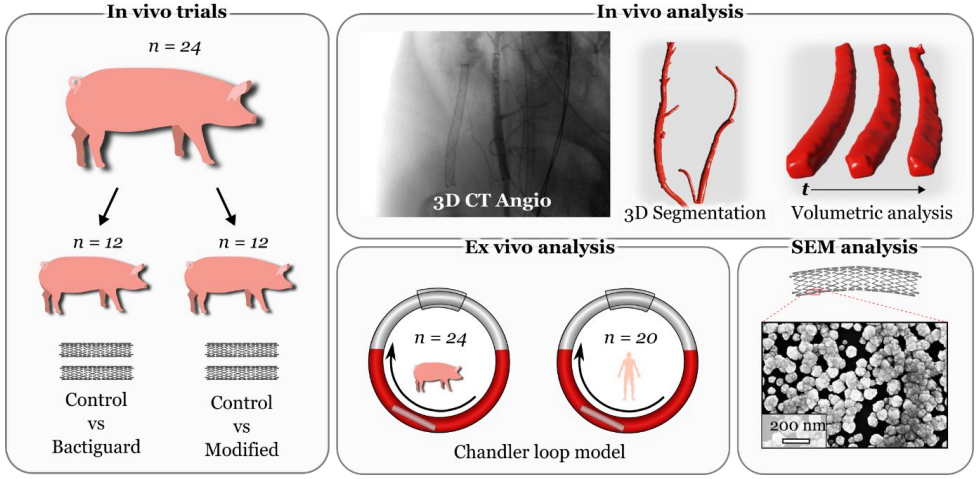

Figure 10. Study design of the stent implantation and chandler loop experiments. In vivo analysis in the form of 3D CT angiography scans was performed in parallel with in vitro analyses in chandler loop experiments. The stent coating was examined in an SEM prior to and after the implantations.

An open-source software, ITK-Snap, was used to extract the volumes from the CT data from the experiments. The volumetric analysis will reveal disruptions in the flow of contrast due to thrombotic complications associated with the implant surface. Volumes were acquired through a semi-automatic active contour segmentation based on voxel intensity thresholds set by the user and were initiated on closed curves also supplied by the user, mainly in the vicinity of the stent volume. The procedure is intended to highlight the difference in the flow between the different time points as well as between different implants. Efforts were made to standardize the segmentation procedure in terms of measuring the average voxel intensity of the vessel segments proximal to the stent and applying threshold values in the segmentation procedure in relation to this value. These methodologies, however, yielded sporadic segmented volumes that were either discontinuous or did not accurately represent what was seen in the original images. Instead, manual threshold values were applied to mimic what was observed in the 3D data.

The volumetric data was compared both in terms of the raw voxel count in the software and normalized based on the volume acquired at the time of the implantation. The normalization is performed to account for different vessel sizes between the left and right-hand sides of the animal, as well as between different animals. Exclusion criteria for analysis were selected as extensive unilateral vasospasm after implantation. The *in vitro* analysis consisted of experiments performed in Chandler loop experiments, where coated and uncoated nitinol tubes were compared separately. These experiments are performed in polyurethane tubes, with the nitinol tubes mounted inside, in which blood is circulated for a period of time. These experiments were performed in porcine (n = 24) and human blood (n = 20). Afterward, a number of blood markers relevant to the coagulation cascade is measured and compared between baseline, control, and coated materials as well as an empty loop, to account for the spontaneous activation of the experiment. Ultimately, the coating integrity is also compared before and after implantation in an SEM.

3.3.2 Blood marker analysis

The levels of thrombin-antithrombin complex (TAT), polymorphonuclear elastase (PMN), beta-thromboglobulin (β-TG), adenosine diphosphate (ADP), and thrombin receptor activating peptide (TRAP) were measured when the chandler loop experiments concluded. These markers were selected to highlight the activation of platelets and leucocytes as well as to reveal the total activation of the coagulation pathway. The activation in porcine and human blood as well as the difference between the coatings, were compared as well. Furthermore, the amount of protein deposited on the surface was evaluated optically after the chandler loop experiments, expressed as the percentage of the tube that was covered.

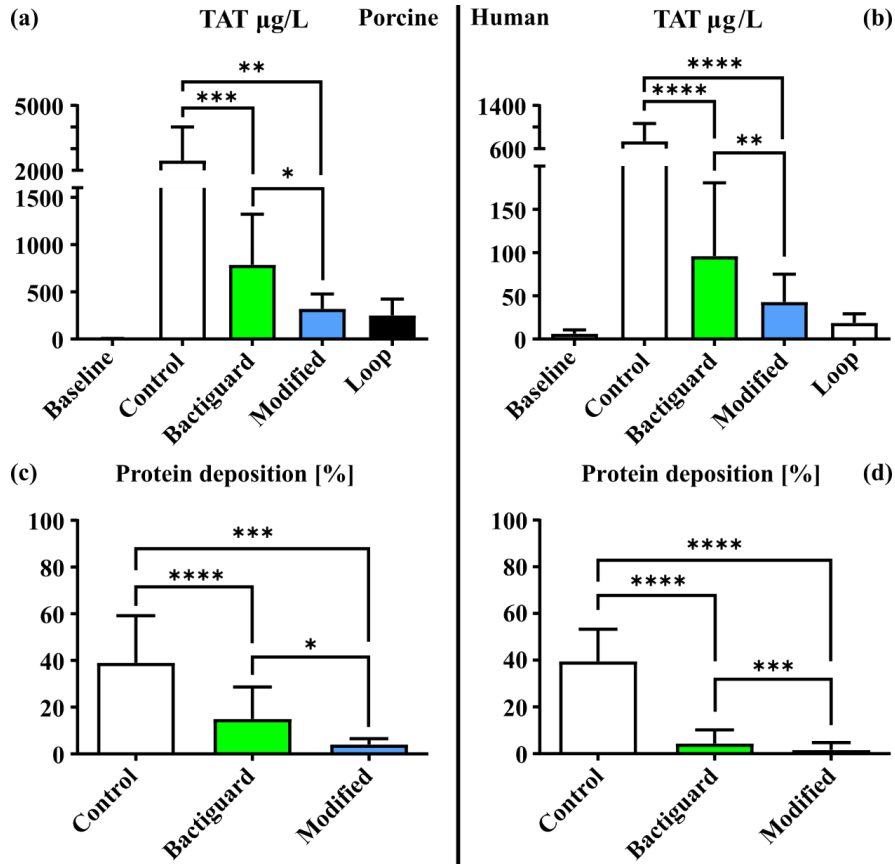

Figure 11. Results from the measurement of the TAT complex after the chandler loop experiments (a & b) as well as the optical measurement of protein deposits covering the tube surface after the experiments (c & d).

The main findings of the analysis of blood markers are in the activation of the TAT complex as well as protein deposition, Figure 11. There is a substantial decrease in the TAT activation for both coated materials, with a further significant decrease for the modified coating compared to the Bactiguard coating. The same results are observed

for the deposited proteins. Among the other blood markers, there were significant decreases for the modified coating in the β-TG in porcine blood and the PMN marker in both porcine and human blood. The other blood markers did not reveal any statistically significant difference.

3.3.3 In vivo thrombus formation

Six measurements, three from each group, were excluded from the analysis based on the exclusion criteria, yielding 9 data points in each group of stents. The measurements did not reveal any difference between the stents with the Bactiguard coating and controls, either for the raw or normalized volumes. When looking at raw volumes, there was no significant difference for the stents with the modified coating versus their respective controls. However, there is a significant improvement in favor of the modified coating for the normalized volumes, Figure 12.

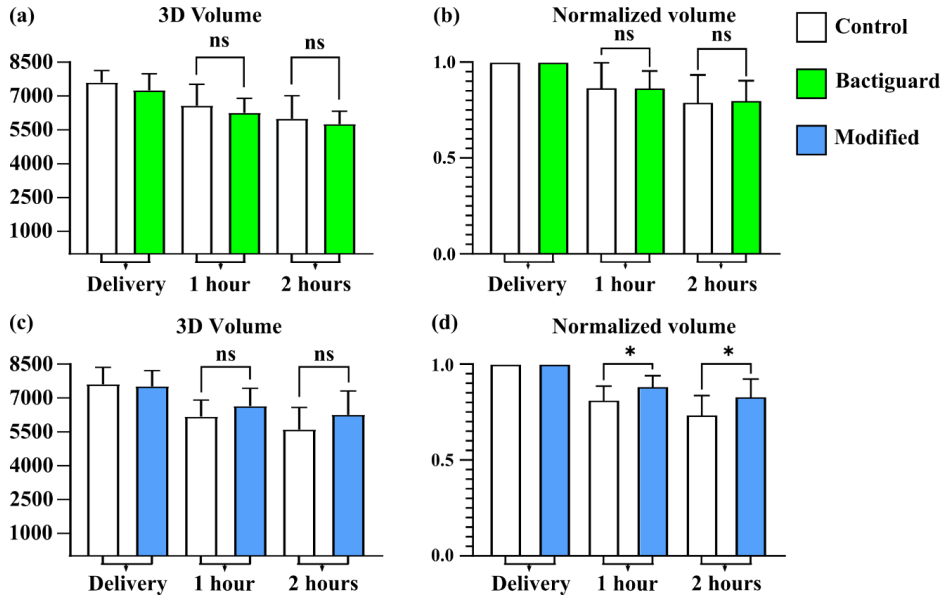

Figure 12. Results from the volumetric analysis. The analysis is presented both as the raw voxel counts as well as normalized based on the volume from the first time point. (a & b) Raw voxel and normalized volumes of the Bactiguard coated stents versus their respective controls, respectively. There was no significant difference in performance in this coating. (c & d) Raw voxel and normalized volumes of the stents with the modified coating versus their respective controls, respectively. There is no difference in the raw voxel volume, although a trend is visible. There is a significant difference in the normalized volumes in favor of the modified coating.

3.3.4 Coating integrity

The coating was examined before and after the implantation in an SEM to investigate adverse effects. The images did not reveal any damage or discontinuities to the coating. A thin build-up of a protein film was observed across the coatings, Figure 13.

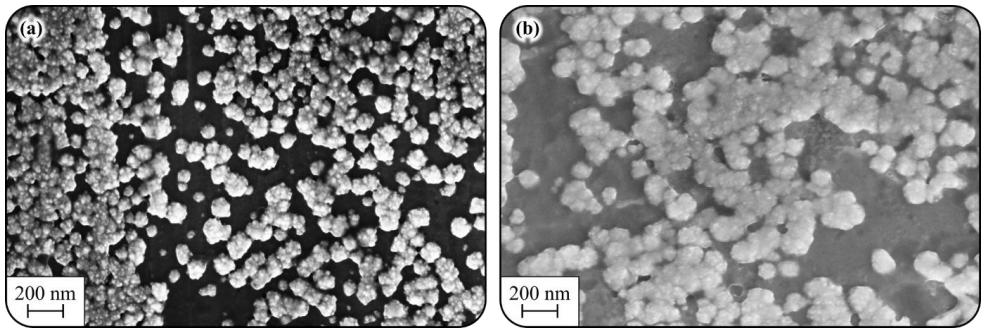

Figure 13. SEM examination before (a) and after implantation (b). There is no notable change in the coating structure, coverage, or integrity other than a thin protein film deposited on the surface.

3.4 Conclusions

The results indicate that the modified coating shows promise as an implant addition. Not only do we see significant improvements in Chandler loop experiments, indicating a reduction in the activation of the coagulation system, but we also reveal similar effects *in vivo*. The improvement in the acute phase of implantation has implications for potential alterations to the DAPT regimen in the acute phase, potentially reducing it in scope.

Chapter 4 – Endothelial cell sampling

This chapter dives deeper into the anatomy of the blood vessel, the challenges that are associated with sampling strategies attempted in literature, and the path that was followed to address these.

4.1 Overview of blood vessel anatomy

The blood vessel's size, shape, and function vary depending on its location and what organ it supplies blood to. Apart from the capillaries, all blood vessels generally consist of three layers: tunica externa, tunica media, and tunica intima, Figure 14.

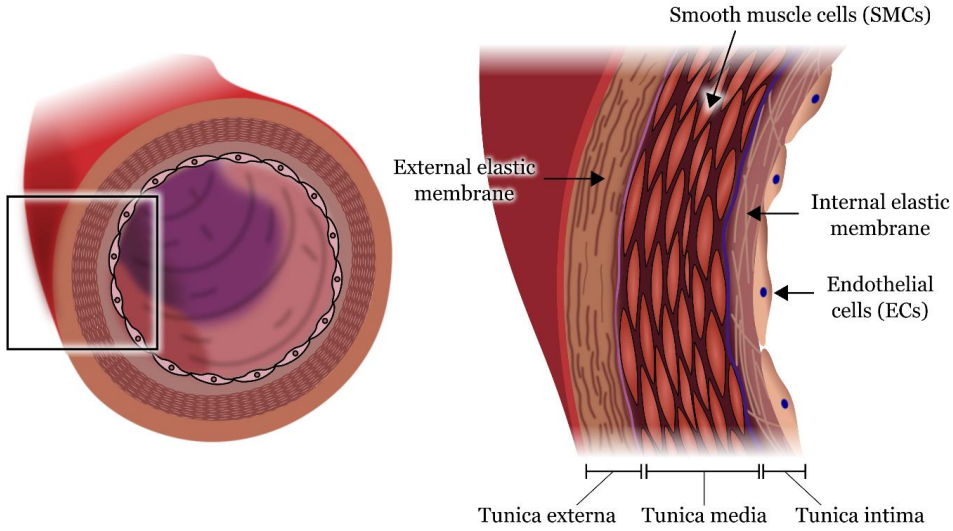

Figure 14. Anatomy of the blood vessel. Depending on vessel type, the thickness of the respective layers varies. The capillaries only consist of the endothelium.

The external layer acts as structural support, and the medial layer is composed of some elastic and muscular tissue and regulates the blood vessel diameter. The thickness of these two layers depends on the type of blood vessel, where, e.g., arteries have a thicker layer of elastic tissue to be able to handle the increased pressure. The innermost layer is what all blood vessels share, the endothelium[85]. The endothelium consists of a layer of connective tissue, the internal elastic membrane, and endothelial cells (ECs). These cells have several crucial functions, including, but not limited to, regulation of vascular tone and substance transport into and out of the vessel. As such, many conditions are initiated by changes in the function of these cells, such as atherosclerosis, coronary artery disease, edema, and many others[86]. Some studies further reveal that there are functional variations of ECs between organs and even within the same organ and that they are active in several neurodegenerative diseases[87, 88]. The ECs could harbor secrets about how these pathological changes are caused, and if they could be selectively harvested, one could illuminate the complex interactions responsible for these diseases.

4.2 Challenges with endothelial cell sampling

Dedicated sampling of the endothelium is not a procedure that is performed clinically. There has been substantial research on the function of the ECs and how their role varies at different sites of the body[87-89] and a number of attempts at extracting these cells through the endovascular route[22, 23, 90-98]. There are interesting studies garnered toward understanding how the cells differ in terms of genetic expression at various sites[87, 88]. These studies, however, rely either on extracting cells post-mortem or from surgically removed tissue. The studies attempting to extract the cells in vivo rely on methods that either extract a low number of cells or are contaminated by blood. Furthermore, they utilize endovascular devices without a dedicated sampling mechanism, relying on stochastic interaction with the endothelium.

Despite the shortcomings in the cellular extraction methods, there is significant interest in understanding how ECs behave, highlighting the need for a new, selective biopsy tool. Part of this thesis presents a device that selectively interacts with the endothelium for cell extraction without blood contamination.

4.3 Exploring different designs

The path to the design presented in Paper IV is paved with a variety of iterations. Initial designs were aimed at solving the lack of a dedicated sampling mechanism on endovascular devices. The intended procedure for sampling ECs was designed based on the mantra to "*detach, catch and contain*" the cells of interest. This mantra means that the device should only interact with the blood vessel wall, detach the ECs, make sure that these cells are caught inside or on the device, and are contained upon device extraction. Additionally, the blood vessel wall interaction would preferably be ensured by an actuation mechanism. The design considerations were also aided by what has been done previously. For example, it has been shown that with the application of external pressure and navigating a guidewire in superficial blood vessels, one can remove ECs[23], as was also verified by control experiments in Paper IV. This sampling fails on the basis of catching and containing the cells, relying on the fact that some cells will adhere to the surface and remain during the guidewire extraction.

4.3.1 Micrograter solution

Based on the above, we conceptualized a design that featured a 3D-printed rotational cutting mechanism[99]. This device consists of a 0.38 mm nitinol tube with an inner channel of 0.28 mm. At the distal end, 3D-printed structures and a gold marker are mounted, Figure 15. The 3D-printed structures are cylindrical and feature three cutting edges, similar to a grating structure; underneath those, internal channels lead to its center. These channels are aligned with laser-cut holes in the nitinol tube. Reciting the mantra of detach, catch, and contain, cellular detachment is achieved by cutting edges in the tangential direction, where the sampling is actuated by rotating the device. The catching and containing aspects are facilitated by leading the tissue that is detached into channels within the tube, and nothing interacts with this space while moving the device axially.

These devices were tested in a porcine model and navigated to peripheral kidney vessels. While the device successfully achieved a dedicated interaction with the blood vessel wall, this design was deemed too invasive. The cellular composition of the samples was not further investigated, but the resulting tissue samples are believed to be a mixture of the blood vessel wall and some surrounding tissue, creating unnecessary damage in the vasculature. Subsequently, the subsequent iterations were further reduced in size.

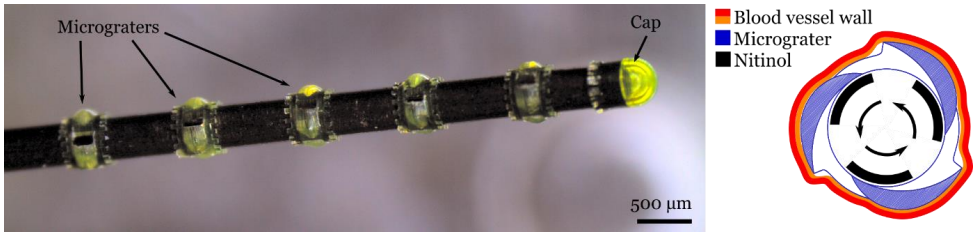

Figure 15. One of the earliest prototypes featured 3D-printed rotationally symmetric microgaters aligned with laser-cut holes in a 0.38 mm nitinol tube (left). A conceptual sketch of the intended vessel wall interaction (right). The figure contains elements reproduced from IEEE, with permission[99].

4.3.2 Miniaturized brush designs

The design aspects of the iterations following the micrograter were more considerate of the thickness and properties of the blood vessel wall. As the endothelium is no more than a few micrometers thick, and the ECs even less than 1 micron in thickness, one would potentially not need features much larger than this to achieve an interaction. Additionally, the tube used for the micrograter designs was replaced in favor of a smaller, more flexible wire. This was done in order to reduce the stiffness and the overall invasiveness of the procedure. The 3D prints were heavily modified, Figure 16, to be incorporated on the smaller wire, and the sampling mechanism was changed. Instead of relying on a cutting mechanism, a cylindrical structure with several radially protruding elements was conceived. Instead, the idea was to create a structure that only interacted with the blood vessel wall a certain distance (limited by protrusion depth), with a large surface area for cells to get trapped in.

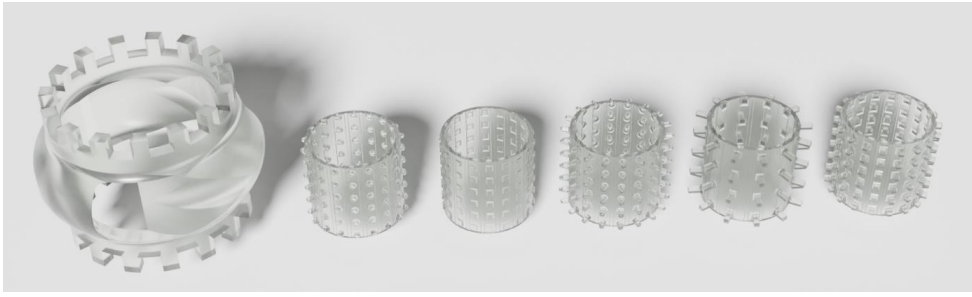

Figure 16. Rendering of the micrograter (far left) next to updated iterations.

These brushes were tested *ex vivo* on porcine hearts in the coronary vessels. Several different brush designs were considered, varying the protrusion shape, length, and density, and ultimately compared in terms of how many cells were captured, leading to the decision of the final device to be tested *in vivo*.

4.4 Evaluation of final design

The final device consists of the smaller 0.23 mm nitinol wire, 3D-printed brush elements, Figure 17, and a radiomarker placed 5 mm from the distal end. The final 3D-printed design features cubic protruding elements with a rounded base connecting it to its' cylindrical base. The wire and brush assembly is housed inside a polytetrafluoroethylene (PTFE) tube.

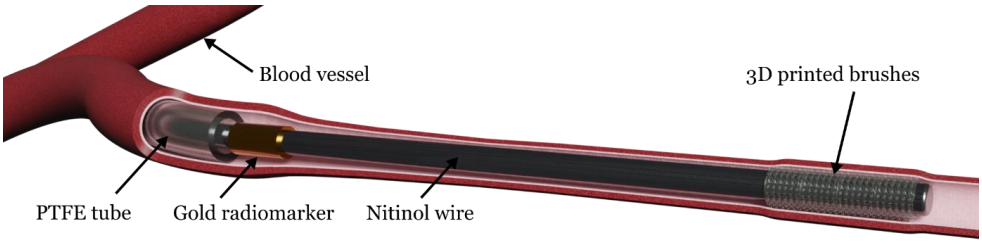

Figure 17. 3D rendering of the final design as its intended to be used inside a blood vessel. The figure contains elements reproduced from Wiley-VCH GmbH under Creative Commons License CC-BY 4.0[100].

Briefly, the sampling is achieved through three separate motions. The full assembly is initially navigated into a wedged position with the wire-brush assembly protected within the PTFE tube. The wire-brush assembly is navigated further at this stage until another wedged position has been reached. This sequence is important, as the first wedging prevents blood from flowing around the device, and the second wedge ensures selective blood vessel wall interaction. The wire-brush assembly is proximally rotated at the last wedge, engaging the brush structure with the blood vessel wall. Lastly, the wire-brush assembly is retracted within the PTFE tube, protecting the extracted sample within it. The device can then be extracted from the vasculature, and the sample can be analyzed.

4.4.1 Device manufacturing and assembly

The final device consists of a 0.23 mm nitinol wire over which 3D-printed microbrushes and a radiopaque gold marker are threaded. The 3D-printed prototypes were printed with a 2PP process, where the printing process for the final design was performed with a 25X objective, 1 µm layer thickness, and solid internal scaffold. The radiopaque marker is produced by coiling a rolled gold strip onto a separate section of the same wire used for the device and cutting off a 1mm section of the gold with a scalpel. The microbrushes are manually mounted on the wire and fixated onto the surface with cyanoacrylate glue. The inner lumen of the microbrushes contains grooves to increase the surface area in contact with the glue. One device consists of eight microbrushes, mounted in two sections of one mm each, with a one mm distance between the two sections, and a radiopaque marker placed five mm from the distal tip. The radiopaque marker enables visualization of the device during fluoroscopy and guides the user on the location of the distal tip. The PTFE tube housing the device has an outer diameter (OD) and an inner diameter (ID) of 483 and 330 µm, respectively.

4.4.2 Study design

The device was tested in a porcine model (n = 6) to evaluate the function and safety of the device, Figure 18. The number of devices tested (n = 81) was divided into liver (n = 41) and kidney (n = 40). The selection of organs was based on the ease of endovascular navigation to the target site and to be able to evaluate differences between two separate organs in terms of the quality of the sample. The device was compared to control samples of several categories: the full device navigated similarly but without rotation of the brush (n = 16), devices without brushes (n = 27) navigated the same way as well as blood samples (n = 3*)* and surgically extracted vascular tissue (n = 4).

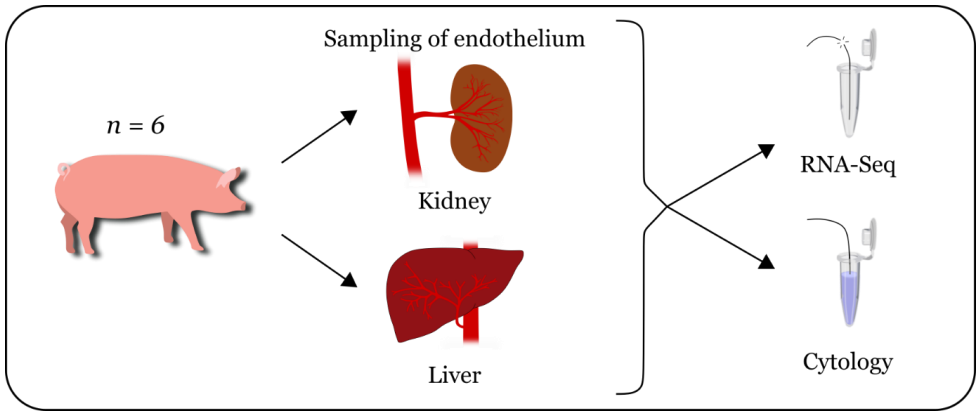

Figure 18. Study design of paper IV. The final design was evaluated in a series of experiments (n = 6) where samples were taken from peripheral vessels in the kidney and liver vasculature. The resulting samples were evaluated with RNA-Seq and cytology. Sampling was also performed with guidewires and control devices without brushes to be able to compare sampling efficacy.

The resulting samples were analyzed with cytology and RNA-Seq. The latter two control sample categories were used as a contrast in the sequencing analysis. Safety aspects of the device use were evaluated in terms of induced vascular hemorrhages and device integrity.

4.4.3 Performance

The devices were inspected visually after each sampling event to assess the presence of tissue. This assessment indicated that tissue was wrapped around the entire brush in 80% (52/65) of the procedures, and 12% (8/65) contained a lesser amount of tissue. In 8%, we found no sample. Samples taken from control devices (regular devices without rotation, wires without brushes, or conventional guidewires) did not yield visible samples.

4.4.4 Cytological staining

The cytological staining was performed on a subset of samples (n = 52), both directly on the device (n = 10) to maintain everything that was sampled, and on dissociated samples (n = 42). Antibody staining of the samples still on the device was performed to visualize the EC-specific marker CD31 and the cell nuclei with 4',6-Diamidino-2-Phenylindole (DAPI). The dissociated samples added stains for the white blood cell (WBC) specific marker CD45 and α-SMA to stain for smooth muscle cells (SMC). The staining, Figure 19, illustrates an overlap between EC-specific markers and cell nuclei and a noted absence of cells from other sources. However, the brush structures auto fluoresces, making analysis of these samples more difficult. These were then supplemented with an analysis of dissociated samples. The staining of these samples confirmed the absence of SMCs and WBCs. The captured cells were counted across the stained samples, revealing an average cell count of 349 for the device and 0.5 for the control device.

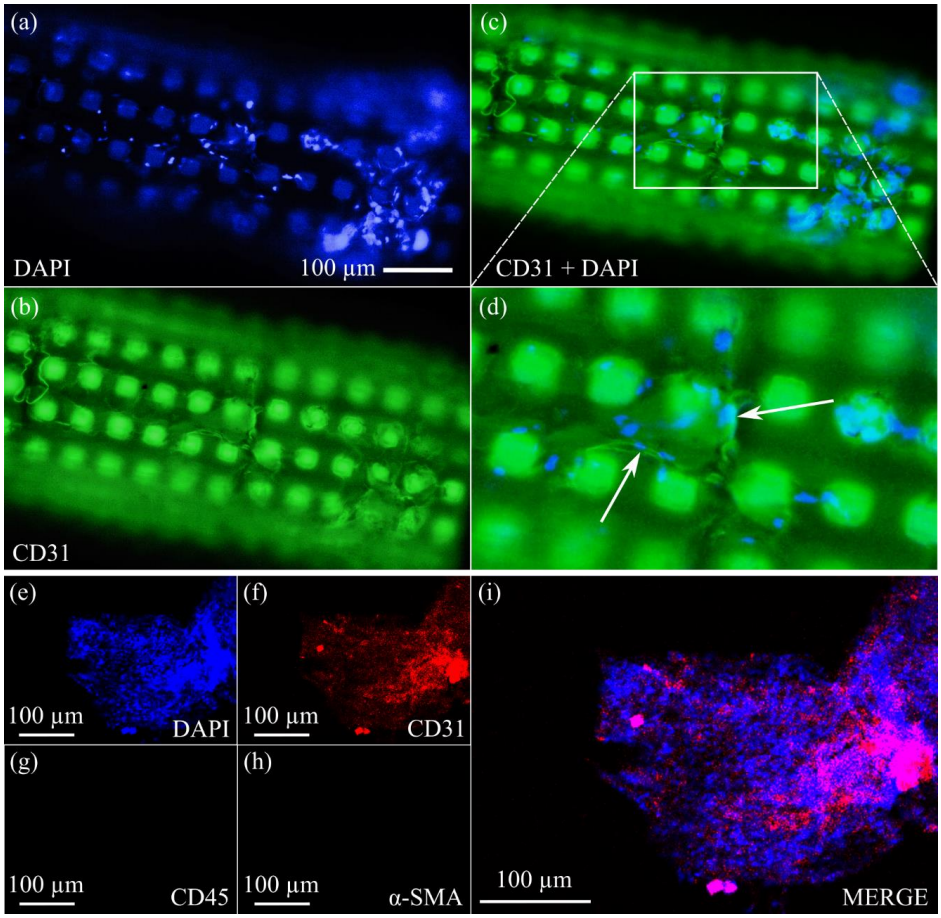

Figure 19. Cytological staining of the device (a-d) revealed an overlap of the DAPI and CD31 stain. Supplementary staining of dissociated samples (e-i) reveals the same and the absence of WBCs and SMCs. The figure contains elements reproduced from Wiley-VCH GmbH[100] under Creative Commons License CC-BY 4.0.

4.4.5 RNA-Seq

A subset of the samples collected with the device (n = 10), control devices (n = 4), and blood and vascular control samples were analyzed with RNA-Seq. A custom protocol to extract the RNA developed for the heart biopsy samples in Paper I was used. The resulting RNA samples were prepared for sequencing through the generation of a cDNA library and sequenced using 2 x 50 base pair reads on the Illumina NovaSeq platform. Three samples (one blood sample and two samples from the device) were excluded due to a low number of reads uniquely mapped to the genome. The control devices were included in the sequencing, but their data was removed from the analysis once the cell count was established.

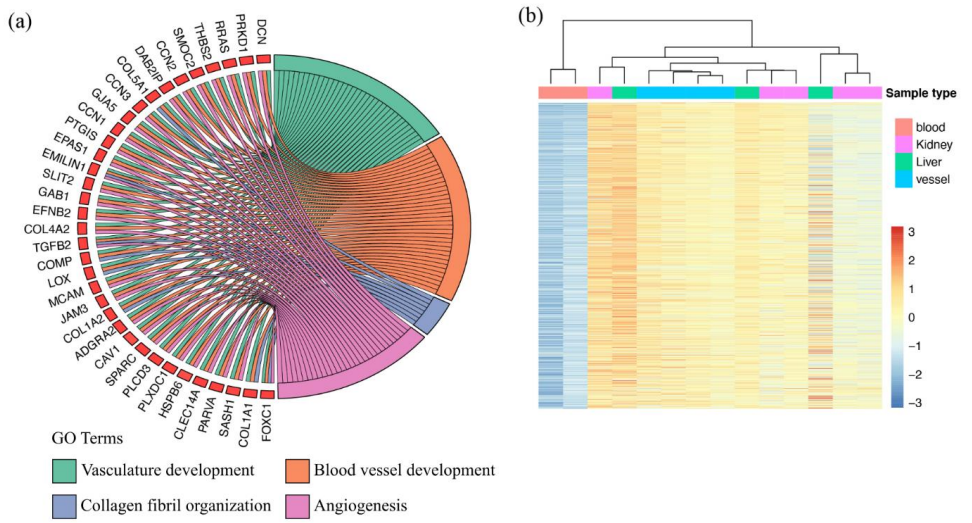

Figure 20. (a) Chord plot of upregulated genes revealing gene ontology terms relating to vascular function. (b) Heat map of differentially expressed genes comparing blood samples, surgically extracted vascular samples, and samples from the device. The heatmap illustrates the similarity between the vascular control samples and the difference compared to the blood samples. The figure is reproduced from Wiley-VCH GmbH[100] under Creative Commons License CC-BY 4.0.

The sequencing results show that the samples are undoubtedly of vascular origin, showing similarities between the vascular control samples and marked differences from blood, Figure 20. Furthermore, among the upregulated genes, there were several genes associated with endothelial cell function, such as EPAS1, CLEC14A, and MCAM[101-103]. This data is in agreement with the cytological data as well.

4.4.6 Safety aspects

The incidence of bleeding in the vasculature, defined as extravascular contrast pooling after sampling, in the device group was 11% (7/65), and in the control device group, it was 11% (3/27). These bleeding events were transient, resolving themselves within minutes after sampling. As there is no difference between the two groups, the incidence of bleeding must be related to other aspects than the brush structure itself. As the device was manufactured manually without adhering to any manufacturing standard, and the method of cell extraction is completely new, there are several aspects that can be responsible for these bleedings. The sampling procedure requires the device to be wedged into a vessel of a similar dimension as the device, which is not obvious when it occurs during angiographic guidance. This, in combination with using a fully metallic wire, could lead to a situation where the device is protruded a little bit too far, damaging the blood vessel wall unnecessarily.

The device integrity was examined after each sampling event, looking for damaged brush sections or other issues. On two occasions, damage was revealed, either in the form of a broken or detached brush section.

4.5 Conclusions

This thesis presents a method of selectively extracting ECs, as demonstrated by cytological staining and sequencing data. It represents an important development to enable access to ECs *in vivo*. However, a few shortcomings in the study need to be addressed. When it comes to cytological data, one should be careful in making sweeping claims, as the selection of cellular markers inherently limits it. For example, based on this information, there is no way of proving that the extracted cells are not pericytes or fibroblasts. On the other hand, the cytological evaluation is not the most appropriate evaluation method for this device, seeing as there were difficulties with stain visualization on the device and that dissociation of the samples was inadequate in many cases.

Chapter 5 – Endomyocardial biopsy

5.1 Overview of the anatomy of the heart

Briefly, the heart is divided into four separate chambers, receiving and pumping blood to and from different parts of the body. As biopsies of the heart is the focus of this chapter, the anatomy of the heart wall is of interest, Figure 21.

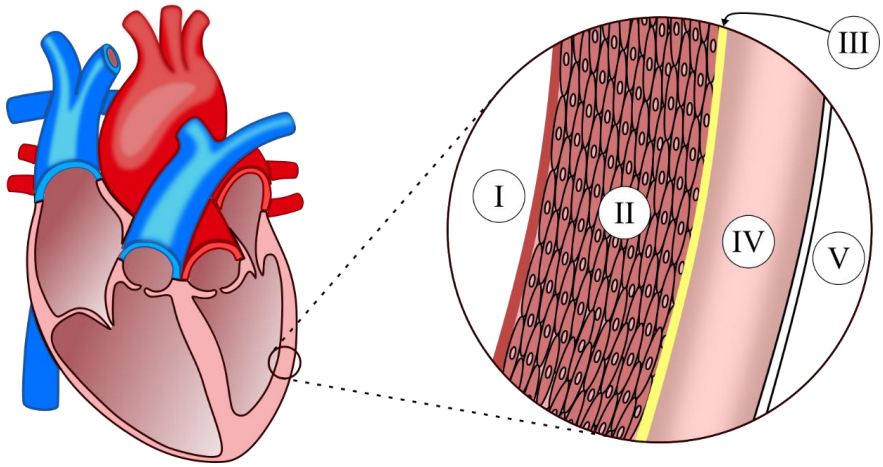

Figure 21. Anatomy of the heart. The left and right ventricles of the heart (left image) have different properties and output pressures, putting different requirements on the outer heart wall. The thickness of the heart wall in the right ventricle is notably thinner than its' left counterpart. The heart wall is divided into three layers; (I) the endocardium, (II) the myocardium, and (III) the epicardium. The heart is surrounded by a pericardial cavity (IV) and the pericardial layer (V).

The innermost layer of the heart is the endocardium, analogous to the endothelium of a blood vessel, covered with endothelial cells. These endothelial cells, however, are different from those in the blood vessel in that they respond to differences in exerted pressure and can regulate blood vessel dilation and heart contraction[104, 105]. The myocardial layer consists of a complex 3D network of cardiomyocytes and other connective tissues, referred to as the syncytium[106]. The outermost layer of the heart is the epicardium, a thin layer of mesothelial cells, connective tissues, nerves, and blood vessels[107]. Lastly, the heart is surrounded by the pericardial sac and the pericardial layer. The pericardial sac acts as a physical barrier against infections and contains pericardial fluid that lubricates the heart surface. The pericardial layer is divided into the parietal and visceral pericardium[108], covering the entire heart. The full anatomy and function of these layers are beyond the scope of this thesis, but the overall structure is important to understand to identify issues related to biopsies.

5.2 The endomyocardial biopsy technique

Biopsy of cardiac tissue is performed with an endovascular device and is most often performed in the case of heart transplantation to monitor for tissue rejection. Other indications exist, including, but not limited to, myocarditis, cardiomyopathies, and amyloidosis [109]. The procedure usually involves accessing the vasculature through the jugular vein, providing a relatively straight path into the right ventricle, Figure 22.

However, other access points, such as the femoral or radial artery, can also be used to access the left ventricle[16]. The endomyocardial biopsy (EMB) device was initially developed for percutaneous use in the 1960s. It was in the shape of cutting claws that open and close with the push and pull of an internal wire [110].

5.2.1 Challenges in the EMB procedure

The EMB device has not been extensively refined in function or size for the reasons mentioned concerning histopathology, whereas current clinically used devices are almost identical. The main drawback of the EMB device is its' size and stiffness, limiting navigability inside of the ventricle, usually targeting the apex of the right ventricle. One of the most important aspects concerning the challenges of EMB lies in the difference in thickness in the different regions of the heart. The apex of the right ventricle is the region of the heart wall where it is thinnest, leading to a risk of lethal complications if the heart wall is inadvertently punctured.

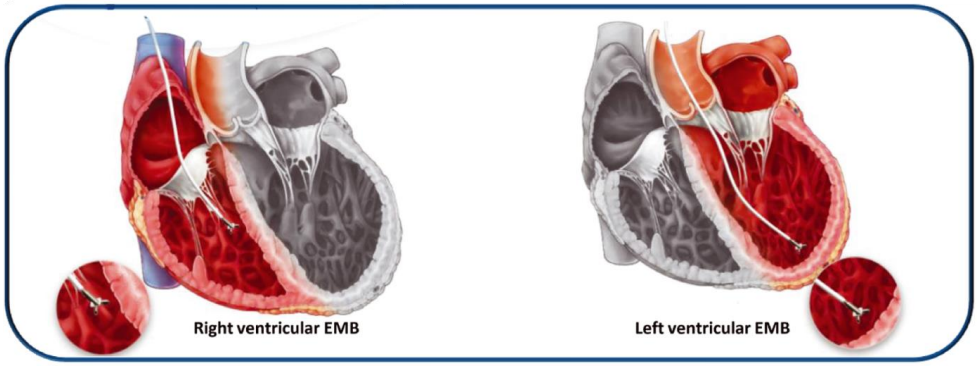

Figure 22. Schematic illustration of the EMB procedure with the clinically used device. Biopsies of the LV are possible but are more technically challenging due to the stiffness of the device. Furthermore, the device stiffness impedes navigation within the ventricle, leading to similar sites being targeted in between sampling events. Image reproduced from John Wiley and Sons [109] with permission from the publishers.

Although complications in EMB procedures are infrequent (~1%), they can be severe, some being potentially lethal[111]. In the case of heart transplant monitoring, the device is especially troublesome since repeated biopsies are required[109]. The limited flexibility of the EMB device results in biopsies being taken in similar areas between each procedure, potentially of scarred or weakened tissue, increasing the associated risk and reducing diagnostic accuracy. Furthermore, since the right ventricle is the preferred sampling site and there is limited navigability, certain heart diseases are difficult to assess with a biopsy. Many heart conditions affect the left ventricle, most notably heart failure [112]. Meanwhile, other conditions, such as sarcoidosis, affect only parts of the heart, where substantial benefits could be gained by targeting specific areas of the heart [113]. Given the shortcomings of the clinically used EMB device, a lot can be gained with a miniaturized device. In doing so, one gains navigability by reducing the stiffness, reduces invasiveness by reducing the footprint inside the heart, and provides access to tissue from other heart diseases. Lastly, due to mechanical scaling laws, the solution to device miniaturization is not to simply reduce the size of the currently used device. The EMB device as it is today already houses intricate mechanical features to facilitate the mechanism that opens and closes the forceps jaw. A further reduction in

size would most likely result in device failure or reduce the strength of the mechanism to such a degree that it is impossible to retrieve tissue samples. The solution, as presented in Paper I-III, lies elsewhere.

5.2.2 Exploring different designs

Many of the early prototypes were constructed with the same idea: to utilize an anchor hook approach, tearing tissue apart upon device retrieval. These, however, were highly variable in their sampling accuracy.

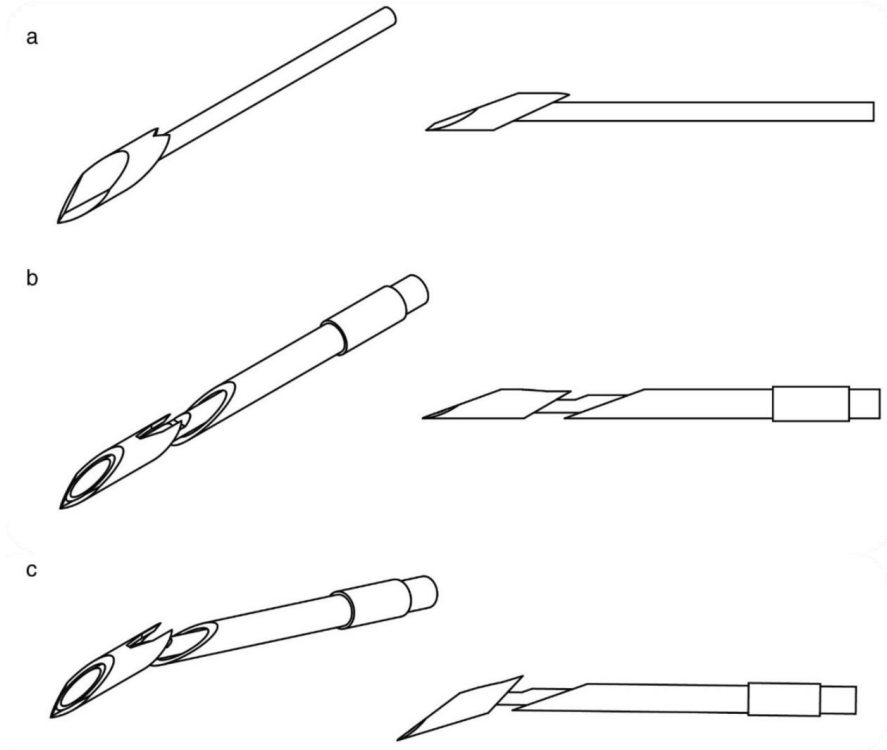

Figure 23. Panels a-c collectively illustrate the device iterations in chronological order. (a) The earliest concept was simply a laser-machined device mounted on a wire, providing a sharp rear end intended to tear tissue apart, with no mechanism for securing the resulting sample. (b) This iteration added a tube with a radiomarker and ground tip, intended to provide a surface where a sample could be clamped upon axially moving the internal wire. Additionally, the wire had a laser-machined pocket to increase the sample size. (c) The last iteration prior to the successful device added an angle to the distal laser machined head, intended to improve the cutting aspect of device retrieval. The figure contains elements reproduced from Springer Nature[114] under Creative Commons License CC-BY 4.0.

Several trials with a variety of nitinol-based designs were performed. Up to 65 different device designs were evaluated based on three conceptually similar approaches, Figure 23. These three approaches combined led to the device that was ultimately successful, Figure 24.

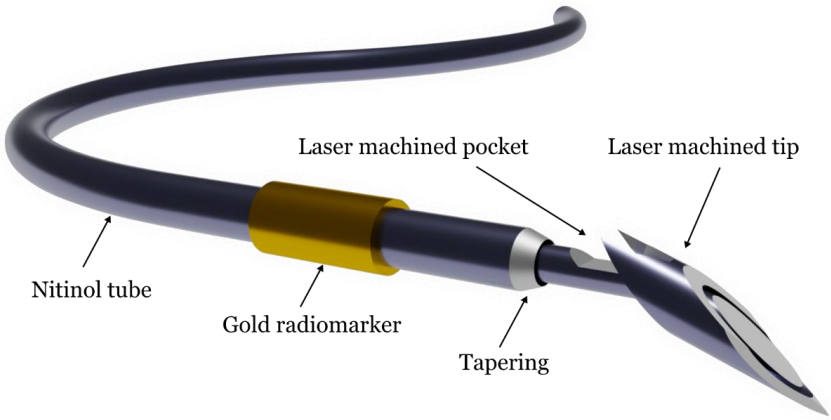

Figure 24. 3D rendering of the device that was ultimately selected. The ID and OD of the nitinol tube is 0.28 and 0.38 mm, respectively. The tube houses a nitinol wire with a diameter of 0.23 mm that has a laser-machined tip at the distal end. The laser-machined tip is glued to the wire with cyanoacrylate glue, sits at an angle with respect to the axis of the wire and tube, and has two sharp edges oriented proximally. The inner wire is movable with respect to the tube and is designed to tear apart tissue and clamp it between the tip and tube edge.

Papers I-III of this thesis collectively present the proof of concept of the novel device, referred to as the micro-EMB device, its' potential use in disease diagnostics as well as the safety aspects of device use.

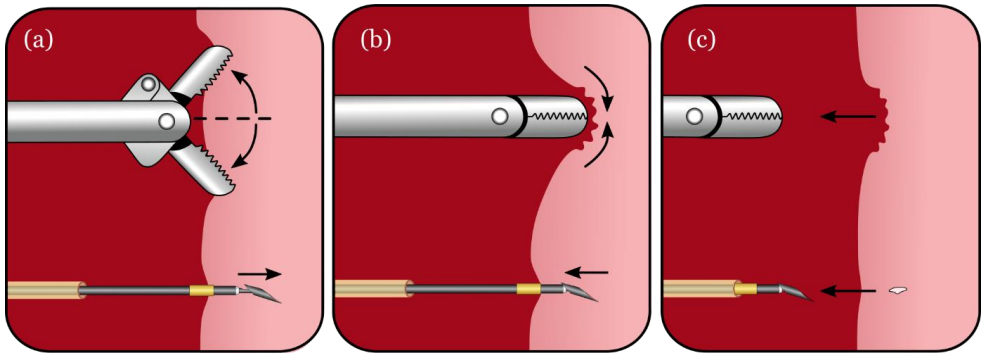

Figure 25. Comparison of size and sampling mechanism between the micro-EMB and conventional device. (a) Initially, both devices engage the heart wall. The micro-EMB device penetrates a certain distance dictated by the radiomarker. The inner wire of the micro-EMB device is further protruded. The forceps open and grip the heart wall. (b) In the next stage, the inner wire of the micro-EMB device is retracted, tearing a sample from the myocardium and trapping it between the tube edge and tip. The forceps close, tearing a sample from both the endo- and myocardium. (c) Finally, both devices are withdrawn from the heart wall. The micro-EMB device extracts a significantly reduced sample and causes less damage at the sampling site.

The device has a substantially reduced diameter, 0.38 mm, compared to the current EMB device and a completely new method of extracting tissue, Figure 25. The device features a movable bidirectional cutting tip attached to a wire housed inside a 0.38 mm OD tube with a 20-degree tapering at the distal end. The tube further features a penetration depth-limiting radiologically visible flange. The tip extends beyond the cutting tube and can be advanced a limited distance coaxially in relation to the tube. The device penetration depth can be varied by altering the position of the radiopaque flange during manufacturing. The key development that increased the sampling accuracy was the addition of a circumferential tapering of the tube that ensures that no matter the orientation of the distal laser machined device, there will always be a clamping effect to trap a potential sample. The micro-EMB device, by virtue of the novel mechanism, obtains a sample from the myocardial layer and not from the endocardium. This difference carries some weight depending on what disease is of interest, where this device might see the most use in diseases affecting the heart muscle. Furthermore, the sample size is roughly 1/200th compared to the samples extracted by the forceps device.

5.2.3 Device manufacturing and assembly

All device prototypes were constructed in-house. Grinding procedures were performed with a custom benchtop grinding machine that features a grinding disc that can be angled 0-90 degrees and a fiber chuck that can be rotated. Three-facet grindings, as well as rotational tapering, can be produced without issue. Laser machining of the prototypes was done with a picosecond laser setup (Talisker 1000 355-10, Coherent, CA, USA) that further featured a custom-built 5-axis stage for movements in 3D as well as two additional rotational stages. The device manufacturing will be described in terms of the wire-tip assembly and the tube in which the wire-tip assembly is housed. All nitinol parts of the device are made from a nitinol tube of 0.38 and 0.28 mm OD and ID, respectively, and a nitinol wire of 0.23 mm in diameter.

The manufacturing of the wire-tip assembly is initiated by grinding the 0.38 mm tube to form a sharp tip. Grinding angles utilized are 17.5 degrees for the primary grinding followed by a 22.5-degree grinding after rotating the tube +/-45 degrees offset to the original orientation. After grinding, the tube is mounted in the picosecond laser setup. The bidirectional cutting mechanism is produced by cutting a V-shaped pattern a certain distance behind the tip, rotating 90 degrees, and cutting off at a 30-degree angle. The 30-degree cut coincides with the V-pattern and, once cut off, produces two sharp features with the V-pattern between. The total tip length varied and was 2 mm in papers I and II, and modified to be 1.5 mm in paper III to increase the safety profile potentially. This tip is positioned on a 0.23 mm nitinol wire that is pre-bent at an angle, represented by the tip in Figure 23 (c). This angle varied and was between 16-19 degrees (Paper I and II) and 19-23 degrees (Paper III), where a shorter tip could tolerate a larger angle. The tip is glued to the wire tip with cyanoacrylate glue. The angle is intended to orient the sharp elements outside of the OD of the nitinol tube once assembled to improve the tearing aspects of the device. At this stage, the wire-tip assembly is mounted in the picosecond laser setup again. A pocket is laser machined into the wire directly proximal to the tip. It was cut off if the wire was protruding at the distal end of the tip (beyond the sharpened tip). After these steps, the wire-tip assembly is completed.

The nitinol tube is manufactured by rotationally grinding the tip at a 20-degree angle, producing the tapered end. Any eventual grinding burr was machined away in the picosecond laser, producing a clean edge. Afterward, a gold coil is manually

assembled, glued onto the tube, and positioned at a certain distance from the distal end. This distance was varied between 2 mm (Paper I and II) and 0.5 mm (Paper III). At this stage, the tube is complete.

The wire-tip assembly is mounted inside the nitinol tube, and the assembly is complete. The distal end is operated through the use of a torque device (Merit Medical, USA), where the distance can be manually set. In this size range, there were no issues translating a proximal motion to a distal one.

5.3 Micro-EMB proof of concept

The proof of concept of the device was established in a porcine model. The study was conducted in two stages, Figure 26.

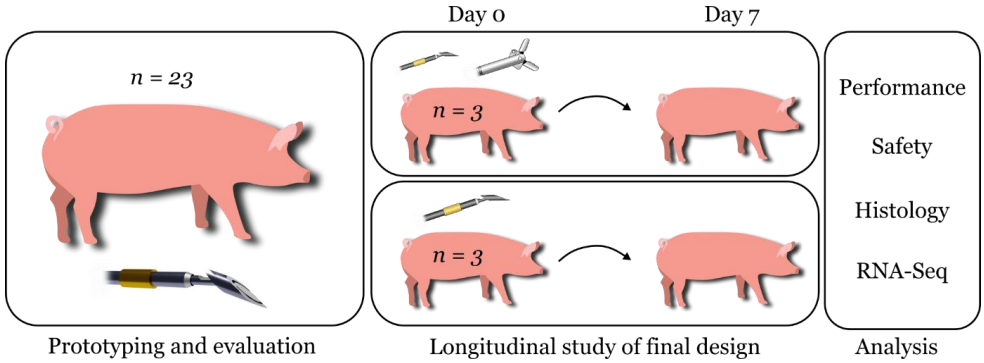

Figure 26. Study design of paper I. The early prototypes were evaluated in a series of animals (n = 23), whereas a final design was selected. The final design was longitudinally evaluated in animals (n = 6), divided into two groups. In one group, samples were taken with the conventional EMB device and the novel device, and in the other group, only the novel device was tested. The analysis consisted of evaluating the sampling performance, certain safety aspects, and histology and RNA-Seq of the resulting samples.

The initial prototyping stage in a series of 23 animals was done to evaluate device prototypes and optimize the RNA isolation protocols. Afterward, a longitudinal study of 6 animals was performed, Figure 26. The longitudinal part of the study was intended to evaluate several aspects of the device use: (i) The performance of the micro-EMB device in terms of sampling accuracy. (ii) Brief examination of the safety in terms of arrhythmias or similar complications. The reason for dividing the longitudinal group in two was to be able to identify the safety aspects of the micro-EMB device separately. (iii) The sample quality and feasibility of using histology and RNA-Seq on the resulting samples. Control samples in the form of skeletal muscle and blood were extracted as contrast in the sequencing data,.

5.3.1 Device performance

A total of 157 sampling events were performed with the novel device; out of those 127 were considered successful. The success was based on an arbitrary visual assessment from 0-4, where 0 indicated no sample, and 4 indicated a sample that protruded extensively outside of the intended confinement zone proximal to the device tip. A score of 2 or higher was deemed successful, Figure 27.

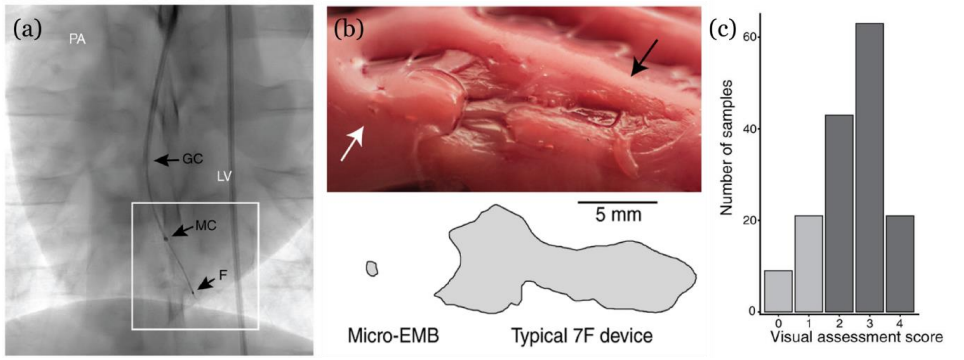

Figure 27. (a) Fluoroscopy image of the novel device inside the right ventricle, assessed from the posteroanterior view. The guide catheter (GC), the microcatheter (MC), and the radiopaque marker of the micro-EMB device (F) are highlighted. (b) The difference in tissue damage at the site of sampling between the conventional device (black arrow) and micro-EMB device (white arrow). Silhouettes of the sampled area are highlighted underneath. (c) The distribution of sample scores based on the visual assessment. The figure contains elements reproduced from Springer Nature[114] under Creative Commons License CC-BY 4.0.

The device could be successfully navigated inside the ventricle due to its' reduced stiffness. The average weight of the collected samples was 0.052 mg (n = 6) and showed a substantial reduction in tissue damage at the site of sampling.

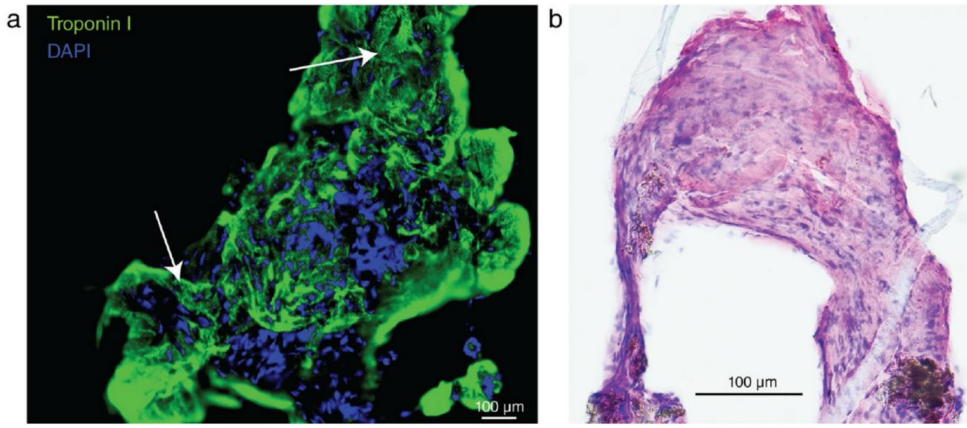

Figure 28. (a) Immunofluorescent staining for troponin I and DAPI of a sample extracted with the micro-EMB device. Characteristic striations of heart muscle tissue are indicated with white arrows. (b) H&E staining of another sample with crush artifacts illustrates the difficulty of using this analysis method for such small samples. The figure is reproduced from Springer Nature[114] under Creative Commons License CC-BY 4.0.

5.3.2 Cytological analysis

Immunofluorescent staining was used to evaluate the presence of troponin I in a selection of samples (n = 7). As previously discussed in the introduction, the small nature of the tissue samples made it difficult to assess the samples properly. We did, however, reveal the presence of characteristic striations relevant to heart muscle tissue, Figure 28. These difficulties were expected, however; hence the focus was oriented toward RNA-Seq.

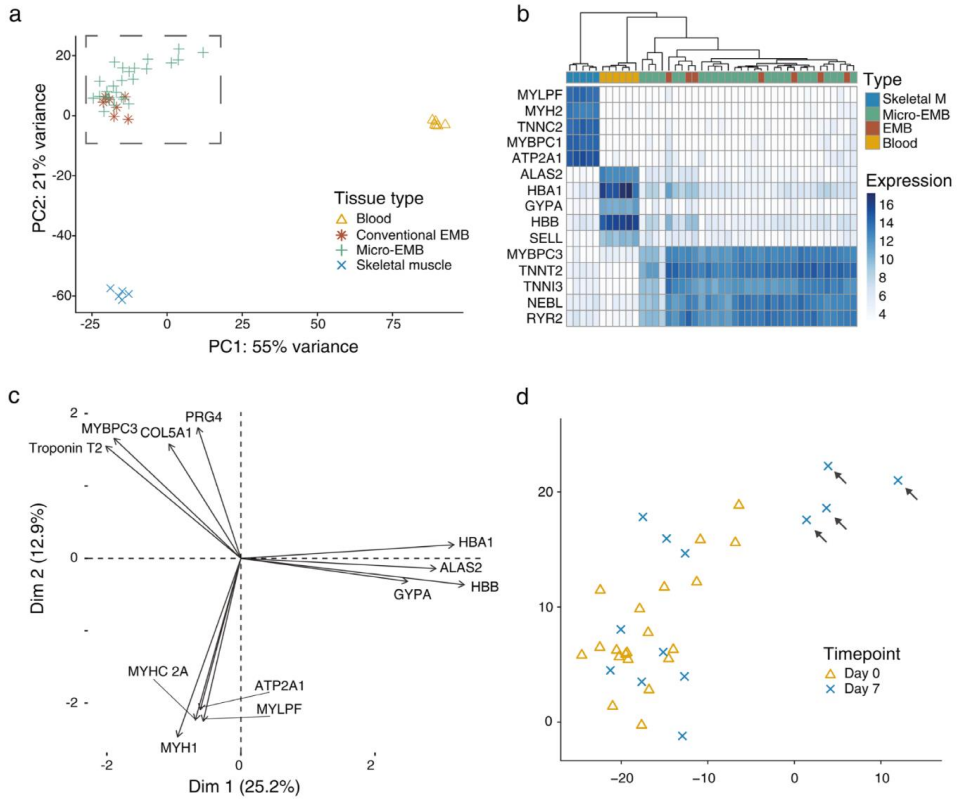

Figure 29. (a) Principal component analysis (PCA) plot illustrating the clustering seen among the different sample types. The samples from the micro-EMB device and conventional EMB device cluster together, indicating their similarity. (b) Heatmap of the 5 top differentially expressed genes of each sample type. The color grading is based on the $\log_2$ fold change of the differential expression analysis. (c) PCA loadings plot showing the top four weighing genes in the first three principal component axes. (d) Magnification of the dashed area in (a). The visual representation of the sample is different depending on the time point. All outliers are from the follow-up experiment, indicating these samples were somehow affected by the previous experiment. The figure is reproduced from Springer Nature[114] under Creative Commons License CC-BY 4.0.

5.3.3 Feasibility of RNA-Seq

Samples from the micro-EMB device, conventional EMB, skeletal muscle biopsies, and blood were analyzed with RNA-seq. Initial quality control was performed based on parameters such as mapping rates and the number of expressed genes. A majority (29/32; 91 %) of the micro-EMB samples and all control samples (22/22; 100 %) passed the quality control. Seven samples representing all tissue types were excluded due to signs of blood contamination. The ultimate inclusion rate was 81 % for the samples extracted with the micro-EMB device. The results of the RNA-Seq are presented as a PCA plot and a heatmap of differentially expressed genes, Figure 29. First, this data shows that the samples extracted with the micro-EMB device have similar genetic expression compared to those extracted with the conventional method. Second, the genetic expression of these samples is notably different from control samples.

5.3.4 Device safety

Several aspects of the safety of device use, such as pericardial effusion, irregularities in the heart rhythm, and post-operative behavior, were examined during and after the in vivo experiments. No adverse events aside from transient arrhythmias, common during catheterization procedures in the heart, were observed.

5.3.5 Influence on subsequent research

Paper I successfully demonstrated that the micro-EMB device procures samples from the heart wall that are similar to those extracted with the conventional device, at least in terms of their genetic makeup. The conclusion drawn from this is that the genetic information contained within samples of reduced size is not inherently different from larger ones and could potentially be used for diagnostic purposes. However, the potential for detecting pathological changes in the tissue was not the study's objective, which warranted a disease model and further work.

5.4 Potential of micro-EMB in disease diagnostics

Paper II was designed to explore the diagnostic potential by utilizing an infarct model in swine, Figure 30. The device's diagnostic capability was examined in a porcine myocardial infarction (MI) model. The chosen model was selected due to the simplicity of the procedure, where the left anterior descending artery (LAD) is occluded with a balloon for 60 minutes. Additionally, there are studies showing that MI models show changes in genetic expression early[115, 116].

The presence of the infarction was confirmed by evaluating the electrocardiogram, examining the heart tissue post-mortem, and by troponin assays. All the samples (n = 164) were extracted from the LV. Samples were taken at various time points: baseline (n = 15), during the one-hour occlusion (n = 14), up to two hours after re-perfusion (n = 49), after two days (n = 33), and finally after 14 days (n = 53). The samples were divided according to whether they were extracted in the infarcted region or outside of it. A subset of the samples (n = 85) was analyzed with RNA-Seq to evaluate the gene expression over time. Some samples were excluded from the analysis due to failed quality control (n = 24), blood contamination (n = 2), and being identified as outliers (n = 6). This led to 53 samples being included in subsequent analyses. These analyses consisted of differential gene expression analysis and a deconvolution analysis to estimate sample cell proportions.

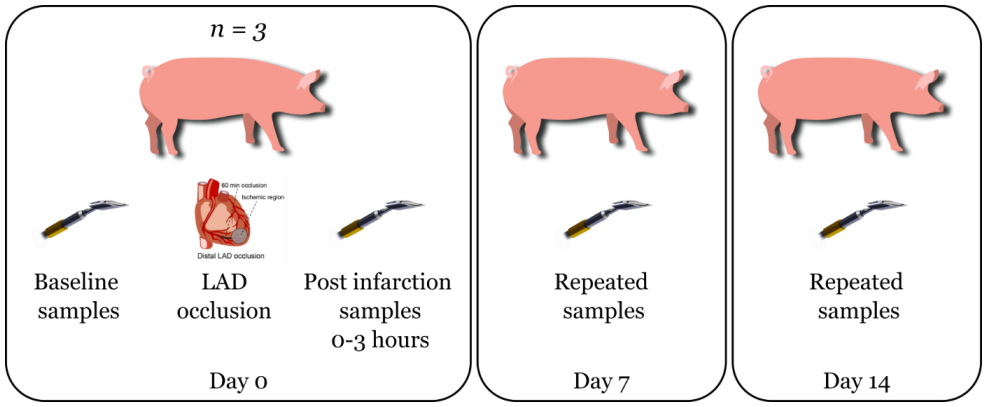

Figure 30. Paper II is a longitudinal study where baseline samples were compared to samples extracted after the induction of a heart attack by occluding the LAD. Samples taken after the infarction were taken at days 0, 7, and 14 to examine whether any transient changes in the genetic expression could be detected. The post-infarction samples were taken from the infarcted region as well as outside of it.

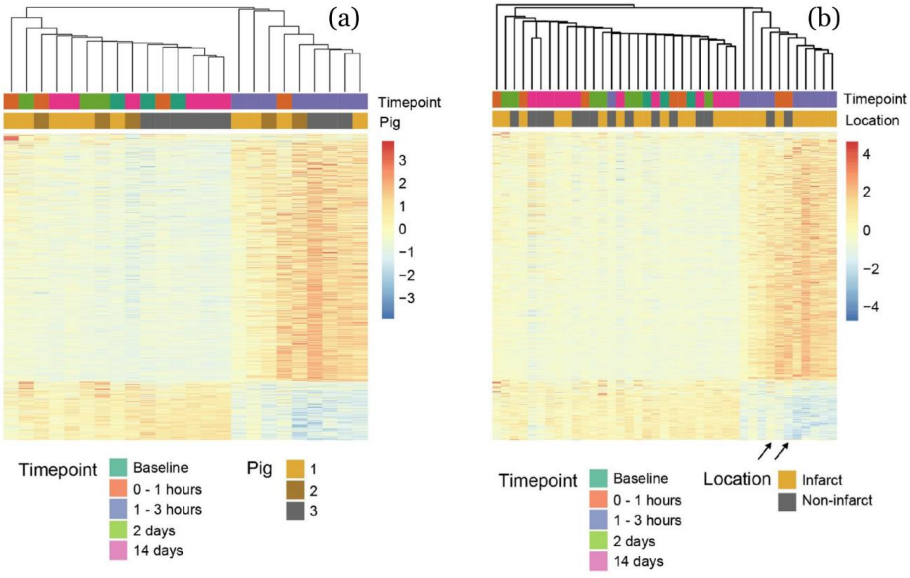

Figure 31. (a) Heatmap of differentially expressed genes across samples extracted from the infarcted region. Samples extracted at the 1-3 hour time points cluster together, indicating a change in their genetic expression. (b) Heatmap of differentially expressed genes across all samples. Here, two outliers from the non-infarcted region are clustered with the infarcted samples. The figure is reproduced from the Public Library of Science[117] under Creative Commons License CC-BY 4.0.

5.4.1 RNA-Seq to detect pathologic changes

The analysis of the sequencing data is presented here as a heatmap of differentially expressed genes, both when comparing all samples extracted from the infarcted region and across all samples, Figure 31. The differential gene expression did not reveal any major changes in the group of samples extracted at 2 and 14 days. The deconvolution data, Figure 32, supplements this analysis in that it does reveal changes in the estimated cell proportions in the samples in the later time points.

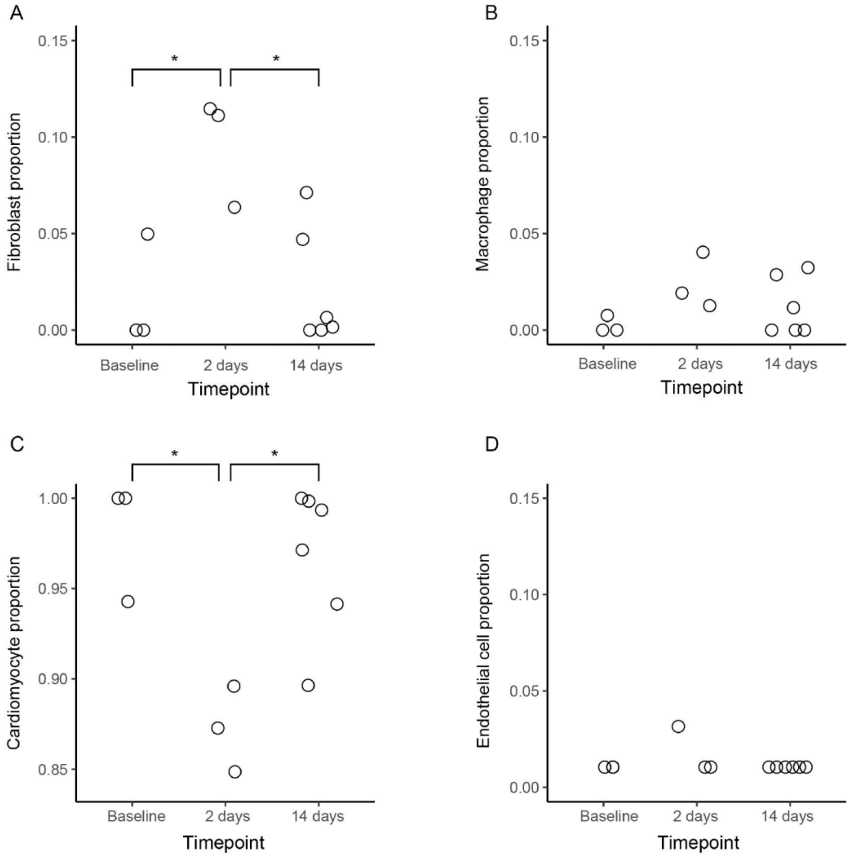

Figure 32. Deconvolution analysis of the RNA-Seq data from a subset of samples. The analysis considered the ratios of (a) fibroblasts, (b) macrophages, (c) cardiomyocytes, and (d) endothelial cells. There was a significant increase in the estimated fibroblast proportion and a decrease in the estimated cardiomyocyte proportion. The figure is reproduced from the Public Library of Science[117] under Creative Commons License CC-BY 4.0.

5.4.2 Device safety

In this study, the safety of the micro-EMB was also examined, although not the main intention of the study. No major complications were observed in any of the animals regarding tamponade or sustained arrhythmia. This fact, coupled with repeated

sampling events, the induction of an infarct, and the longitudinal nature of the study, further indicates the safety of the micro-EMB device.

5.4.3 Influence on subsequent research

Paper II demonstrates that it is possible to detect changes in the genetic expression levels even when extracting very small samples. The RNA-Seq data indicate a clear clustering of samples in the earlier time points after the induction of an infarction, however, not at the later time points. A deconvolution technique was applied to estimate changes in the estimated cellular proportions at the later time points, which showed a difference in the fibroblast and cardiomyocyte populations. However, the deconvolution technique requires the input of genetic data from known cell types, which, in this case, was extracted from a mouse database[116]. Any conclusions drawn from the deconvolution data have to be verified in future studies with a more representative database. Certain aspects of the study design can partly explain the difficulty in detecting later changes. First, the induced infarction was relatively small. Second, as only fluoroscopy was used to guide navigation inside the heart, the accuracy of the sampling was reduced. Lastly, there were relatively few replicates in each sample category. Despite these weaknesses, however, changes were detected, which might be further proof of the method's potential in diagnostics. We believe that the micro-EMB device at this stage has been properly benchmarked in pre-clinical animal studies in terms of proving that it works for RNA-Seq and is at the same level as the conventional device. Future work with the micro-EMB device in terms of establishing it as a method for diagnostics is best suited to studies in humans. However, as discussed for the endothelial cell brush, this device requires a proper manufacturing procedure and relevant testing of biocompatibility, mechanical testing, etc., before human trials can begin. Papers I and II serve as good proxies for safety data, but as neither study was designed to investigate safety explicitly, this warranted an additional study.

5.5 Safety evaluation

Paper III is explicitly designed to evaluate the safety profile of the micro-EMB device. This was done by benchmarking it to the conventional EMB device in a porcine model, Figure 33. Major complications were defined as a cardiac event, such as pericardial effusion, causing death or sustained hemodynamic compromise.

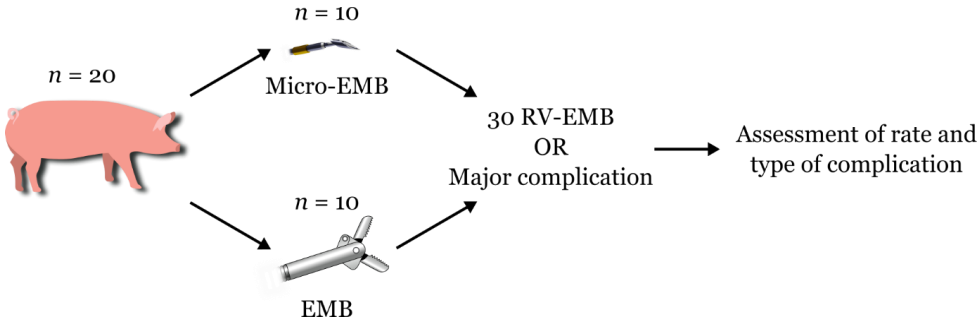

Figure 33. Study design of Paper III. A group of 20 animals were divided into two groups of 10, each being subjected to either the micro-EMB or conventional EMB. Endpoints were selected as 30 confirmed biopsies taken from the right ventricle or the incidence of a major complication. If these happened, they would be assessed in terms of incidence rate and type.

The hemodynamic compromise was defined as a mean artery pressure lower than 45 mmHg for more than 20 minutes. The complications were assessed continuously during the trial by ultrasound investigations of the heart after each sampling event, checking for excess pericardial fluid, and monitoring the blood pressure. Hemodynamic compromise coupled with the discovery of excess pericardial fluid was defined as a tamponade. After the trials, a sternotomy of the heart was performed, where the amount of pericardial fluid and its characteristics in terms of the level of blood contamination were examined. Ultimately the rate and type of complications were compared between the two device groups.

5.5.1 Comparison of complication rate

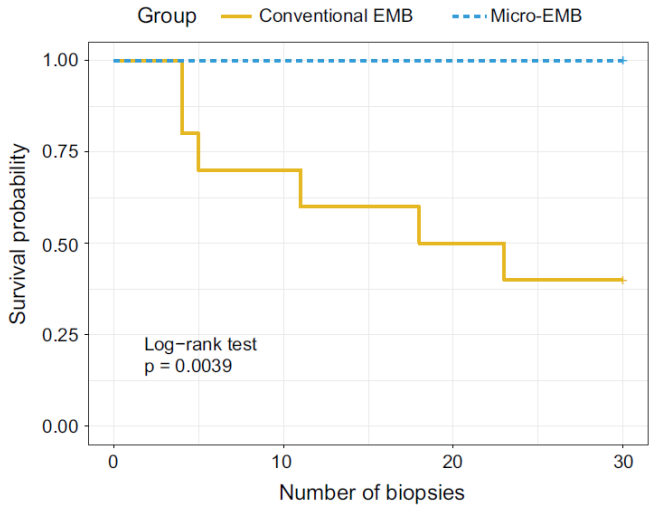

Figure 34. Kaplan-Meier survival plot for both groups. The micro-EMB group showed no complications, and all animals survived the procedure. In the conventional EMB group, the first major complication happened after four biopsies in one animal, with a total of 6 animals suffering major complications. The figure is reproduced from Springer Nature[118] under Creative Commons License CC-BY 4.0.

The main results of Paper III are in the form of a survival plot comparing the two groups, Figure 34, and the assessment of the complication rate and type, Figure 35.

The survival plot illustrates a clear difference between using the micro-EMB and conventional EMB device in terms of complication rate, seeing no adverse events for the micro-EMB device. In contrast, the conventional EMB leads to a 40% survival rate. The assessment of the rate and type of complication in the EMB group was exclusively in the form of a tamponade, causing blood to leak into the pericardial sac. The examination of the pericardial fluid characteristics revealed an excess of 100 mL of blood-contaminated fluid in the animals with a major complication. There were incidences of blood-contaminated pericardial fluid in the micro-EMB group as well; however much lower in volume, which did not lead to hemodynamic compromise.

The study clearly demonstrates a safety advantage of using the micro-EMB device in terms of acute complications, although certain weaknesses are present in the study. The number of biopsies is not representative of a clinical scenario, as one commonly

extracts around four biopsies in an ordinary procedure during heart transplant monitoring[119]. However, since healthy animals were used, it is deemed unlikely that complications would occur with such a small number of replicates. This would require a larger number of animals to be employed to illustrate a difference, which presents an ethical issue. Thirty biopsies were selected to accelerate the incidence of complications to be able to illustrate the safety comparison more clearly in a smaller number of animals. Additionally, only the acute complications were monitored. Longer-term complications, such as damage to the valves or scarring of the myocardium, were not assessed, which would warrant additional studies.

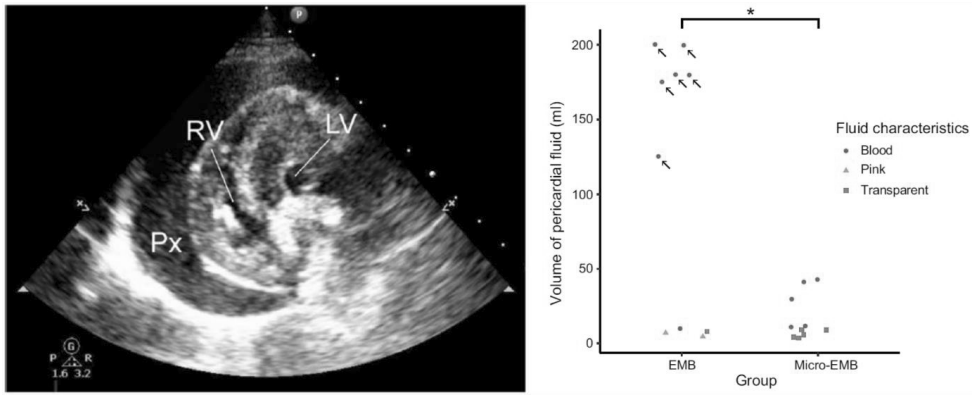

Figure 35. Example of a transthoracic echocardiogram (left) illustrating an excess of pericardial fluid (Px) around the RV. The pericardial fluid characteristics across all animals (right) illustrate the volume and color of the fluid. All animals with a major complication (marked with an arrow) had an excess of 100 mL of blood-contaminated liquid in the pericardial sac, indicating a tamponade. The figure is reproduced from Springer Nature[118] under Creative Commons License CC-BY 4.0.

5.6 Conclusions

Paper I demonstrates that the micro-EMB device is capable of extracting tissue samples of radically smaller size than the currently used devices with high accuracy. Furthermore, Paper II demonstrates that it is not only possible to extract information from the extracted samples, but the information generated is also potentially useful as a diagnostic aid. Lastly, paper III reveals that the micro-EMB device is much safer to use.

Chapter 6 – Soft tissue biopsy

6.1 The Extroducer trans-vessel wall technique

Analogous to the Seldinger technique that enables safe entry into the vasculature, referred to as the introducer, the trans-vessel wall technique (Extroducer) is a method developed in 2010 that enables safely exiting the vasculature[120]. This technique involves the use of a nitinol tube with a sharpened tip housed in a PTFE tube. Using conventional fluoroscopic guidance to navigate the vasculature, the Extroducer can be safely guided in the vessels while in the PTFE tube and, once the target site has been reached, can be pushed forward to penetrate the vessel wall to exit the vasculature[121]. Early Extroducer prototypes were designed to feature a detachable tip, leaving a part of the distal device behind. The incoming blood flow through the tip is too low to induce thromboembolic complications[120]. However, depending on the organ and whether the arterial or venous system is accessed, some applications do not require tip detachment[122]. This method can create a working channel from outside the body into most locations within and is particularly beneficial in areas that are harder to reach with percutaneous procedures, such as the pancreas, liver, or brain. Other devices on the market principally achieve the same effect, although with substantially larger diameters and a design targeted for an otherwise specific purpose [123]. This technique was initially conceived to deliver substances, such as drugs, mRNA, cells, or otherwise, super selectively without risking systemic side effects.

6.1.1 Extroducer manufacturing

The Extroducer devices utilized in this thesis are constructed in-house from nitinol tubes. Two tube dimensions were tested; one with 255 and 175 µm OD and ID, respectively, and the other with 246 and 147 µm OD and ID, respectively. The smaller of the two represents the original Extroducer dimensions, and it also features a distal tapering of the last 25 cm down to a distal OD of roughly 190 µm. Both tubes are sharpened in the benchtop grinding machine described in Chapter 5 with a primary and secondary angle of 12.5 and 17.5 degrees, respectively. Similar to the other devices, they feature a gold coil designed as a penetration limiter and as a guide for fluoroscopic visualization. At the proximal end, depending on the device iteration, there is a syringe connector to be able to apply pressure through the channel.

6.2 Exploring device operations in the Extroducer

Paper V is based on the idea that this working channel could instead be used to extract cells for analysis. The trans-vessel wall technique and the minimal diameter of the Extroducer represent the essence of the innovation. However, this is also what presents numerous challenges when attempting to manufacture a device that would fit inside. With an inner diameter of 147 µm, this sets the stage for what is feasible to fit inside. The path to reaching the design presented in paper V is paved with several iterations, made of silicon through the MEMS technology platform and through 3D printing.

6.2.1 MEMS designs

The MEMS technique was utilized to construct the silicon devices and was designed on SOI wafers. The MEMS manufacturing resulted in the silicon devices freely suspended on top of the handle layer of the wafer, with breakaway structures connecting it to the remainder of the device layer. From this point, the devices could be manually aligned to a laser-machined nitinol wire, broken off, and glued with cyanoacrylate glue. The assembled device consists of a nitinol wire small enough to fit

inside the Extroducer, with a distal device attached. The dimensions of the wire depended on which design iteration was used but were either 99 or 127 µm in diameter. The designs of the silicon devices were varied in length and prong thickness, but the more successful devices were 1 mm in length with a 10 µm thickness. The operating procedure of the assembled device would be to operate the wire at the proximal end, translating to a motion on the distal end of the Extroducer. The core idea of the attached silicon devices was to achieve an expansion once the device protruded out of the Extroducer channel and a subsequent contraction once retrieved back in. The device designing was an iterative process evaluated in gelatine models in terms of whether any gelatine was pulled into the Extroducer channel. The first attempts were made with a double beam design with sharp features in the distal orientation and barbs oriented proximally. These designs did not expand laterally into the gelatine once protruded but remained the same shape. However, there was some success in extracting gelatine into the channel. The design was altered to feature a similar two-beam design but with a pre-opened shape to achieve the expansion effect that was sought after. The idea was that this device, while inside the channel, would be in a stressed, contracted state since the devices were manufactured to be wider than the Extroducer channel. Once protruded, it would expand by virtue of releasing the stress. The success of these devices was evaluated in ex vivo testing and DAPI staining of the resulting samples, Figure 36.

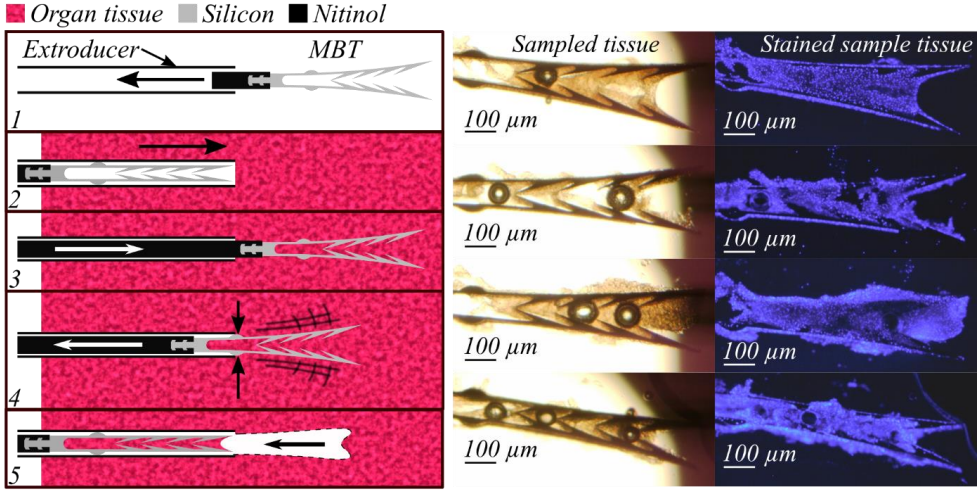

Figure 36. One of the early prototypes showed success in ex vivo benchtop sampling. (1-5) Schematic of device operation with preloading, leading to a contracted state, followed by subsequent expansion when protruding the device into tissue. Lastly, retracting it tears a tissue piece that is dragged within the Extroducer. The right panel shows corresponding brightfield microscopy and DAPI staining of acquired samples. Adapted, with permission, from[61].

Once a silicon prototype was manufactured that was deemed successful[61], it was tested in porcine models. The porcine trials revealed two things primarily. First, the pushability of the nitinol wires is very low, resulting in difficulties protruding the device past the Extroducer opening whilst inside parenchymal tissue. Of note is that these issues were not present inside the lab. Ex vivo tissue and the gelatine model were easy to access even with a full-length device, even when the system was bent, similar to what

would be experienced in the vasculature. Second, on the instances that the device was possible to protrude, they were structurally too weak to pass through the parenchyma of softer organs without breaking when tested in large animals. From this, we ascertained that tissue in vivo behaves rather differently compared to ex vivo in terms of mechanical stiffness. Unfortunately, these issues were difficult to visualize because the system was too small to be seen in fluoroscopy. These findings were repeatable through many silicon device dimensions, unfortunately.

6.2.2 3D-printed designs

The finding that devices break in the porcine trials was thought to be inherent to the silicon devices since silicon as a material is strong but brittle. Using 2PP to create 3D-printed designs was therefore tested as an alternative. The assembly process was similar for these devices, manually mounted onto the nitinol wire and glued with cyanoacrylate glue in laser-machined cavities in a nitinol wire.

Naturally, the 3D-printing process makes the 3rd dimension accessible, in contrast to the 2.5D approach of the MEMS platform. One of the earliest 3D-printed prototypes was designed with the silicon devices in mind, with three rotationally symmetric pre-bent prongs, each with a sharp tip and proximally oriented barbs. It was thought that this design would present a similar penetration behavior but, by virtue of being less brittle, not break as easily, Figure 37. Although this design did not break the same way, it was bent or otherwise deformed after sampling was attempted in vivo.

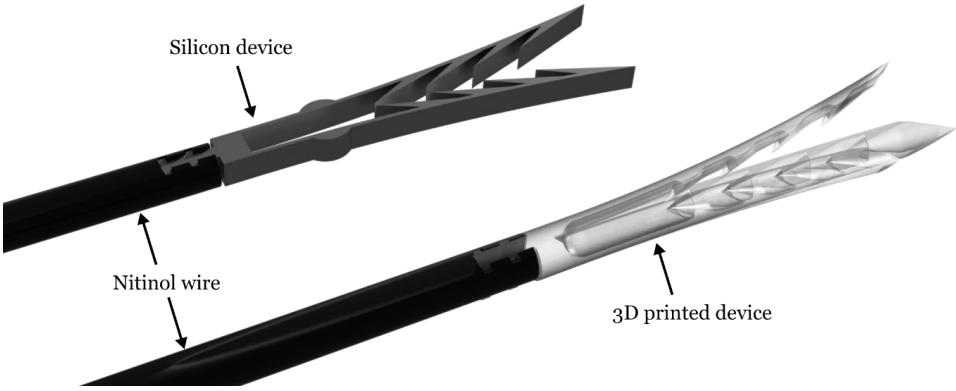

Figure 37. 3D rendering of the original silicon design (left) and 3D printed alternative (right) as mounted on the nitinol wire. Both designs are structurally too weak to survive tissue penetration in vivo.

A variety of additional design modifications in the shape of needle-like structures were tested in an attempt to address this. Unfortunately, these were also breaking during device insertion, cementing the notion that a device mounted on a wire of these dimensions would likely break.

6.2.3 Mechanical considerations of the distal device

At this stage, the breaking of both the silicon and 3D-printed devices was attributed to the small dimensions of the prong design. The thickness of the polymer prongs was similar to the silicon devices, in the range of 10 μm, with varying lengths up to 1 mm. Comparing the two materials' mechanical properties, the polymer material has a yield

strength of roughly 1 GPa compared to the 7 GPa of silicon. This difference in yield strength is compensated for by the different geometry of the prongs, where they are instead curved, producing a higher area moment of inertia.

As both materials and geometries failed, it was hypothesized that a slightly larger diameter of the Extroducer tube could be the solution to the observed mechanical issues. The larger tube had a length of 1.7 m and an outer and inner diameter of 255 and 175 µm, respectively. By virtue of the same mechanical scaling laws, even a slight increase in dimensions will increase the mechanical strength with a certain power, depending on the geometry. Unfortunately, the same upscaled geometries were attempted with the larger tube, with the same end result of broken devices. Given the nature of device fractures, attempting devices with an intended mechanical actuation mechanism was deemed infeasible, i.e., with moving elements or protruding features.

After the publication of paper IV, combined with the failed attempts at creating a 3D-printed device with the Extroducer, we hypothesized that the brush designs might also work well for this application. The brush design was therefore adjusted to fit within the Extroducer channel and to feature a sharpened wire tip to lower penetration forces. Exposing a device with a large surface area and sharp edges aligned well with the idea of not having mechanically actuated elements on the device. Additionally, given the results of using brush structures for endothelial cell sampling, there was confidence in that this solution would not be as sensitive to fractures and that it could actually sample cellular material. Initial attempts with these devices were unsuccessful, but not in terms of device fractures. Instead, the mode of failure was in device delivery into the parenchyma of the organs. This fact, coupled with the earlier device fractures, led to an investigation of what was required to penetrate the tissue and increase the force generated at the distal end.

6.2.4 Investigation of force relations

As discussed earlier in this chapter, the pushability of the wire, loosely defined as the ability to transfer force along the wire from the proximal to the distal end, is very low when using wires of these dimensions. When navigating through tortuous vascular paths, the degrees of bending that the system is subjected to might lead to one being unable to push the wire through the catheter. This problem is exacerbated when the dimensions are drastically reduced, resulting in several issues when attempting traditional, manual manipulation of the wire during endovascular navigation. First, several forces are at play in catheter systems, as described in Chapter 2, that hinder wire movement. These forces are primarily influenced by the degrees of bending that the catheter system is subjected to and the wire stiffness. Second, a confounding factor is that, in addition to these forces, there is a mechanical obstacle, the tissue, on the other end of the catheter that also needs to be overcome. A low penetration force of the wire is, therefore, also of crucial importance to enable access to the tissue.

Understanding this interplay of forces was necessary to find a way of addressing the shortcomings of low pushability. The force required to pull a wire through the tube as a function of the degrees of bending was investigated with the 255 µm tube combined with a 99 µm nitinol wire, Figure 38. The pulling force was measured with a force sensor (LSB200, Futek, USA) connected to the wire as the catheter system was bent a number of rotations. These measurements were repeated three times for each rotational setting. The bending radius was found not to have a significant influence on the force response unless very small (< 1 cm).

A subset of the wire tips was sharpened in the benchtop grinding machine and examined in an SEM to investigate the tip radius and appearance, Figure 39. The influence of the tip shape on the penetration force of the 99 µm wire was examined in ex vivo muscle tissue. These tests were performed with a tissue piece placed on top of the force sensor used in the pulling force measurements and the wire mounted in a Z-stage. The penetration was imaged with a microscope and correlated with the resulting force-time curve. The peak force was extracted for each measurement for sharpened (n = 30) and blunt wires (n = 6).

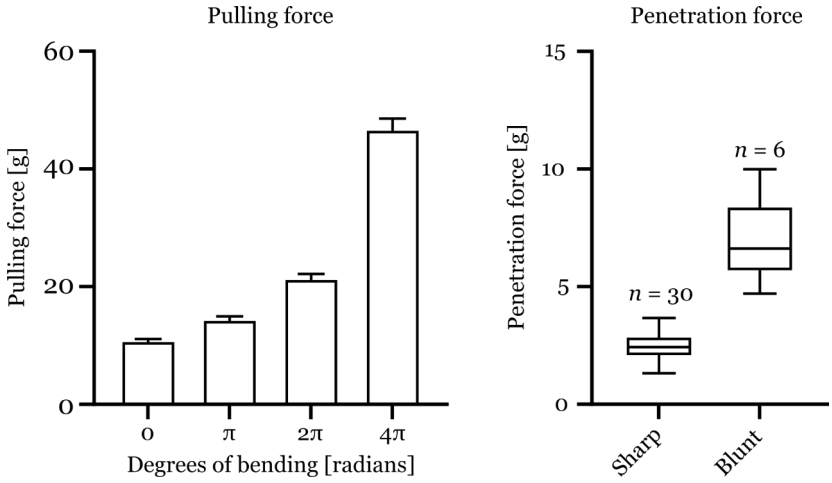

Figure 38. Pulling force as a function of the degrees of bending for the 255 µm tube and 99 µm in combination (left). The bending radius of the experiments displayed here was 43.5 cm. The penetration force in ex vivo muscle tissue, comparing sharpened and blunt wires (right).

The results of these experiments indicated that the force response closely resembles the relation described by the Capstan effect. Additionally, the penetration force was significantly lower for the sharpened wires.

These data, coupled with the failed deployment of these devices in vivo, set the stage for what a solution would require. One, it needed to be insensitive to the degrees of bending, and two, it needed to increase the force generated at the distal end. These experiments served as a precursor for investigating what solutions exist in the literature to similar issues and to the final device that was eventually tested in papers V and VI.

6.3 Proof of concept for tissue sampling through the Extroducer

The final device design is depicted in Figure 40 and is intended to be used as a tool to enter parenchymal tissue by exiting the vasculature and deploying the inner wire for sampling. The device has been tested with two tube variations, with the larger nitinol tube used in liver and kidney and the smaller tube used in the brain. The same wire size was used for both variations, so the micropiston size was adjusted to fit into either tube. The larger tube was believed to increase the force generation by virtue of being a larger system but was simultaneously believed to be more difficult to navigate and steer into the region of interest.

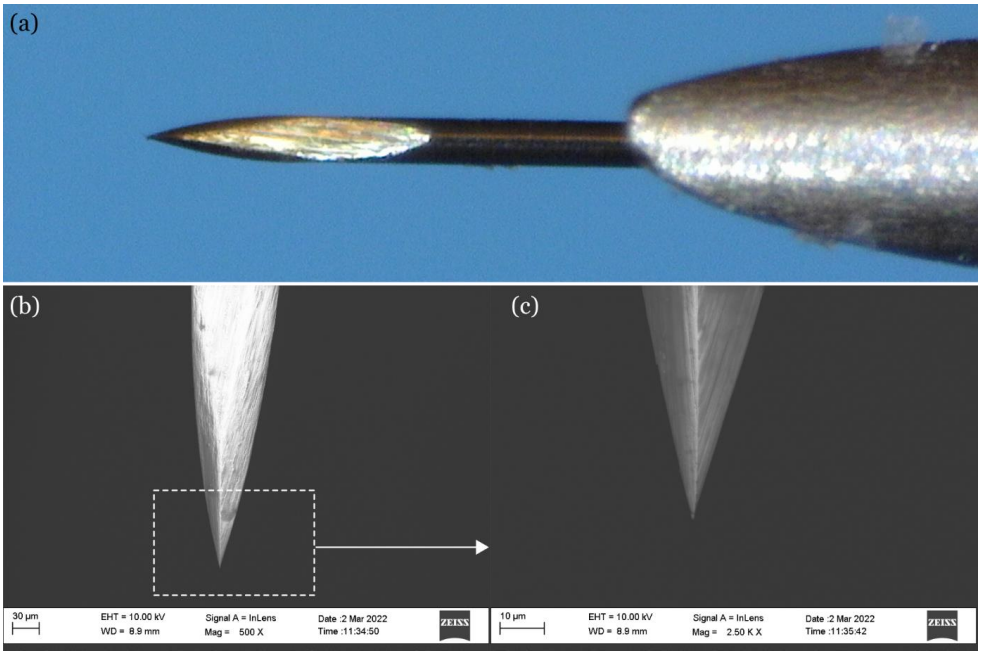

Figure 39. (a) A 99 µm wire as sharpened in the grinding machine, showing a 3-facet grinding. (b) SEM image of a sharpened wire and (c) a zoom in of the inset in (b). The tip radius was 2.1 (±1.2) µm for the investigated tips (n = 10).

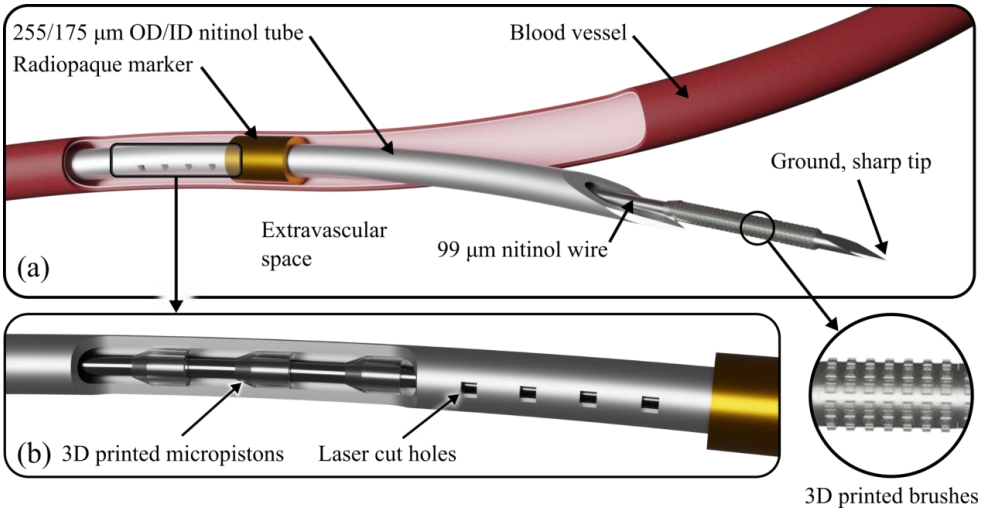

Figure 40 3D rendering of the device as it is intended to be used in an endovascular procedure. (a) The tube exits the vasculature, whereas the inner wire can be deployed, putting the brushes in contact with tissue and retracted, withdrawing cellular material into the tube opening. (b) Zoom in on the internal micropiston arrangements.

6.3.1 Device manufacturing and assembly

The full device is composed of three parts: (i) an inner, sharp nitinol wire with a set of 3D printed pistons and brushes, (ii) an outer, sharp nitinol tube with a radiopaque gold marker and laser-cut holes on the proximal side of the marker and (iii) a PTFE tube that houses the inner system of the nitinol tube and wire.

The 3D-printed pistons and brushes are mounted on a nitinol wire with an OD of 99 µm. The individual brushes are hollow cylinders of height 250 µm, OD 125 µm, and ID 110 µm, with radially protruding square pillars of width 15 µm and height 7.5 µm. The pillars are rounded at the base with a 5 µm radius and equidistantly positioned across the outer cylinder surface at 12 angular and 7 axial positions. The pistons are also hollow cylinders with a height of 250 µm with a conical tapering of 20 degrees, an OD of 165 µm for the larger tube, 145 for the Extroducer tube, and an ID of 105 µm for both designs. There are 4 pistons arranged 25 mm proximal to the wire tip and 4 brushes arranged directly proximal to the wire tip. The 3D-printed parts are printed with a 2PP process. The printing process for the final design was performed with a 25X objective, 1 µm layer thickness, and solid internal scaffold. The wire with the 3D printed pistons and brushes is housed inside the Extroducer, with two different dimensions as described in section 6.1. The laser-machined holes on the Extroducer are arranged in pairs of 4 instances of 50 µm squares, cut through the tube at the center axis, spaced 250 µm apart along the axis, and 250 µm behind the radiopaque marker. The radiopaque marker is produced and assembled identically to previous devices described in this thesis. At the proximal end of the nitinol tube, a syringe connector is glued, allowing the injection of liquid through the tube. The wire-tube assembly is lastly housed inside a PTFE tube of 483 and 330 µm, respectively.

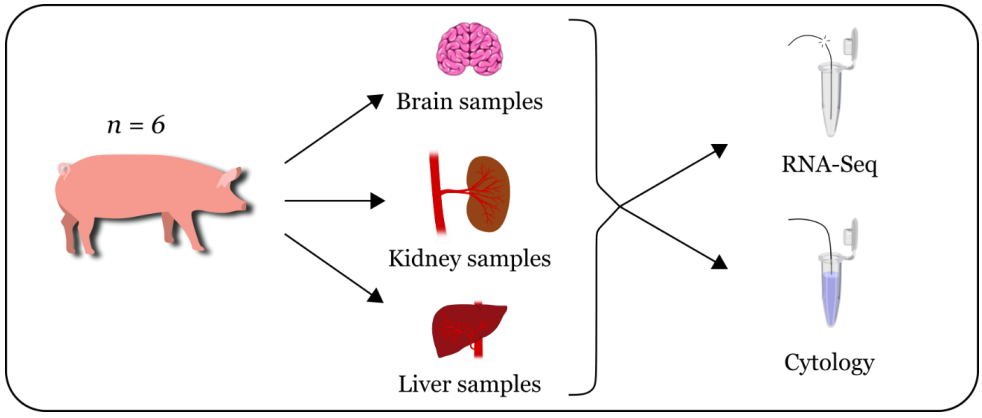

Figure 41. Study design of Paper V. A series of 6 experiments were executed with kidney, liver, and brain sampling performed in 2 experiments each. The samples were evaluated with cytology and RNA-Seq.

6.3.2 Device operation and performance

Once a target site has been reached through the Extroducer technique, the internal device is actuated by applying hydraulic pressure. The hydraulic actuation is designed to overcome frictional issues and increase force generation and solves the previously described issues with wire delivery.

The mechanics of the actuation mechanism is outlined in later subsections relating to Paper VI. The pressure is the driving force pushing the wire forward, aided for the most part by the micropiston features. The distance that the wire moves is dictated either by the laser cut holes in the tube, designed to act as a pressure release once the pistons have advanced past them, or by a proximal stopper, added as a safety feature in case the wire would advance too far. Once the device has entered the tissue, it is left inside for 30 seconds and retracted manually inside the opening of the nitinol tube. Any sample obtained by the brush is protected inside the tip of the catheter assembly and can be safely extracted and examined. The devices were tested in the liver, kidney, and brain and evaluated with cytology and RNA-Seq, Figure 41. Two experiments were dedicated to each organ, and, similar to Paper IV, the devices were compared to control devices without any brush elements. Additionally, surgically extracted kidney, liver, and muscle tissue controls were stained to verify the staining protocol.

Table 1. Overview of locations targeted, how many samplings that were attempted and the associated success rate.

Location	Sampling events	Success rate
Liver	26	77% (20/26)
Kidney	23	48% (11/23)
Brain	28	71% (20/28)

The control devices were tested in the liver (n = 3) and kidney (n = 3) and did in one instance, each show a tissue sample at the tip of the wire.

6.3.3 Cytology

Immunofluorescent staining was performed on samples from the liver (n = 9), kidney (n = 11), and surgically extracted control samples (n = 3). The primary antibodies used for the staining were: GPT/ALT1 mouse anti-porcine monoclonal antibody as the liver-specific marker and NKCC2/SLC12A1 rabbit anti-porcine polyclonal antibody as the kidney-specific marker.

Similar to all sampling projects in this thesis, this visualization procedure is lined with certain challenges due to the size of the sample. The antibodies utilized for these samples are chromophores as opposed to the fluorophores used in papers I-IV. This change was made in an attempt to mitigate the problems with the autofluorescence of the 3D-printed material. The results, Figure 42, illustrate a slight difference between liver and kidney samples in terms of a color shift but are difficult to interpret. A green shift in color represents the liver-specific marker and the kidney-specific marker will appear red. To verify the staining protocol, control samples were stained in the same batch, which does show clear differences in appearance.

6.3.4 RNA-Seq

These results were supplemented with RNA-Seq data, which is currently being analyzed. At the time of writing this thesis, the kidney (n = 10) and liver (n = 16) samples show successful generation of cDNA libraries and sequencing, except from two liver samples. Brain samples are currently being prepared for RNA isolation.

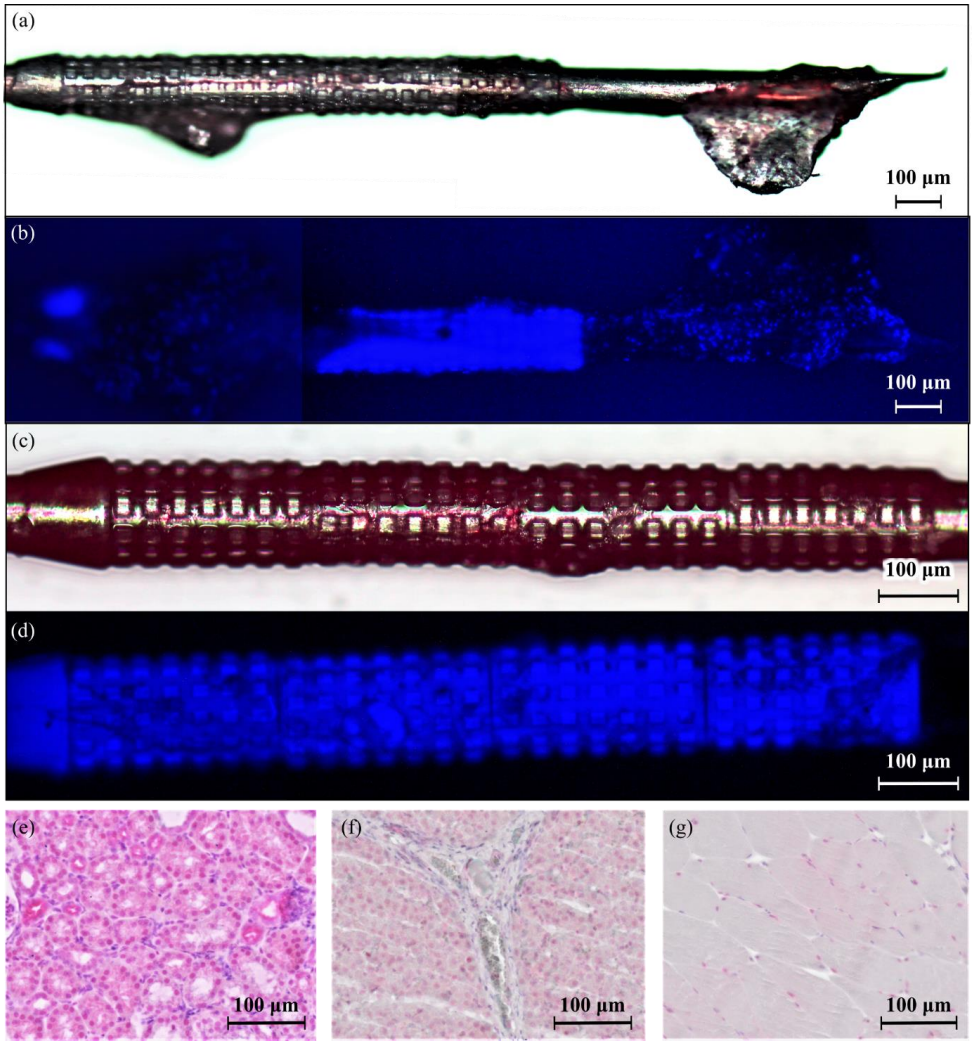

Figure 42. (a) Bright-field microscopy of a stained liver sample attached to the brush. (b) Corresponding DAPI stain of the same sample. (c) Bright-field microscopy of a stained kidney sample attached to the brush. (d) the corresponding DAPI stain of the same sample. Sectioned and stained (e) kidney sample, (f) liver sample, and (g) muscle sample extracted surgically.

6.4 Micropiston solution

Adding the micropistons to the Extroducer system made sampling possible, and, as described in the introductory parts of this chapter, a lot of effort went into finding this solution. Paper VI is a technical evaluation of the micropiston system in terms of the force generated, benchmarked to conventional manual pushing and applying pressure without the micropistons.

Prior to arriving at the final solution, it was known that utilizing pressure in catheter systems, referred to as the flushing technique, is an efficient way of alleviating the friction experienced when a catheter system is subjected to extensive degrees of bending[71]. This was attempted with some prototypes in the in vivo experiments but was unsuccessful as well in delivering the wire into the tissue. In essence, the internal wire is possible to navigate inside of the channel both with manual pushing and the application of a flushing technique. However, as soon as the wire engages with tissue outside of the channel, any solution prior to the micropiston system fails.

The inspiration for the micropiston idea came from a solution in the cable installation industry, as described in the introduction of this thesis. The reported solution is a way of vastly increasing installation distances through pre-constructed channels. By attaching pressure-absorbing structures on large-scale cables and applying liquid pressure, installation distances of several km can be achieved[72]. The cable installation problem is a close analogy to catheter systems, and we therefore hypothesized that this could be directly applied to our system. The requirements of the solution, however, are different. The question is whether this could increase the force generated at the distal end.

6.4.1 Evaluation of force generation

The requirements of the system are not only to increase the force generated at the distal end. It also needs to provide increased force generation as the system goes through several degrees of rotation. The force response as a function of applied pressure was evaluated in a custom-built setup, Figure 43, featuring a pressure chamber where the catheter system and a high-pressure syringe could be connected.

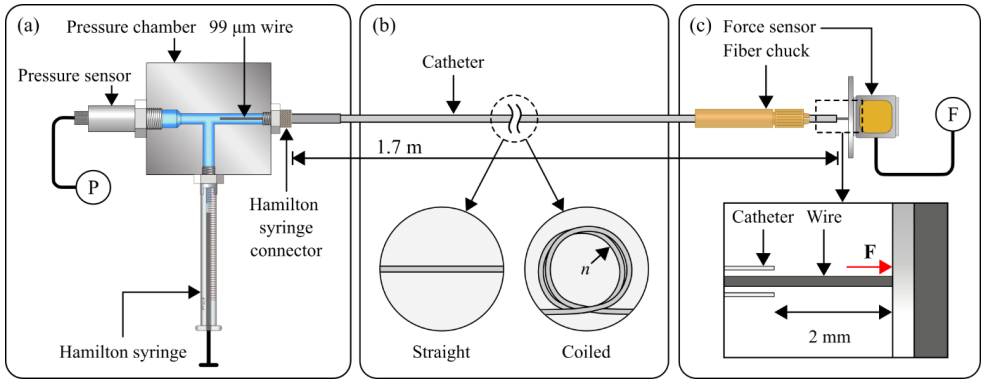

Figure 43. Experimental setup for force and pressure measurement. (a) Pressure chamber with threaded fittings for a pressure sensor with inlets and outlets for Hamilton connectors. (b) The arrangement of the catheter system, either in a straight setting or wound a number of rotations n. (c) The distal part of the catheter is clamped in a fiber chuck and positioned with the tube opening 2 mm from a force sensor plate.

The pressure in the pressure chamber was measured with a pressure sensor, and the force at the distal end of the catheter system was measured with a force sensor. We evaluated three types of wire actuation: (i) micropiston actuation, i.e., applying pressure proximally to a catheter containing a wire with micropistons attached to its distal end; (ii) flushing, i.e., applying pressure proximally to a catheter containing a wire without micropistons, and; (iii) manual pushing, i.e., applying manual force to the

proximal end of a wire without micropistons. Each set of experiments was performed for the following geometric configurations: catheters wound with 0, 1, 2, 3, or 5 rotations with a 5 cm bending radius (rotational experiments) and catheters in an artificial vasculature path modeled after a full-body human angiography[124]. Each experiment was repeated 3 times.

6.4.2 Force response as a function of pressure

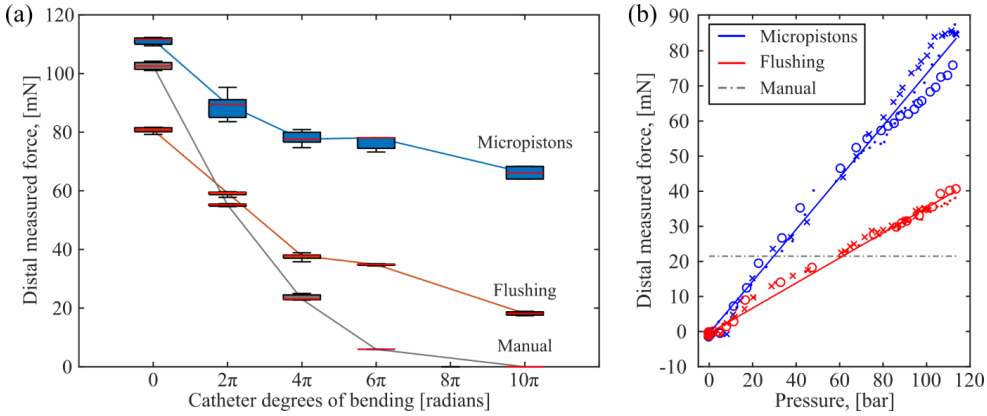

Figure 44. (a) Results of rotational experiments illustrate the benefit of using the micropiston system in terms of the force generated across all experimental settings. (b) The distal force generated by the three actuation mechanisms for different proximal actuation pressures. Circles, dots, and stars indicate measurement results for different experiment repetitions. Solid lines are least square error linear curve fits. The force from the manual operation is not dependent on pressure, and the mean value is represented with a dashed line.

There is a clear advantage of using the micropiston system, especially at larger degrees of bending, Figure 44. The manual setting closely resembles that of the Capstan effect, quickly dropping to almost no distal force transfer after more than 3 full rotations. The flushing technique provides an improvement compared to manual pushing at large degrees of bending as well, as expected from the literature. However, it performs poorly compared to the micropiston system.

6.5 Conclusions

Papers V and VI collectively represent an important step in enabling minimally invasive sampling of soft organs through the Extroducer technique. Further work is needed to verify the method in terms of the sequencing aspects of the acquired samples. Initially, the results of sample preparation look promising in terms of cDNA library and sequencing data generation; however, the results from this analysis are still pending.

Chapter 7 – Summary and outlook

7.1 Summary

This thesis work represents a step towards realizing the next generation of tissue sampling and implantation towards reduced invasiveness. The motivation for addressing the invasiveness of established devices used for tissue sampling stems from the development of next-generation sequencing technologies and how they hold promise as an alternative platform for diagnostics. Sequencing technologies could provide data from minute amounts of genetic material, rendering current devices unnecessarily invasive if sequencing were to be implemented. The sampling devices presented in this thesis work for tissue sampling leverage this development, producing samples too small to be reliably analyzed with histopathology and providing sufficient material for sequencing. The motivation for reducing the invasiveness of endovascular implants stems from the foreign body response associated with the foreign material, necessitating extensive medication to counteract platelet activity and subsequent thrombosis. Concluding remarks will be made with respect to the thesis objectives presented in the introduction. Achievements according to the objectives are listed below:

1. **Establish less invasive methods of obtaining tissue samples through the endovascular route.** Several devices were prototyped and evaluated, leading to three distinct devices for different purposes. First, for endomyocardial sampling, we demonstrate an endovascular sampling device that is substantially smaller than existing devices used for sampling. Second, for EC sampling, we demonstrate a device for sampling endothelial cells in sub-mm vessels with an increased selectivity compared to existing sampling methods. Third, we demonstrate a device to be used with the Extroducer platform for sampling soft tissue that successfully samples tissue from the kidney, liver, and brain.

2. **Validate the new devices in terms of the quality of the produced samples.** Through evaluation with cytology and RNA-Seq, we demonstrate good quality of extracted samples, as evaluated in all sampling projects. In summary, all devices produce too small samples to be reliably analyzed with cytology, even more so for the devices used for endothelial cells and soft tissue. However, samples were successfully prepared for RNA-Seq, yielding data that can be effectively analyzed and compared. The micro-EMB device is at a more mature stage, where we have further demonstrated the capability of differentiating between healthy and sick tissue.

3. **Verify the safety profile of the devices used for sampling.** We demonstrate a drastic improvement in the safety aspects of using the micro-EMB device through benchmarking with a conventional device. The safety profile of the EC sampling device was a consideration in paper IV but not the explicit objective of the study. The monitored data indicate no difference compared to control devices for the endothelial cell sampling device. For the device used in conjunction with the Extroducer, complications were also monitored, indicating no adverse effects during or after sampling, which aligns with the already established safety profile of the Extroducer platform.

4. **Reduce protein adhesion and thrombosis formation on endovascular implants.** Two conceptually similar coatings were applied to stents and evaluated

in vivo and *in vitro* in a blinded study. Both coatings show promise in terms of a significant reduction in coagulation *in vitro*. However, only one of them showed an improvement *in vivo*.

7.2 Outlook

The path forward for the projects oriented toward tissue sampling is, ultimately, to reach clinical implementation. By virtue of being preclinical studies, many aspects pertaining to the manufacturing standards of the devices, the biocompatibility, mechanical integrity, etc., has not been optimized or tested to the proper extent. All devices have been assembled manually in a non-certified lab environment. To fully translate the use of this device to humans, this needs to be addressed by producing it in a proper manufacturing facility with the required testing capabilities. Including miniaturized devices in clinical practice also requires adequate implementation of molecular analysis tools since classic histology is not feasible for the procured samples. This transition is already seen in some aspects of diagnostics, mainly in oncology, and is believed to be implemented in other areas as well[31]. For example, a genetic expression profile test called the Molecular Microscope based on a microarray is available in heart transplant monitoring[125]. Briefly, this platform shows promise in that it can further classify samples based on the type of rejection in greater detail than histology. Time will tell whether the transition from traditional histology and cytology to omics techniques holds true. Apart from requiring this transition, each project has a few weaknesses that need to be addressed in future research endeavors.

The micro-EMB device represents the most mature development in this thesis, having an established proof of concept, verification of its safety, and use in diagnostics. The natural next step is incorporating it into human studies, requiring the above-mentioned steps to achieve a certified device. A potential target for such a study is the main indication for heart biopsy today; heart transplant monitoring. Sampling in this cohort is done on up to 14 separate occasions in the first year[119]. A head-to-head comparison of the micro-EMB and regular device could be incorporated, comparing the diagnostic outcome, provided that a molecular analysis tool is used. There are other indications for heart biopsy, such as heart failure or myocarditis[109]. Some of these conditions present focal patterns inside the heart, which could be challenging to target with the conventional, stiffer device, which could also be interesting to target with a future study. In general, scenarios where a clinician would traditionally avoid biopsies due to the risks, could potentially be studied with the micro-EMB device, providing valuable molecular information about these conditions.

Regarding the EC sampling device, the incidence of bleedings, damaged devices, and the material used for the 3D prints warrants further studies with a device series that has been properly manufactured. The reason for the bleedings and observed damages are briefly speculated upon in Chapter 4 and can be addressed by improvements in device design. For example, tailoring the mechanical stiffness of the core wire similar to guidewire designs[69] to reduce the tip invasiveness or improve the brush's adhesion mechanism to the nitinol wire. Additionally, a few shortcomings in the cytological analysis need to be addressed. Future studies should consider additional stains for cells of interest to verify the method's selectivity completely. However, as with all the sampling projects, the power lies in producing samples that are feasible for RNA-Seq. This analysis provides much more data and could, ideally, replace the need for cytological analysis. For example, cell populations in the sample can be estimated based on genetic data using deconvolution matrices[126]. These analyses could potentially provide information about how the cell proportion in the sample changes

over time, potentially replacing cytology once the sequencing technique has been perfected. Apart from addressing this, additional studies will have to be performed, similar to the path taken for the micro-EMB device, to verify the potential of acquiring diagnostic information. A disease model of interest is the induced stroke model with an endovascular device[127]. An envisioned procedure would be to induce a stroke for a period of time and take samples from the endothelium from healthy, perfused areas as well as from vessel segments distal to the induced stroke. A comparison of genetic expression between these groups could highlight transient, acute changes in the ECs. This information could also be coupled to imaging analyses of the tissue of interest, yielding further information about what happens in the gradient of tissue injury around the stroke. Another area of interest is in vascular malformations, where certain efforts are made to understand the genetic expressions responsible, potentially providing information on abnormalities that can be targeted with a tailored treatment[128]. Lastly, the role of ECs in neurodegenerative disease has been highlighted[88]. The EC sampling device could further elucidate the role of ECs in these conditions, although the clinical implementation of such a sampling procedure might present difficulties.

The implications of the Extroducer-based device are similar to the device for EC sampling. The cytological evaluation does indicate that we are sampling the correct tissue type. However, these devices are even smaller than the EC sampling device, which makes cytological evaluation nigh on impossible to draw conclusions from. The exact nature of the samples will have to be revealed with sequencing. If sequencing yields good data, the implications are vast. The device would enable sampling from areas that are considered hard to reach, such as the brain, without causing hemorrhagic complications. Brain sampling today is usually performed with stereotactic frames with reported post-biopsy morbidity rates of up to 13% and permanent neurological impairment for up to 3.9% of patients[129]. Patient safety would increase drastically if the endovascular route could be chosen instead. The implications of the device extend beyond sampling as well. By virtue of being able to position a sharp wire in soft tissue, other applications can be envisioned, such as delivering miniaturized implants.

Lastly, while promising, the study on the stent coating leaves room for plenty of additional studies. First, by studying the coating in an acute setting, sweeping conclusions on the effects when applying the coating in clinical use cannot easily be drawn. There is much to be learned about what happens at later stages. Several additional studies can be envisioned and would be required to argue for clinical implementation. The most interesting study, arguably, is of the mechanism of action responsible for the increased blood compatibility. As mentioned at the beginning of section 3.3, there is speculation as to how the coating interacts with adhered proteins and their subsequent activation. This could be verified by proteomic assays of the protein film that eventually forms on the surface. This way, the relative abundance of specific proteins can be ascertained, as well as if they undergo conformational changes. Comparing the results with controls will likely reveal differences in the protein composition, highlighting what proteins are interfered with and to what extent. Naturally, a longitudinal *in vivo* study would be required to be able to examine the long-term effects. At longer time frames, other factors come into play, such as the interaction with the vessel wall as well as the stability of the coating. Even further ahead, the coating would have to be benchmarked with other commercial platforms to prove either that it works better or that it is not inferior.

Acknowledgements

I'd like to express my gratitude to my many supervisors for the opportunity to work both with you and on this research project. To my main supervisor at KTH, **Göran Stemme**, thank you for investing your time in me and for hosting such a diverse research group. Thank you to my main supervisor at KI, **Staffan Holmin**. I remember the first time I entered your office in the old Karolinska hospital, feeling both insecure and excited during our interview. Thank you for believing in me then and for what it ultimately led to today. To my co-supervisor **Niclas Roxhed**, sometimes it felt like you were more passionate about my research than I was, so thank you for the motivation that it provided. To my co-supervisor, **Wouter van der Wijngaart**, thank you for the efforts you made in improving the research and the discussions about life that came up somewhere in between it all. Last but not least, I'd like to thank my co-supervisor **Stefan Jonsson**. In many aspects, you were the catalyst that enabled this career path for me, and for that, I'll always be grateful.

I'm also grateful to my many friends and colleagues at MST. **Valentina**, my trusted office mate, and confidant: thank you for having the patience required to share offices with me and for giving me the tough love that I (sometimes) needed throughout the various events in my life. *Ευχαριστώ*. **Henar**, my gym partner extraordinaire: I really appreciate being able to confide in you not only matters of life but also research. Thanks for the support, and here's hoping for many more split squats *y conversaciones en español* to come. **Argyris**, my partner in crime in all matters of in vivo experiments: Thanks for being the laid-back, supportive presence I need when I'm stressing out inside and outside of the lab. It truly made a difference. **Theocharis**, the Balkan presence that I didn't know I needed and didn't deserve: Thanks for all the good times shared, whether it was playing on the Switch, playing padel, or hanging out at the country house. Don't lose hope in me; eventually, I'll realize the importance of world history. **Laura**, my gym rat equivalent at MST: Thanks for all the laughs, gym sessions, and language exchanges. I hope I improved your impression of Stockholm the way you improved mine of Spain. **Pierre**, my ever-present lunch partner: Thanks for being a good friend, the padel sessions (and tournaments), and the laughs. For the record, my financial advice was never illegal, the disclaimer, however unnoticeable, was always stated. **Arne**, one of the few people who have seen me out of my wits during festivities, and who I was fortunate enough to spend two weeks in Canada with. Thanks for the associated memories and your continued support. **Emre**, my fellow MST entrepreneur, although you've made it considerably farther: thanks for that one time we went to the gym, and all the help throughout the years. **Jibbe**, my primary source of minority complex at the office: thanks for allowing me to win in our gaming sessions, it can't have been easy to suffer through my subsequent verbal torment. **Filipe**, in many aspects my equivalent in the medical device arena at MST: thanks for sharing ideas, wires and tubes, and for saying that Swedish football (in one aspect) actually has something to offer internationally. **Kerem**, the only one I felt I could comfortably pass on the 3D printer responsibility to: thank you for unloading that burden and for showing me proper Turkish fortune telling. **Saumey**, when we met at the MST course way back, I could tell that you were an intelligent guy with a passion for research and I was not surprised to see you enroll at MST as a fellow PhD student not long after. Thanks for showing me and others that passion, and I am happy that we became friends. **Gaehun**, the calming presence that every office needs and that never says no to going out for lunch: thanks for showing us the ways of the Nanoscribe and for proving my point that buying an apartment is the only reasonable thing to do.

Mohammad, my badminton nemesis: thanks for always presenting a cheerful mood in the office and for cementing my role as the undefeated badminton champion. **Cecilia**, our resident clean room magician, I honestly don't know where any of our research would have been without your help. Thanks for having patience with me in my early Kista-faring years. **Micke**, also a wizard in his own right and invaluable to MST: I always found it incredible how I could send a 3D file, wait a few days, and then a replica of it magically appeared on my desk—many thanks for your efforts. There are many more to be thankful to at the department; thanks to all who made MST the amazing research environment that it is.

The research group at KI deserves praise as well. **Rikard**, my peer on the medical side of this research project: thank you for sharing a major part of this journey. Seeing your technical skills compared to my own has been humbling, impressive, and motivating. Here's hoping for many more years of collaborative efforts in the medical device and 3D printing industry. **Arvin**, my other medical counterpart throughout this research endeavor: thank you for your tremendous additions to the sequencing aspects of this research. If you ever need a position as a machine learning engineer, I think you don't need to learn anything extra. Also, thank you for providing valuable perspectives in matters of life. **Jonathan**, arguably the researcher at all of KI who's most eager to do research and figure things out: thank you for the assistance throughout most of my experiments and for providing humbling advice in the dating arena. **Jeroen**, although we only occasionally worked together, having a fellow engineer on site felt good. Thanks for the support, and I hope we get to work together more in the future. **Victoria**, working with you always felt effortless, and I enjoyed our discussions and occasional gossip during the experiments. Thank you for that, and if you ever need another 3D print, let me know! **Fabian**, you always felt like somewhat of a guiding presence in my early, insecure years in the research group. Thanks for being patient and relaxed with me during that time. **Pellina**, probably one of the most important people in this thesis, as you've been involved in every single one of my experiments: thank you for your patience in correcting my poorly filled order forms and assisting me when I reach out for information months later. Thanks to everyone in the group for supporting me and making it easy for an engineer to fit in.

I also wish to thank the other research collaborators I encountered throughout the projects. **Javier**, thank you for your patience in educating me on the history of blood research and for the hours we spent fine-tuning our manuscript. **Robert**, you were always supportive of whatever I chose to do, and I'll always remember the time we spent collaborating.

I also want to thank all of my friends. **Martin, Jennifer, Micke, Nathalie, Sara, Christine, Oskar, Mimmi, Martin, Sofie & Rikard**: you all have been a presence for most of my adult life, and many of my cherished memories are from times spent with you. Thank you for the past years and for thinking that what I do is impressive, it gave me motivation and perspective. **Martin, Guisella, Linus, Amanda, Leo, Sam, Jonathan & Evelina**: the times spent with you both on- and offline was a much needed escape from the realities of the research struggle, although the time spent online provided a different kind of stress. **Erik**, the friend that I knew I could always turn to whenever I felt troubled or when I, or you, wanted to try a fun project. Thanks for the friendship, side ventures and the recent lessons in Frisbee golf. **David & Elin**, I am happy that our time at MST coincided and that we became friends. I'm looking forward to our continued friendship and the future trips together. **Sanna, Karl & Natasha**, the colleagues-turned-friends, thank you not only for the good times outside of the office but also for being the Swedish presence I lacked inside of it.

Simon, and by extension, your family, **Victoria, Leah & Aron**: I can't thank you enough for the hours spent grinding in the gym, throwing bars, dumbbells, and ourselves around ad infinitum. It gave me much valued time to reduce stress and think about other things. **Celine**: Thank you for your undying support and companionship throughout the years we've known each other. Thank you for continuously striving to make both yourself and me a better person. Thank you for showing me what truly matters in life.

Slutligen är jag tacksam för min släkt och familj. **Mats**, i egenskap av storebror har du alltid varit en förebild och den person som jag till alla pris måste bli bättre än, på gott och ont. Jag tror att du haft en större inverkan på mina beslut än vad både du och jag inser. I slutändan är jag tacksam för den relation vi har och hur den kommer fortsätta forma våra liv. **Mamma och pappa**, vars tidvis orimliga övertro på min förmåga nog är den största anledningen till att jag är där jag är idag. Jag fick höra när jag var yngre att det första val man gör i livet är sina föräldrar, och där kunde jag nog inte valt bättre.

References

[1] S. I. Seldinger, *Acta Radiologica*. **1953**, *39*
[2] F. Ahmad, T. Sabharwal, A. Adam, *Surgery (Oxford)*. **2008**, *26*
[3] M. M. Payne, *Tex Heart Inst J*. **2001**, *28*
[4] T. F. Meaney, M. A. Weinstein, E. Buonocore, W. Pavlicek, G. P. Borkowski, J. H. Gallagher, B. Sufka, W. J. MacIntyre, *American Journal of Roentgenology*. **1980**, *135*
[5] U. Sigwart, J. Puel, V. Mirkovitch, F. Joffre, L. Kappenberger, *New England Journal of Medicine*. **1987**, *316*
[6] A. M. Spiotta, M. I. Chaudry, F. K. Hui, R. D. Turner, R. T. Kellogg, A. S. Turk, *Journal of NeuroInterventional Surgery*. **2015**, *7*
[7] S. T. Kee, L. Kinoshita, M. K. Razavi, U. Nyman, C. P. Semba, M. D. Dake, *Radiology*. **1998**, *206*
[8] A. Pomoni, C. Sotiriadis, F. Gay, A.-M. Jouannic, S. D. Qanadli, *European Radiology*. **2018**, *28*
[9] D. C. H. Cheng, J. Martin, A. Lal, A. Diegeler, T. A. Folliguet, L. W. Nifong, P. Perier, E. Raanani, J. M. Smith, J. Seeburger, V. Falk, *Innovations*. **2011**, *6*
[10] K. B. Quencer, K. Anand, *Techniques in Vascular & Interventional Radiology*. **2021**, *24*
[11] A. Khalifa, D. C. Rockey, *Current Opinion in Gastroenterology*. **2020**, *36*
[12] D. Berger, V. Desai, S. Janardhan, *Clinical liver disease*. **2019**, *13*
[13] V. Nair, J. Butany, *Journal of Clinical Pathology*. **2010**, *63*
[14] G. Ortner, E. Tzanaki, B. P. Rai, U. Nagele, T. Tokas, *Turkish Journal of Urology*. **2021**, *47*
[15] C. R. Weiss, S. G. Nour, J. S. Lewin, *Journal of Magnetic Resonance Imaging*. **2008**, *27*
[16] T. Ahmed, A. Goyal, StatPearls Publishing, **2021**
[17] X. Yao, M. M. Gomes, M. S. Tsao, C. J. Allen, W. Geddie, H. Sekhon, *Current Oncology*. **2012**, *19*
[18] C. S. Kaufman, M. R. Cretcher, *Techniques in Vascular & Interventional Radiology*. **2021**, *24*
[19] N. J. Khati, J. Gorodenker, M. C. Hill, *Ultrasound Quarterly*. **2011**, *27*
[20] I. C. Tsai, W.-L. Tsai, M.-C. Chen, G.-C. Chang, W.-S. Tzeng, S.-W. Chan, C. C.-C. Chen, *American Journal of Roentgenology*. **2009**, *193*
[21] A. M. From, J. J. Maleszewski, C. S. Rihal, *Mayo Clinic Proceedings*. **2011**, *86*
[22] D. L. Cooke, D. B. McCoy, V. V. Halbach, S. W. Hetts, M. R. Amans, C. F. Dowd, R. T. Higashida, D. Lawson, J. Nelson, C.-Y. Wang, H. Kim, Z. Werb, C. McCulloch, T. Hashimoto, H. Su, Z. Sun, *Translational Stroke Research*. **2018**, *9*
[23] S. W. Waldo, D. A. Brenner, J. M. McCabe, M. D. Cruz, B. Long, V. A. Narla, J. Park, A. Kulkarni, E. Sinclair, S. Y. Chan, *PloS One*. **2015**, *10*, e0118081
[24] M. Titford, *Journal of Histotechnology*. **2006**, *29*
[25] B. Naylor, *Acta Cytologica*. **2000**, *44*
[26] W. Gray, G. Kocjan, Elsevier Health Sciences, **2010**
[27] S. Behjati, P. S. Tarpey, *Archives of Disease in Childhood. Education and Practice Edition*. **2013**, *98*
[28] M. Arya, I. S. Shergill, M. Williamson, L. Gommersall, N. Arya, H. R. Patel, *Expert Review of Molecular Diagnostics*. **2005**, *5*
[29] A. Butte, *Nature Reviews Drug Discovery*. **2002**, *1*
[30] Z. Wang, M. Gerstein, M. Snyder, *Nature Reviews Genetics*. **2009**, *10*

[31] D. S. Rogawski, N. A. Vitanza, A. C. Gauthier, V. Ramaswamy, C. Koschmann, *Translational Research*. **2017**, *189*
[32] F. Tang, C. Barbacioru, Y. Wang, E. Nordman, C. Lee, N. Xu, X. Wang, J. Bodeau, B. B. Tuch, A. Siddiqui, K. Lao, M. A. Surani, *Nature Methods*. **2009**, *6*
[33] B. D. Piening, A. K. Dowdell, M. Zhang, B.-L. Loza, D. Walls, H. Gao, M. Mohebnasab, Y. R. Li, E. Elftmann, E. Wei, D. Gandla, H. Lad, H. Chaib, N. K. Sweitzer, M. Deng, A. C. Pereira, M. Cadeiras, A. Shaked, M. P. Snyder, B. J. Keating, *The Journal of Heart and Lung Transplantation*. **2022**, *41*
[34] J. da Silva, F. Grönberg, B. Cederström, M. Persson, M. Sjölin, Z. Alagic, R. Bujila, M. Danielsson, *Journal of Medical Imaging*. **2019**, *6*
[35] M. Barton, J. Grüntzig, M. Husmann, J. Rösch, *Frontiers in Cardiovascular Medicine*. **2014**, *1*
[36] J. Y. Moon, F. Franchi, F. Rollini, D. J. Angiolillo, *Progress in Cardiovascular Diseases*. **2018**, *60*, 478
[37] S. Torii, H. Jinnouchi, A. Sakamoto, M. Kutyna, A. Cornelissen, S. Kuntz, L. Guo, H. Mori, E. Harari, K. H. Paek, *Nature Reviews Cardiology*. **2020**, *17*
[38] D.-H. Lee, J. M. de la Torre Hernandez, *European Cardiology Review*. **2018**, *13*
[39] D. Hoare, A. Bussooa, S. Neale, N. Mirzai, J. Mercer, *Advanced Science*. **2019**, *6*
[40] H. Jinnouchi, S. Torii, A. Sakamoto, F. D. Kolodgie, R. Virmani, A. V. Finn, *Nature Reviews Cardiology*. **2019**, *16*
[41] J. W. Drelich, J. Goldman, *Current Opinion in Biomedical Engineering*. **2022**, *24*,
[42] I. H. Jaffer, J. I. Weitz, *Acta Biomaterialia*. **2019**, *94*
[43] J. L. Brash, T. A. Horbett, R. A. Latour, P. Tengvall, *Acta Biomaterialia*. **2019**, *94*, 11
[44] M. Gorbet, C. Sperling, M. F. Maitz, C. A. Siedlecki, C. Werner, M. V. Sefton, *Acta Biomaterialia*. **2019**, *94*, 25
[45] M. Weber, H. Steinle, S. Golombek, L. Hann, C. Schlensak, H. P. Wendel, M. Avci-Adali, *Frontiers in Bioengineering and Biotechnology*. **2018**, *6*, 99
[46] T. Gori, A. Polimeni, C. Indolfi, L. Räber, T. Adriaenssens, T. Münzel, *Nature Reviews Cardiology*. **2019**, *16*
[47] K. Zhang, T. Liu, J. A. Li, J. Y. Chen, J. Wang, N. Huang, *Journal of Biomedical Materials Research, Part A*. **2014**, *102*, 588
[48] S. M. Dizaj, A. A. Rad, N. Safaei, S. Salatin, E. Ahmadian, S. Sharifi, S. Z. Vahed, F. Lotfipour, S. Shahi, *Journal of Pharmacy & Pharmaceutical Sciences*. **2019**, *22*, 501
[49] M. Vafa Homann, D. Johansson, H. Wallen, J. Sanchez, *Journal of Biomedical Materials Research, Part B*. **2016**, *104*, 1359
[50] G. Björling, D. Johansson, L. Bergström, A. Strekalovsky, J. Sanchez, C. Frostell, S. Kalman, *Journal of Biomedical Materials Research, Part B*. **2018**, *106*, 2337
[51] B. Magnusson, Y. Kai-Larsen, P. Granlund, Å. Seiger, L. Lindbo, J. Sanchez, D. Johansson, *Therapeutic Advances in Urology*. **2019**, *11*, 1756287219854915
[52] Y. Kai-Larsen, S. Grass, B. Mody, S. Upadhyay, H. L. Trivedi, D. K. Pal, S. Babu, B. Bawari, S. K. Singh, *Antimicrobial Resistance & Infection Control*. **2021**, *10*, 40
[53] A. R. Pelton, S. M. Russell, J. DiCello, *The Journal of The Minerals, Metals & Materials Society*. **2003**, *55*
[54] D. Stöckel, *Endovascular Update*. **1998**, *1*
[55] V. Birman, *Applied Mechanics Reviews*. **1997**, *50*
[56] S. Thompson, *International Endodontic Journal*. **2000**, *33*

[57] A. Badrou, N. Tardif, A. Even, P. Chaudet, N. Lescanne, J. Szewczyk, A. Gravouil, N. Hamila, A. Bel-Brunon, *Cardiovascular Engineering and Technology*. **2022**, *13*
[58] J. W. Judy, *Smart Materials and Structures*. **2001**, *10*
[59] M. Tanaka, *Microelectronic Engineering*. **2007**, *84*
[60] A. M. Hynes, H. Ashraf, J. K. Bhardwaj, J. Hopkins, I. Johnston, J. N. Shepherd, *Sensors and Actuators A: Physical*. **1999**, *74*
[61] M. Sandell, R. Grankvist, S. Jonsson, W. M. v. d. Wijngaart, G. Stemme, S. Holmin, N. Roxhed in Proc. 2020 IEEE 33rd International Conference on Micro Electro Mechanical Systems (MEMS), 18-22 Jan. 2020, **2020**
[62] R. Srinivasan, E. Sutcliffe, B. Braren, *Applied Physics Letters*. **1987**, *51*
[63] K. Sugioka, Y. Cheng, Femtosecond laser 3D micromachining for microfluidic and optofluidic applications, *Springer London*, **2013**
[64] P. Pou-Álvarez, A. Riveiro, X. R. Nóvoa, M. Fernández-Arias, J. del Val, R. Comesaña, M. Boutinguiza, F. Lusquiños, J. Pou, *Surface and Coatings Technology*. **2021**, *427*
[65] E. G. Gamaly, A. V. Rode, *Progress in Quantum Electronics*. **2013**, *37*
[66] A. K. Nguyen, R. J. Narayan, *Materials Today*. **2017**, *20*
[67] M. Carlotti, V. Mattoli, *Small*. **2019**, *15*
[68] K.-S. Lee, D.-Y. Yang, S. H. Park, R. H. Kim, *Polymers for Advanced Technologies*. **2006**, *17*
[69] P. Bloss, W. Rothe, P. Wünsche, C. Werner, A. Rothe, G. D. Kneissl, W. Burger, E. Rehberg, *Bio-medical materials and engineering*. **2003**, *13*
[70] J. H. Jung, N. Pan, T. J. Kang, *Tribology International*. **2008**, *41*
[71] K. Makita, S. Furui, T. Irie, J. Hirata, T. Yamauchi, K. Tsuchiya, E. Takenaka, K. Ohtomo, K. Ibukuro, *The British Journal of Radiology*. **1991**, *64*
[72] W. Griffioen, C. Gutberlet, G. Plumettaz, *Journal of Energy and Power Engineering*. **2012**, *6*
[73] I. Cockerill, C. W. See, M. L. Young, Y. Wang, D. Zhu, *Advanced Functional Materials*. **2021**, *31*
[74] J. Rösch, F. S. Keller, J. A. Kaufman, *Journal of Vascular and Interventional Radiology*. **2003**, *14*
[75] D. R. Whittaker, M. F. Fillinger, *Vascular and Endovascular Surgery*. **2006**, *40*
[76] P. McKavanagh, G. Zawadowski, N. Ahmed, M. Kutryk, *Expert Review of Cardiovascular Therapy*. **2018**, *16*
[77] B. E. Claessen, J. P. Henriques, F. A. Jaffer, R. Mehran, J. J. Piek, G. D. Dangas, *JACC: Cardiovascular Interventions*. **2014**, *7*, 1081
[78] D. Stoeckel, C. Bonsignore, S. Duda, *Minimally Invasive Therapy & Allied Technologies*. **2002**, *11*
[79] K. Pendyala Lakshmana, X. Yin, J. Li, P. Chen Jack, N. Chronos, D. Hou, *JACC: Cardiovascular Interventions*. **2009**, *2*
[80] M. F. Maitz, M. C. L. Martins, N. Grabow, C. Matschegewski, N. Huang, E. L. Chaikof, M. A. Barbosa, C. Werner, C. Sperling, *Acta Biomaterialia*. **2019**, *94*, 33
[81] J. Lu, T. J. Webster, *Acta Biomaterialia*. **2015**, *16*
[82] P. Damas, C. Legrain, B. Lambermont, N. Dardenne, J. Guntz, G. Kisoka, P. Demaret, A. F. Rousseau, L. Jadot, S. Piret, D. Noirot, A. Bertrand, A. F. Donneau, B. Misset, *Annals of Intensive Care*. **2022**, *12*
[83] I. Hidalgo Fabrellas, M. Rebollo Pavón, M. Planas Canals, M. Barbero Cabezas, *Enfermeria Intensiva*. **2015**, *26*, 54

[84] T. Funakoshi, K. Furushima, H. Shimada, S. Kojima, *Biochemistry International*. **1992**, *28*, 113
[85] J. A. Rhodin, *Comprehensive Physiology*. **2011**
[86] H. F. Galley, N. R. Webster, *British Journal of Anaesthesia*. **2004**, *93*, 105
[87] E. A. Winkler, C. N. Kim, J. M. Ross, J. H. Garcia, E. Gil, I. Oh, L. Q. Chen, D. Wu, J. S. Catapano, K. Raygor, K. Narsinh, H. Kim, S. Weinsheimer, D. L. Cooke, B. P. Walcott, M. T. Lawton, N. Gupta, B. V. Zlokovic, E. F. Chang, A. A. Abla, D. A. Lim, T. J. Nowakowski, *Science*. **2022**, *375*
[88] A. C. Yang, R. T. Vest, F. Kern, D. P. Lee, M. Agam, C. A. Maat, P. M. Losada, M. B. Chen, N. Schaum, N. Khoury, A. Toland, K. Calcuttawala, H. Shin, R. Pálovics, A. Shin, E. Y. Wang, J. Luo, D. Gate, W. J. Schulz-Schaeffer, P. Chu, J. A. Siegenthaler, M. W. McNerney, A. Keller, T. Wyss-Coray, *Nature*. **2022**
[89] F. J. Garcia, N. Sun, H. Lee, B. Godlewski, K. Galani, B. Zhou, J. Mantero, D. A. Bennett, M. Sahin, M. Kellis, M. Heiman, *Nature*. **2022**
[90] L. Feng, C. Matsumoto, A. Schwartz, A. M. Schmidt, D. M. Stern, J. Pile-Spellman, *Diabetes Care*. **2005**, *28*, 379
[91] D. Onat, S. Jelic, A. M. Schmidt, J. Pile-Spellman, S. Homma, M. Padeletti, Z. Jin, T. H. Le Jemtel, P. C. Colombo, L. Feng, *Journal of Applied Physiology*. **2007**, *103*, 1873
[92] G. P. Fadini, A. Avogaro, *Cardiovascular Research*. **2010**, *87*
[93] D. L. Cooke, H. Su, Z. Sun, Y. Guo, D. Guo, M. M. Saeed, S. W. Hetts, R. T. Higashida, C. F. Dowd, W. L. Young, *Interventional Neuroradiology*. **2013**, *19*, 399
[94] D. L. Cooke, D. Bauer, Z. Sun, C. Stillson, J. Nelson, D. Barry, S. W. Hetts, R. T. Higashida, C. F. Dowd, V. V. Halbach, *Interventional Neuroradiology*. **2015**, *21*, 120
[95] Z. Sun, D. A. Lawson, E. Sinclair, C.-Y. Wang, M.-D. Lai, S. W. Hetts, R. T. Higashida, C. F. Dowd, V. V. Halbach, Z. Werb, *Biotechnology Reports*. **2015**, *7*, 157
[96] N. Jaff, R. Grankvist, L. Muhl, A. Chireh, M. Sandell, S. Jonsson, F. Arnberg, U. Eriksson, S. Holmin, *Neuroradiology*. **2018**, *60*, 759
[97] M. D. Alexander, Z. Sun, M. B. Conrad, D. L. Cooke, *BioTechniques*. **2019**, *66*
[98] K. H. Narsinh, K. Narsinh, D. B. McCoy, Z. Sun, C. Halabi, K. Meisel, T. Tihan, K. Chaganti, M. R. Amans, V. V. Halbach, R. T. Higashida, S. W. Hetts, C. F. Dowd, E. A. Winkler, A. A. Abla, T. J. Nowakowski, D. L. Cooke, *Frontiers in Neurology*. **2021**, *12*
[99] M. Sandell, S. Jonsson, W. v. d. Wijngaart, G. Stemme, S. Holmin, N. Roxhed in Proc. 2021 IEEE 34th International Conference on Micro Electro Mechanical Systems (MEMS), 25-29 Jan. 2021, **2021**
[100] M. Sandell, A. Chireh, A. Spyrou, R. Grankvist, J. Al-Saadi, S. Jonsson, W. van der Wijngaart, G. Stemme, S. Holmin, N. Roxhed, *Advanced NanoBiomed Research*. **2022**, *2*
[101] N. Takeda, K. Maemura, Y. Imai, T. Harada, D. Kawanami, T. Nojiri, I. Manabe, R. Nagai, *Circulation Research*. **2004**, *95*, 146
[102] A. Ouhtit, R. L. Gaur, Z. Y. Abd Elmageed, A. Fernando, R. Thouta, A. K. Trappey, M. E. Abdraboh, H. I. El-Sayyad, P. Rao, M. G. H. Raj, *Biochimica et Biophysica Acta - Reviews on Cancer*. **2009**, *1795*, 130
[103] S. S. Rho, H. J. Choi, J. K. Min, H. W. Lee, H. Park, H. Park, Y. M. Kim, Y. G. Kwon, *Biochemical and Biophysical Research Communications*. **2011**, *404*
[104] H. Zhang, K. O. Lui, B. Zhou, *Circulation Research*. **2018**, *122*
[105] B. Dye, J. Lincoln, *Cold Spring Harbor Perspectives in Biology*. **2020**, *12*
[106] S. Y. Ho, *European Journal of Echocardiography*. **2009**, *10*
[107] P. R. Riley, Current Topics in Developmental Biology, *Academic Press*, **2012**

[108] E. R. Rodriguez, C. D. Tan, *Progress in Cardiovascular Diseases*. **2017**, *59*
[109] P. M. Seferović, H. Tsutsui, D. M. McNamara, A. D. Ristić, C. Basso, B. Bozkurt, L. T. Cooper Jr, G. Filippatos, T. Ide, T. Inomata, *European Journal of Heart Failure*. **2021**, *23*
[110] S. Konno, S. Sakakibara, *Diseases of the Chest*. **1963**, *44*
[111] F. Saraiva, V. Matos, L. Gonçalves, M. Antunes, L. A. Providência, *Transplantation Proceedings*. **2011**, *43*
[112] A. Groenewegen, F. H. Rutten, A. Mosterd, A. W. Hoes, *European Journal of Heart Failure*. **2020**, *22*
[113] D. H. Birnie, P. B. Nery, A. C. Ha, R. S. B. Beanlands, *Journal of the American College of Cardiology*. **2016**, *68*
[114] R. Grankvist, A. Chireh, M. Sandell, A. K. Mukarram, N. Jaff, I. Berggren, H. Persson, C. Linde, F. Arnberg, J. Lundberg, M. Ugander, G. La Manno, S. Jonsson, C. O. Daub, S. Holmin, *Scientific Reports*. **2020**, *10*, 8029
[115] Y. Li, C. Wang, T. Li, L. Ma, F. Fan, Y. Jin, J. Shen, *Cell Death Discovery*. **2019**, *5*
[116] R. Hinkel, D. Ramanujam, V. Kaczmarek, A. Howe, K. Klett, C. Beck, A. Dueck, T. Thum, K.-L. Laugwitz, L. Maegdefessel, C. Weber, C. Kupatt, S. Engelhardt, *Journal of the American College of Cardiology*. **2020**, *75*
[117] A. Chireh, R. Grankvist, M. Sandell, A. K. Mukarram, F. Arnberg, J. Lundberg, C. O. Daub, S. Holmin, *PLOS ONE*. **2021**, *16*
[118] A. Chireh, M. Sandell, R. Grankvist, V. Lövljung, J. al-Saadi, F. Arnberg, J. Lundberg, M. Settergren, S. Holmin, *Heart and Vessels*. **2022**, *37*
[119] V. Nguyen, M. Cantarovich, R. Cecere, N. Giannetti, *The Journal of Heart and Lung Transplantation*. **2005**, *24*
[120] J. Lundberg, S. Jonsson, S. Holmin, *PLOS ONE*. **2010**, *5*
[121] J. Lundberg, S. Jonsson, S. Holmin, *PLOS ONE*. **2011**, *6*
[122] R. Grankvist, M. Jensen-Urstad, J. Clarke, M. Lehtinen, P. Little, J. Lundberg, F. Arnberg, S. Jonsson, K. R. Chien, S. Holmin, *Journal of Internal Medicine*. **2019**, *285*,
[123] J. Lundberg, R. Grankvist, S. Holmin, *Journal of Internal Medicine*. **2019**, *286*,
[124] W. Ajaj, M. Goyen, *An-Najah University Journal for Research-B (Humanities)*. **2010**, *1*
[125] P. F. Halloran, L. Potena, J. D. Van Huyen, P. Bruneval, O. Leone, D. H. Kim, X. Jouven, J. Reeve, A. Loupy, *The Journal of Heart and Lung Transplantation* **2017**, *36*
[126] D. D. Erdmann-Pham, J. Fischer, J. Hong, Y. S. Song, *Genome Research*. **2021**, *31*
[127] P. Little, O. Kvist, R. Grankvist, S. Jonsson, P. Damberg, M. Söderman, F. Arnberg, S. Holmin, *PloS one*. **2017**, *12*
[128] E. Winkler, D. Wu, E. Gil, D. McCoy, K. Narsinh, Z. Sun, K. Mueller, J. Ross, H. Kim, S. Weinsheimer, *Neurology*. **2022**, *98*
[129] M. Riche, A. Amelot, M. Peyre, L. Capelle, A. Carpentier, B. Mathon, *Neurosurgical Review*. **2021**, *44*